ANALYTICAL AND EXPERIMENTAL STUDIES IN NONLINEAR
STRUCTURAL HEALTH MONITORING AND SYSTEM IDENTIFICATION

by

Ahmed Mazen Wahbeh

_____

A Dissertation Presented to the

FACULTY OF THE GRADUATE SCHOOL

UNIVERSITY OF SOUTHERN CALIFORNIA

In Partial Fulfillment of the

Requirements for the Degree

DOCTOR OF PHILOSOPHY

(CIVIL ENGINEERING)

December 2003

Copyright 2003   Ahmed Mazen Wahbeh

UMI Number: 3133349

Copyright 2003 by

Wahbeh, Ahmed Mazen

All rights reserved.

INFORMATION TO USERS

The quality of this reproduction is dependent upon the quality of the copy
submitted. Broken or indistinct print, colored or poor quality illustrations and
photographs, print bleed-through, substandard margins, and improper
alignment can adversely affect reproduction.

In the unlikely event that the author did not send a complete manuscript
and there are missing pages, these will be noted. Also, if unauthorized
copyright material had to be removed, a note will indicate the deletion.

UMI®

UMI Microform 3133349

Copyright 2004 by ProQuest Information and Learning Company.

All rights reserved. This microform edition is protected against

unauthorized copying under Title 17, United States Code.

ProQuest Information and Learning Company
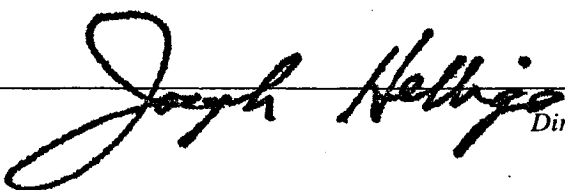300 North Zeeb Road
P.O. Box 1346
Ann Arbor, MI 48106-1346

UNIVERSITY OF SOUTHERN CALIFORNIA
THE GRADUATE SCHOOL
UNIVERSITY PARK
LOS ANGELES, CALIFORNIA 90089-1695

This dissertation, written by

Ahmed Mazen Wahbeh

under the direction of h i s   dissertation committee, and approved by all its members, has been presented to and accepted by the Director of Graduate and Professional Programs, in partial fulfillment of the requirements for the degree of
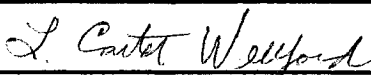
DOCTOR OF PHILOSOPHY

_____
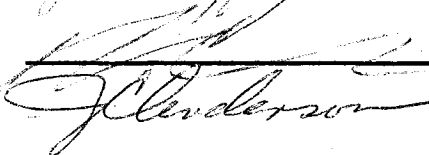   *Director*

Date__December 17, 2003

Dissertation Committee

_____

_____ *Chair*

_____

_____

Acknowledgements

Professor Sami F. Masri has been an advisor like no other. Dr. Masri provided continuous support and guidance throughout my graduate studies; he helped me focus on studies related to my professional career, and he has assisted me in becoming active in technical committees. I would like to thank him for his support, for being there to discuss educational and professional issues, and for the opportunities to explore the different directions the research could lead. I would also like to take this opportunity to show my appreciation to the other members of my Ph.D. committee, Professors James C. Anderson, John P. Caffrey, Petros A. Ioannou, and L. Carter Welford. It has truly been an inspirational experience.

A very special acknowledgement goes to Professor John P. Caffrey, for his immeasurable support and the long hours he spent with me during this study. I would like to thank him for assisting in instrumenting and collecting data from the Vincent Thomas Bridge, sometimes working past midnight, during the optical research portion of this research.

Many USC professors, students, and alumni contributed to the amazing experience of the past years. With this I would like to thank Farzad Tasbihgoo, and Ray Wolfe for their friendship and support, as well as Elena Kallinikidou for her assistance with Mathematica. Dr. Robert Nigbor, thank you for your help and for using your connections to obtain equipment from Kinematrics.

I am grateful to my parents, Abdulrahim and Shaihizar, for the pride they show me and their constant support throughout my education. I would also like to acknowledge my parents-in-law for their encouragement, Leo and Dago Zwinkels.

Most importantly, however, are my wife, Nicole, and my children, Jacob and Jenna without whom I would not be where I am today. Thank you Nicole for all the time you have dedicated to helping me complete my Ph.D., and for taking care of things at home during my absences. Thank you for always being there when I needed you. I know the sacrifices the entire family has made in order for me to obtain my Ph.D. degree. For the times, I could not make it to their soccer games, or school events, I look forward to making my amends.

Contents

vi

List of Tables

vii

List of Figures

Abstract

The research results reported herein consisted of a sequence of analytical, experimental, and field studies involving basic issues that are widely encountered in the field implementation of structural health monitoring (SHM) approaches based on vibration signature analysis. Specifically:

(1) an accurate signal processing procedure was developed and calibrated for obtaining accurate velocity and displacement time history records from corresponding acceleration records containing low-frequency components typically encountered in the response of extended civil structures such as long-span bridges;

(2) a study was conducted to develop, calibrate, implement and evaluate the feasibility of a novel vision-based approach for obtaining direct measurement of the absolute displacement time history at selected locations in dispersed civil infrastructure systems such as long-span bridges;

(3) a previously-developed time-domain system identification approach for obtaining reduced-order multi-input/multi-output models was applied to a large data set of acceleration measurements collected from the extensive instrumentation network installed at the Vincent Thomas Bridge in the Los

Angeles metropolitan region, through the use of a recently installed real-time

structural health monitoring system;

(4) and an investigation was performed with synthetic response data from a

refined finite element model of the Vincent Thomas Bridge to evaluate the

improvement in damage detection accuracy provided by the use of forced

excitations, of known magnitude, in conjunction with dimensionless

measures of the system's transfer function.

Results of the research indicate that while there are potentially powerful tools that

can be used to acquire, process, and analyze vibration response measurements from

dispersed civil structures such as bridges, the lack of sufficiently dense sensor spatial

resolution, coupled with the fact that significant analysis errors are introduced by

relying solely on ambient response measures (as opposed to forced vibration tests),

pose serious handicaps to the reliable implementation of the SHM. However, with

the increasing availability of dense sensor arrays, and the utilization of forced

vibration tests on target structures, more reliable structural health monitoring

strategies will likely evolve in the near future.

Chapter 1

Introduction

1.1 Motivation

In recent years the field of system identification of large structures has been an area of increasing interest in civil structures. There is an explosive growth in technical meetings, workshops and conferences addressing aspects of Structural Health Monitoring (SHM) and being held worldwide at an increasing frequency. This attests to both the importance and breadth of this field, as well as to the abundance of technical hurdles that await investigation and resolution before the full potential of this promising methodology can be exploited by maintenance personnel charged with assessing the condition of dispersed civil infrastructure systems such as bridges. The first international workshop focusing on the use of advance technology for nondestructive evaluation for the performance of civil structures was convened in 1987 under the auspices of the US National Science Foundation (Agbabian and Masri, 1988). Since then, numerous national and international meetings have been held to deal with various aspects of this broad, interdisciplinary field of Structural Health Monitoring (SHM). Information concerning some notable conferences, meetings and papers focusing on SHM are available in the publications of Agbabian et al (1987), Natke and Yao (1988), Housner and Masri (1990), Housner et al (1992), Housner and Masri (1993), Natke et al (1993), Szewezyk and Hajela (1994), Housner et al (1995), Chen (1996), Doebling et al (1996), Housner and Masri (1996),

1

Housner and Kobori (1996), Masri et al (1996), Audenino and Belingardi (1996), Housner et al (1997), Chang (1997), Casciati and Magonette (2000), Smyth et al (2000), Smyth and Masri (2001), Chang (2001), Casciati (2002), Wolfe at al (2002), Chang et al (2002), IABMAS (2002), ICANCEER (2002), and Chang (2003).

New technologies using system identification can assist in satisfying the need to effectively improve the long-term maintenance of critical transportation structures such as large bridges. A relatively new tool, vibration-based signature analysis through system identification, holds promise in identifying degradation or damage in a structure prior to serious consequences, and therefore could be part of a preventative maintenance program.

One of the main problems to be solved, among the numerous challenges to be overcome, is the accurate measurement of the time history of the three-dimensional deformations of complex structures such as flexible bridges, at many locations and orientations, in order to define the evolving (time varying) nature of the structural deformation field of the bridge and its sub-components (such as cable stays, etc). The following summarizes some of the historical development in the SHM field.

Structural Health Monitoring, in the context of a civil structure, is the use of vibration measurements (continuous or periodic) to characterize the global physical properties and to look for changes in these properties, which might indicate degradation or damage. For smaller structures, one can induce vibration through the

2

use of vibration generators; for larger structures, one must realistically rely upon existing ambient vibration from wind and traffic. SHM techniques also have practical applications in the automotive and aerospace industries where dimensions are smaller, operating lives are shorter, and products are of standard designs. Although there is much research on SHM in civil engineering, there are a few practical applications. Some applications to large transportation structures include Roberts et. al., (2000) performed a study to monitor the movement of the Humber Bridge, the third longest suspension bridge in the world, Farrar and Doebling (1999, 1997), Farrar et al (1997), Abdel-Ghaffar and Housner (1977), and Rainers and Selst (1976) performed dynamic analysis of the Loins' Gate suspension bridge in Canada.

System identification is accomplished through a systematic procedure to improve the mathematical model of the dynamic system of intend. In order to achieve such improvements, actual test data from the system is collected and analyzed. To have a relatively accurate model, the collected data, including acceleration response, velocity and displacement must be accurately obtained both in amplitude and phase. In most system identifications studies, only acceleration is measured and the velocity and displacement are then derived by integration. The measured and derived data are then used in obtaining the system properties and analyzing any changes the system might have observed.

3

1.2   Background

There are basically three broad types of identification methods: modal parameter, structural-model parameter, and control-model type. The first and second models are used in structural engineering, whereas the control model identification is used for control-type application, such as the active control of flexible structures.

Methods have been developed in the past decade for studying the active control of flexible structures in the aerospace field, and they are applicable to civil structures. Most of these methods involve similar proving steps consisting of modeling, systems identification, controller designs and verification tests. In both the aerospace and civil engineering fields the most commonly used method in modeling is the finite element method. The finite element model is a well-established method for providing a model useful for structural design analysis. The aerospace industry has adopted additional measures to develop more accurate methods for designing their structures. For instance, once the structure is built, both static and dynamic tests are usually performed in order to establish a mathematical model that characterizes the dynamics of the system. Then, the established mathematical model is used to calibrate the finite element model in order to obtain more accurate models. This type of procedure is referred to as a "closed-loop" system, which involves performing closed-loop dynamic tests. This system identification approach could be implemented in conjunction with civil engineering structures as well.

4

The major advantage of using system identification for modeling purposes is the improvement of the fidelity of the finite element model of the structure. It has been shown that finite element models of structures maybe incorrect by as much as 10% even in the low frequency range. These inaccuracies are attributed to several factors in finite element models, such as the approximations made in the discretization, mis-modeling of structural elements, differences in materials properties, inaccuracy of dimensions, and lack of convergence of the numerical model. Therefore, identified models from experimental measurements are more accurate than the finite element method in providing matches to observations, since the identification method is usually as low as 1% inaccurate in low frequency ranges.

In performing structural system identification, it is important to have a clear purpose of the identification task in mind. For example, in a design control strategy, the ultimate goal is to meet specific performance criteria. Therefore the identification task is to provide a model that will suffice for the input and output of the design. However, the main interest in model testing is to analyze the dynamic properties of the system such as stiffness, damping, frequencies, etc, in which the locations of the actuators are chosen to excite the structural modes of interest, while the location of the sensors measure the structural models of interest. It should always be kept in mind that the purpose of system identification dictates the identification process.

5

Basically there are six steps for performing system identification for complex structures. These steps are summarized as follows:

1. Develop an analytical model of the structure.

2. Establish the common structural dynamic response of the system based on the excitation source utilizing the analytical model.

3. Establish the instrumentation requirement that will provide the required accuracy and spatial resolution for the system.

4. Develop an experimental protocol and record the experimental data.

5. Apply suitable system identification techniques to identify specific characteristics of interest such as input/output relationship, degree of nonlinearity, etc. The system matrices and/or model parameters describe the characteristics of the structure.

6. Feedback the model and/or structure the results of the identified model to refine the analytical model and possibly redesign.

1.3   Research Objective

The objective of this research is to develop a broad foundation for integrating together innovative structural health monitoring and structural control concepts aimed at extending the life of civil structures, and accurately assessing the condition of a structure immediately after a hazardous event.

There is significant need for an accurate dynamic model for structures in the civil engineering field. Structural control monitoring and damage detection is currently an active research area. Significant amounts of research in damage detection and system identification work have been performed on structures subject to ambient excitation. Because most of these studies have been performed on relatively small highway overpass bridges and multi-story buildings, there is strong motivation to validate damage detection methods on a large-scale structure such as a long-span suspension bridge excited by multiple inputs during ambient vibration. This study poses several challenging issues for performing system identification where the structure input is of very small magnitude, and with measurements from a sensor array with low spatial resolution.

In this section, signature-based system identification will be explored not only with regard to dynamic response modeling capabilities, but also for its usefulness in damage detection. The effectiveness of the method is studied by analyzing actual experimental dynamic response data from a large-scale bridge and the finite element model of a large-scale-bridge.

The main objective of this research is to develop an optimized set of data analysis, which can be implemented in the field to monitor changes in the properties of large structures. In order to accomplish this goal, actual physical data were collected from a large structure; a bridge. In addition, synthetic data were generated from a complex, large-scale finite element model. The data was used to develop analytical

7

tools to facilitate vibration signature-based structural monitoring. The Vincent Thomas Bridge (VTB) was used as the test bed for this research, where a significant set of data has been collected over the past decade. In January 2003 a real-time monitoring system was installed at VTB, where data can be collected at any interval specified by the user. Data collected from the real-time system is acceleration data.

In order to perform a reliable parametric or non-parametric dynamic analysis of a structural system, the corresponding data must consist of accurate measurements. In most dynamic analyses the recordings of signals are primarily acceleration records, and therefore the velocity and displacement are obtained through integration of the obtained acceleration data. The degree of accuracy of the integrated data depends on several factors, such as the sampling rate, frequency content of the signal, the length of the record and the nature of the signal. In order to develop an accurate method of integrating acceleration data, one must establish a calibration method for such an algorithm. With the above mentioned in mind, a sequence of tasks was performed to develop, and calibrate needed data-processing algorithms, and subsequently use the aforementioned tasks to analyze a voluminous amount of data collected from the VTB.

Chapter 2 of this study demonstrated a detailed integration algorithm calibration. The integration algorithm calibration was developed to obtain velocity and displacement from acceleration data. The algorithm was then validated by utilizing a finite element method and actual laboratory data. Then the algorithm was validated

8

with both, acceleration and optical field data collected from the Vincent Thomas Bridge, as well as ambient vibration measurements. Chapter 3 of this study focused on further evaluation of the integration algorithm and utilizing the availability of high-performance vision-based system to develop a monitoring system serving a dual purpose; first to enhanced surveillance capabilities, and high-fidelity monitoring of complex deformation of field measuring deformation at selectable locations and orientations. The other goal of this study was demonstrated in Chapter 4, using the real-time monitoring system that was installed on the Vincent Thomas Bridge, the synthetic data to validate the reduced multi-degree-of-freedom (MDOF) model, and to determine the optimum location and number of sensors needed on a large-structure via this specific system identification tool. Chapter 5 explored the use of another identification technique, the transfer function techniques on bridge-like structure. Finally Chapter 6 presented the conclusions of this research, and further studies recommendations.

Chapter 2

Integration Algorithm Development and Validation

2.1 Introduction

In order to perform a reliable dynamic analysis of a structural system on the basis of experimental measurements, the corresponding data must consist of accurate measurements. In most dynamic analyses the recorded signals are primarily acceleration records, and therefore the velocity and displacement are obtained through integration from the obtained acceleration data. The degree of accuracy of the integrated data depends on several factors such as the sampling rate, frequency content of the signal, the length of the record and the nature of the signal.

Furthermore, while in principle one can determine the time history of the displacements by double-integrating the corresponding acceleration, careful studies have clearly established that there are some major pitfalls in various signal processing approaches that can cause significant distortion in the extracted time histories of the estimated displacements. Detailed discussions of some of these problems are documented in the work of Worden (1990) and the work of Smyth and Pei (2000). Consequently, it is essential to develop and calibrate robust procedures for processing acceleration measurements in order to obtain accurate displacement signal.

2.2 Procedure for Obtaining Accurate Displacement Time Histories from Acceleration Measurements

In order to perform a reliable dynamic analysis of a structural system, the corresponding data must consist of accurate measurements. In most dynamic analysis the recordings of signals are primarily acceleration records, and therefore the velocity and displacement are obtained indirectly through integration of the corresponding acceleration records.

To clarify the discussion, consider the basic form of the velocity and displacement measurements after integrating the corresponding acceleration:

$$\dot{x} = \int \ddot{x} dt + c \tag{2.1}$$

$$x = \int \dot{x} dt + ct + d \tag{2.2}$$

It is obvious from basic physics that, for accurate determination of the velocity and displacement signals that are obtained through integration of the corresponding acceleration signals, knowledge of the initial velocity (v_0) and initial displacement (d_0) at the start of the integration interval is needed. The absence of information about the constants c and d appearing in the equations above can lead to severe distortion in the integrated records. Further details about the serious challenges that result from naïve application of the above-listed equations to obtain through integration velocities and displacements from acceleration signals are discussed in the work of Smyth and Pei (2000).

11

In the above mentioned equations, c is a spurious mean level that becomes the linear ramp function in the estimated displacement. This spurious mean level can be removed through mean removal and data de-trending. In theory, if the initial conditions at both x and $\dot{x}$ are zero, then the integration constants c and d will be zero. However in the real world the spurious low frequency error still exists within the integrated signals even after removing the mean and de-trending.

The most common method for obtaining velocities and displacements through integration of acceleration records involves filtering the low-frequency content from the data in order to reduce the effects of (usually) unimportant low-frequency components. However, this operation has to be done with care so as not to filter out significant low frequency components which become more important as the structure becomes larger and more dispersed. This is precisely the situation that is encountered in the monitoring of long-span flexible bridges.

2.3   Integration Algorithm

2.3.1   Background

There are several time-domain recursive integration techniques available for integrating time-domain data. The Trapezoidal method is the one utilized in this study. The method can be summarized in the following equation:

12

$$v_i = v_{i-1} + \frac{\Delta t}{2}(\alpha_{i-1} - \alpha_i) \qquad (2.3)$$

$$d_i = d_{i-1} + \frac{\Delta t}{2}(v_{i-1} - v_i) \qquad (2.4)$$

One can not avoid some sort of noise in digitized acceleration data either from resolution error such as truncation, or from background electrical noise in the data acquisition circuitry. The presence of this low- frequency noise is significantly amplified through integration. Low-frequency spectral content is very critical in civil engineering structures. Thus, this type of magnification disturbances could cause a significant complication in data analysis, and system identification procedures for these structures.

2.3.2 Algorithm Development

The integration algorithm utilizes the trapezoidal integration technique. Usually the input is a time series of acceleration data, either recorded by instrument or a synthetic data generated from a mathematical model. The acceleration data needs to be integrated once to get velocity and once again to obtain displacement.

In order to reduce the errors in the integration procedure due to the missing information concerning the initial conditions, the algorithm whose flowchart is shown in Figure 2.1 was developed and successfully applied here to obtain fairly accurate estimates of the integrated velocities and displacements. An important

13

requirement for accurate data processing is that the acceleration record duration be much longer than the longest characteristic period of interest. As can be seen from Figure 2.1, the main steps in the algorithm are a two-level sequence of band-pass filtering, integration, and de-trending.

```
┌─────────────────────┐
│    Integration      │
│    Algorithm        │
└─────────────────────┘
           │
           ▼
╭─────────────────────────────────────╮
│  Data Record whose length $t_{max}$  │
│  $\gg T_1$, with $dt \ll T_1$, where $T_1$ is │
│  the fundamental period of the       │
╰─────────────────────────────────────╯
           │
           ▼
┌──┬────────────────────┬──┐        ┌──┬────────────────────┬──┐
│  │ Band-pass filter the│  │        │  │ Integrate the acceleration│  │
│  │ acceleration record │  │───────▶│  │ once to obtain the  │  │
│  │ between 0.05 – 30   │  │        │  │ corresponding velocity│  │
└──┴────────────────────┴──┘        └──┴────────────────────┴──┘
                                                   │
                                                   ▼
┌──┬────────────────────┬──┐        ┌──┬────────────────────┬──┐
│  │ Integrate the velocity once│  │        │  │ Band-pass filter the│  │
│  │ to obtain the corresponding│  │◀───────│  │ velocity record between│  │
│  │ displacement record.│  │        │  │ 0.05 – 30 Hz.       │  │
└──┴────────────────────┴──┘        └──┴────────────────────┴──┘
```

Figure 2.1: Flowchart of the integration algorithm structure.

2.4   Algorithm Verification

2.4.1   Finite Element Verification

In order to evaluate the integration approach developed in this study, a finite element model was developed to generate synthetic data utilizing the NASTRAN program.

14

To add realism to the simulation, and in order to generate relatively noise-free data and noisy data, two separate finite element models were analyzed. The first model was a three-degree of freedom system with equal stiffness, masses and damping of two percent (2%). The second analysis was performed on a four-mass system with the fourth mass acting as a high frequency oscillator, since the force was applied at the third mass. Figure 2.1 (a, b) shows the schematic for these two systems.

(a)   (b)
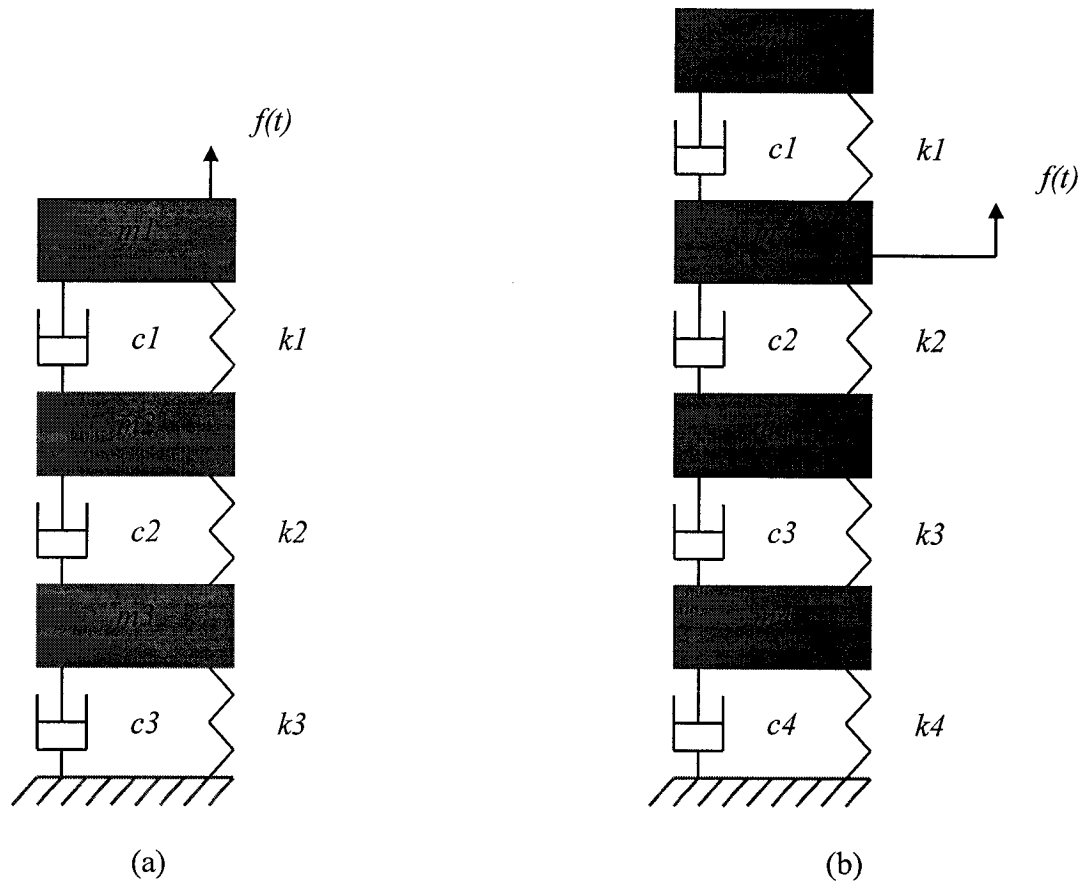
Figure 2.2: (a) Three-mass system, (b) four-mass System.

It was assumed that the masses equal one unit, while the stiffness was calculated from the modal analysis of the system utilizing the NASTRAN program. Based on

15

these eigenvalues, each of the stiffness coefficients, k, was calculated to be 1216 lb/in for the three-mass system and 1427 lb/in for the four-mass system. A two percent damping was utilized in order to realistic oscillation. The damping coefficient, c, was calculated to be 1.395 for the three-mass system and 35.530 for the four-mass system. The time history input file is the excitation force function, $f(t)$, applied at locations shown in above Figure 2.2. The following section describes the signal processing of this input function.

2.4.1.1 Data Input File Generation (Time History)

In order to run the finite element method, a time history file needed to be generated for the input. The following summarizes the steps used to generate the input time history file:

- Time step at 0.005 ($\Delta t = 0.005$) which is equivalent to 200 Hz frequency.

- Number of samples: 200 samples per second.

- Nyquist frequency of 100 Hz.

- Numbers stored in array of 200,000 samples.

- A forward FFT was performed (time to frequency domain).

- The FFT was truncated by removing frequencies higher than 30 Hz.

- An inverse FFT was performed.

- Finally, the DC component was removed (de-meaned) and data was stored in NASTRAN table form.

16

Figures 2.3 through 2.7 highlight steps of the generation of the time history discussed above.
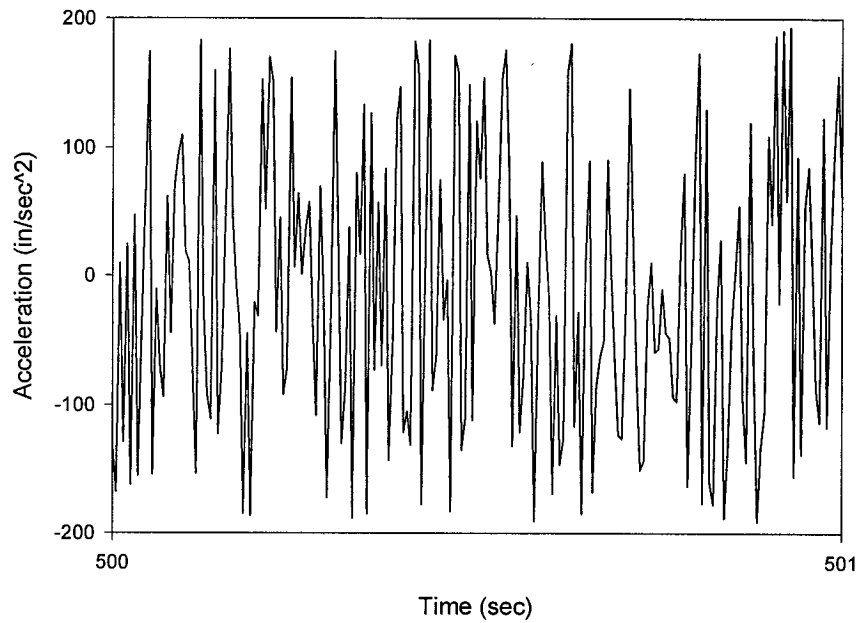
Figure 2.3: Close-up of random loading number.
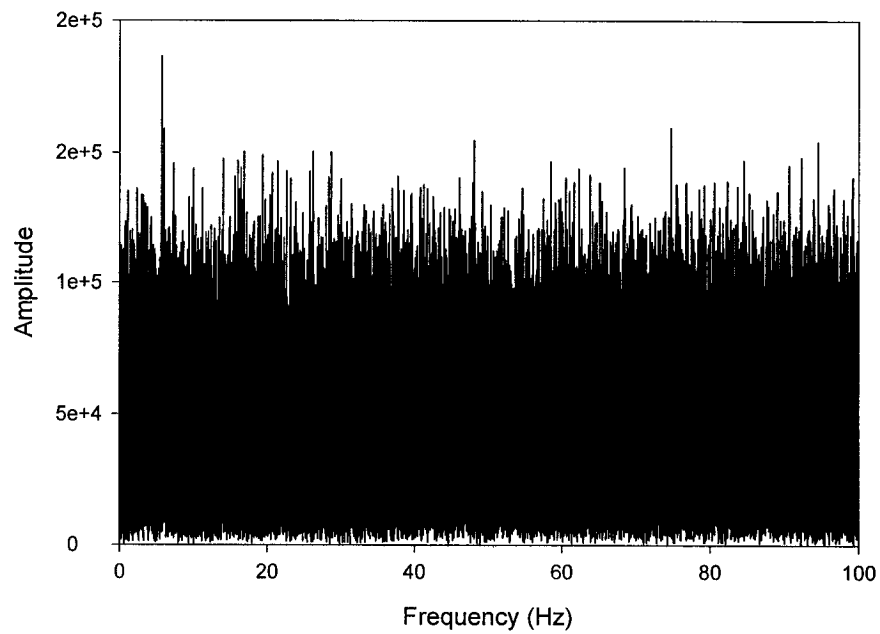
Figure 2.4: Time history after forward FFT and before high frequency truncation.

17
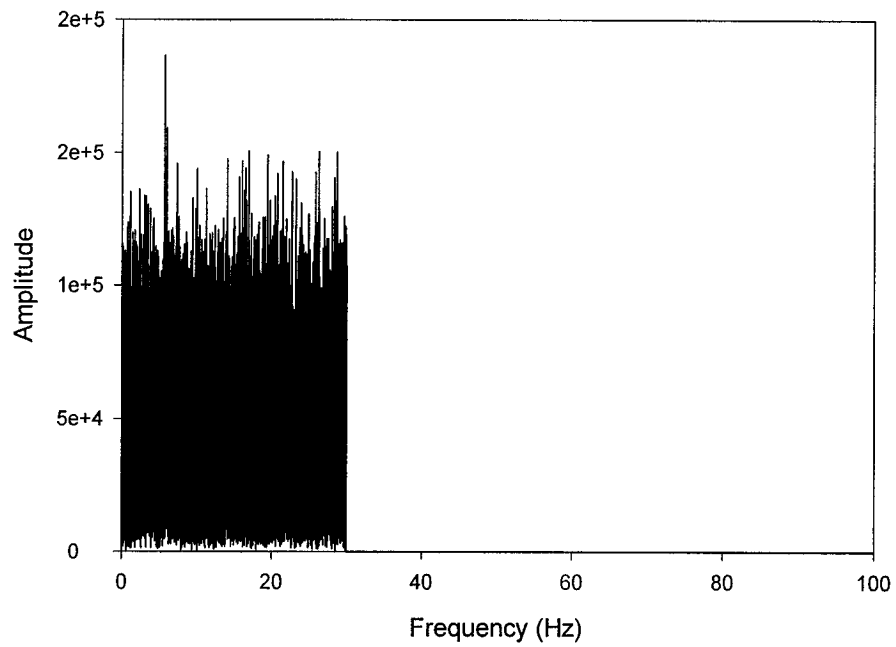
Figure 2.5: Time history after FFT and 30Hz truncation.
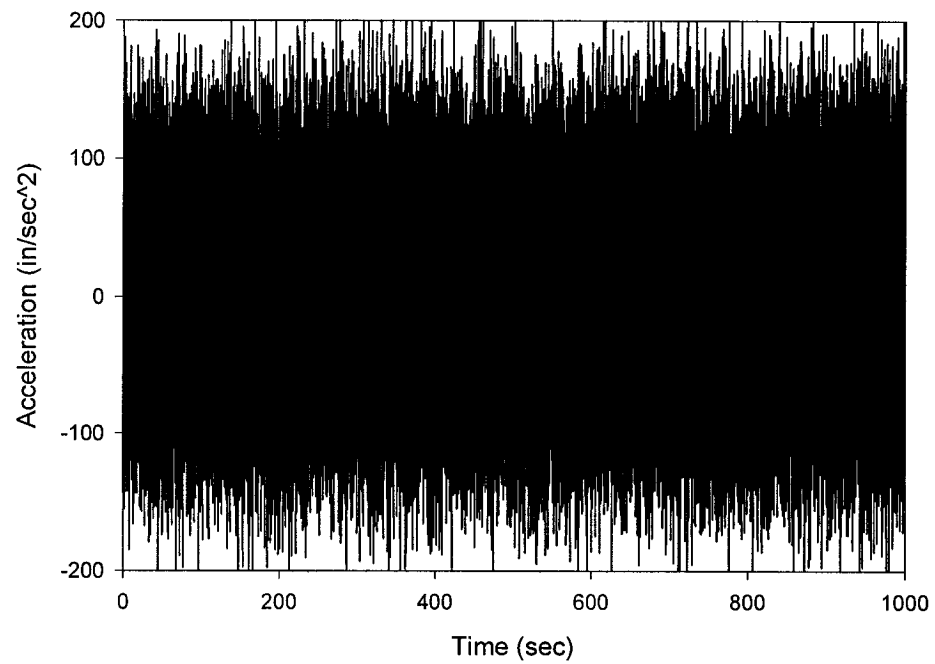
Figure 2.6: NASTRAN time history input file.

18
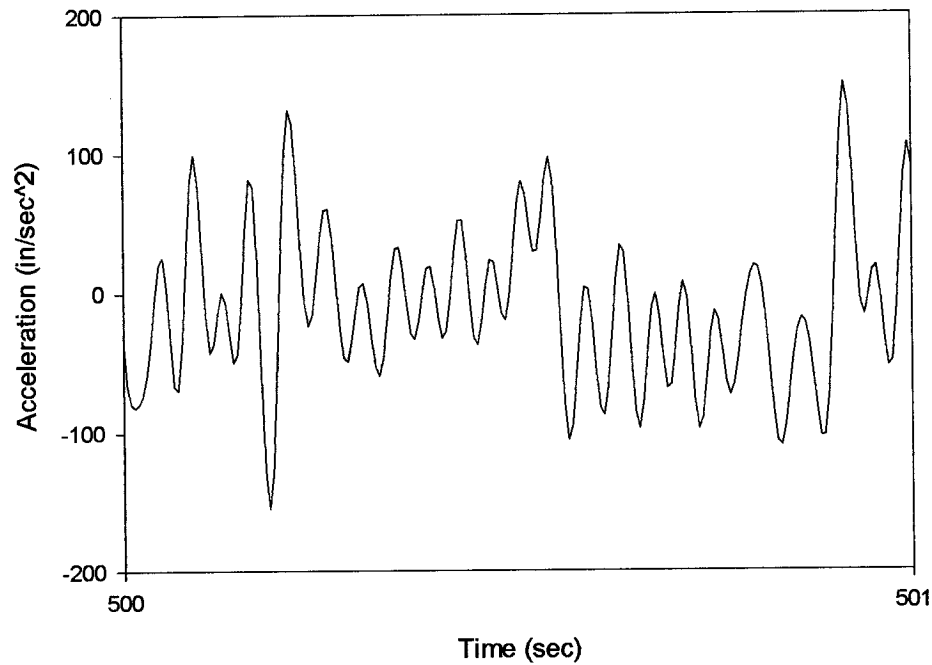
Figure 2.7: Close-up of time history after FFT filtering.

2.4.2 NASTRAN Model Output

Based on the input file and the identified properties of each system, NASTRAN

calculates the corresponding acceleration, velocity and displacement of the two

systems. The finite element program NASTRAN utilizes a direct integration

method, which is essentially a central difference approximation for all output. The

next step of the verification analysis was to obtain the acceleration, velocity and

displacement from the NASTRAN model for both structural systems, and then

compare them with the integrated acceleration data of the NASTRAN output. The

following figure shows the output for both the three-mass system and the four-mass

system.

19
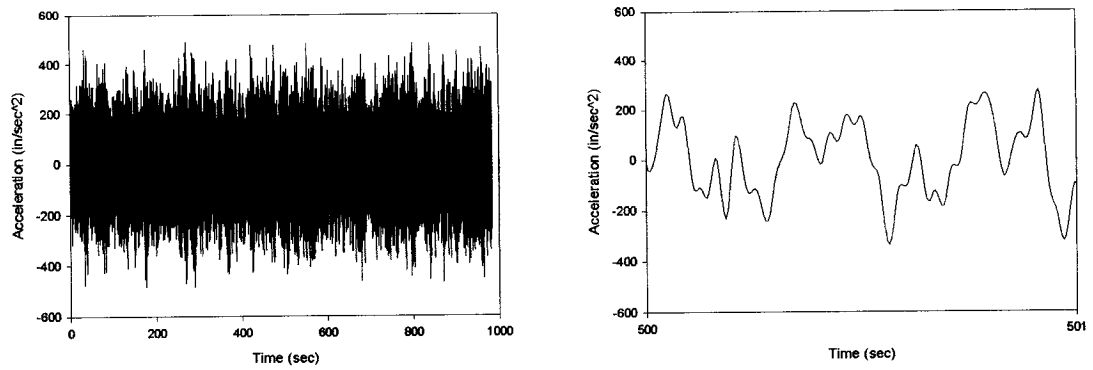
Figure 2.8: Acceleration output of the three-mass system and close-up.
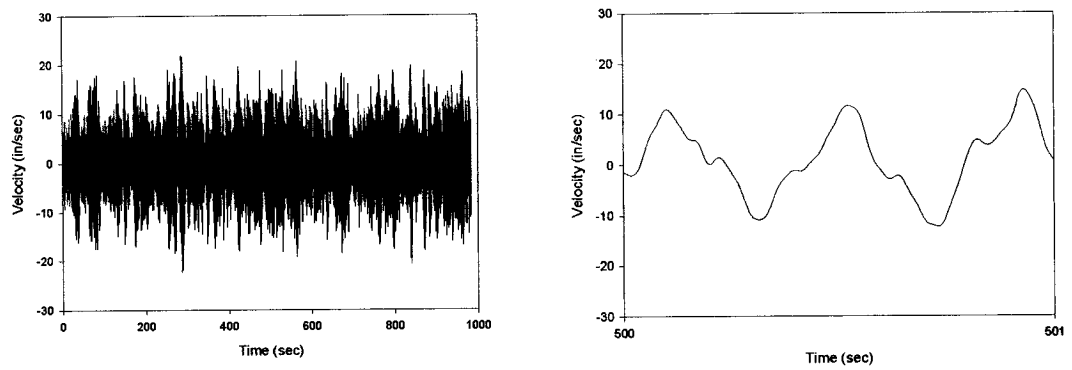
Figure 2.9: Velocity output of the three-mass system and close-up.
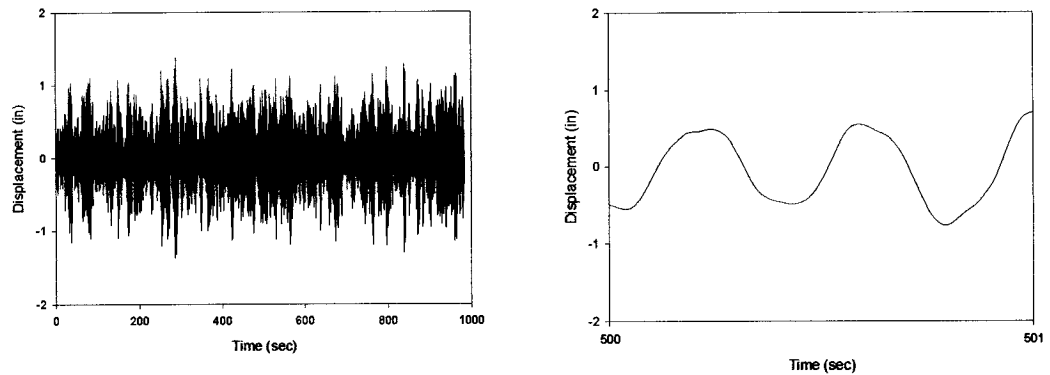
Figure 2.10: Displacement output of the three-mass system and close-up.

20
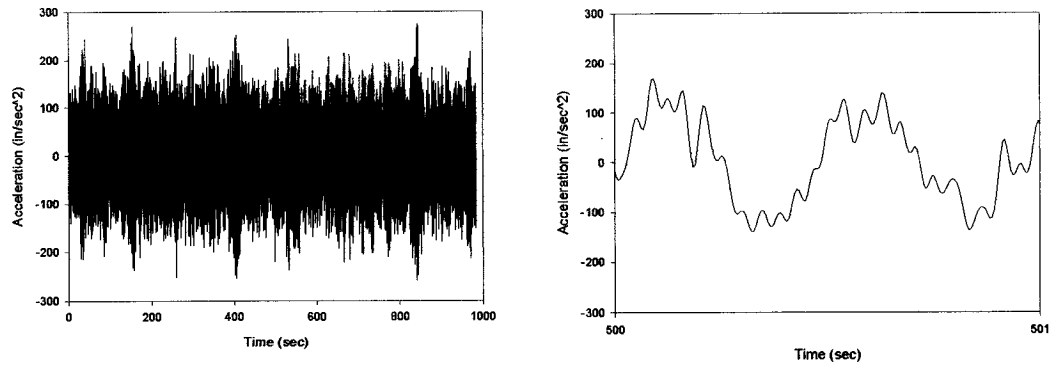
Figure 2.11: Acceleration output of the four-mass system with close-up.
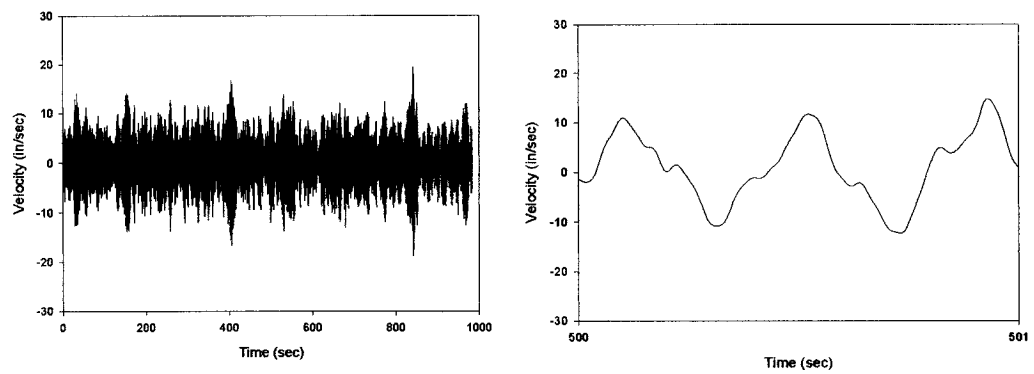
Figure 2.12: Velocity output of the four-mass system and close-up.
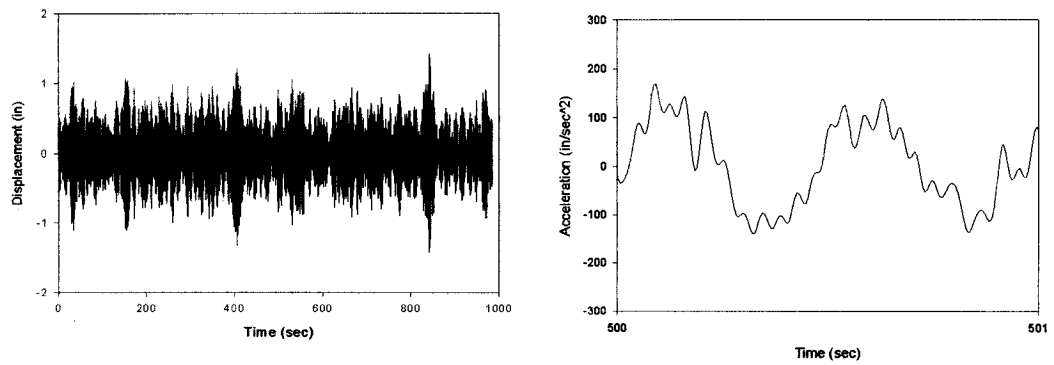
Figure 2.13: Displacement output of the four-mass system and close-up.

The next figures show the output comparison between the Finite Element Models

and the integration algorithm. Only close-ups segments are presented in order to

illustrate the good accuracy of the integration algorithm.

21
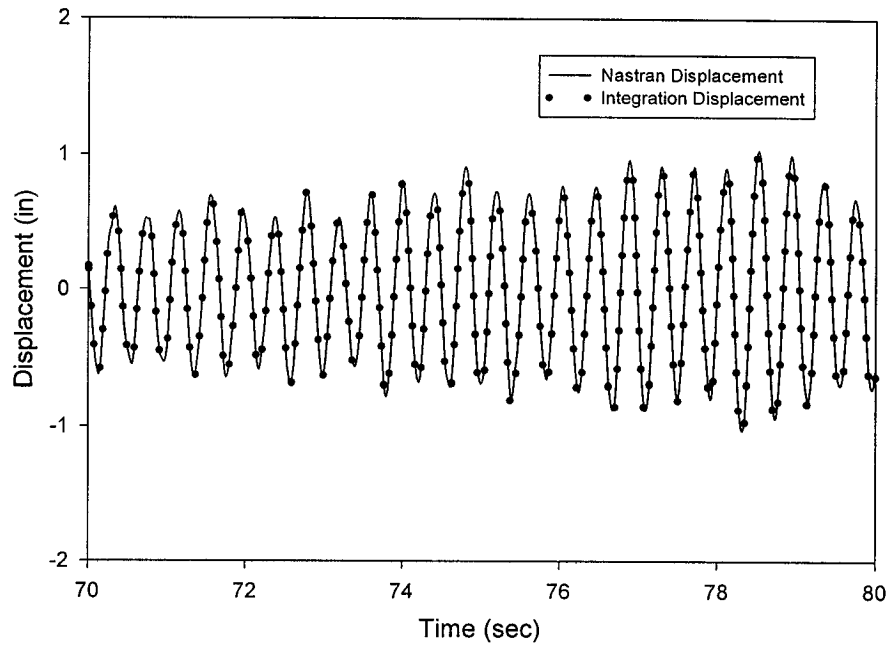
Figure 2.14: Close-up comparison of the output of the double-integration of acceleration data (displacement) versus output of the FEM for the 3-mass system.
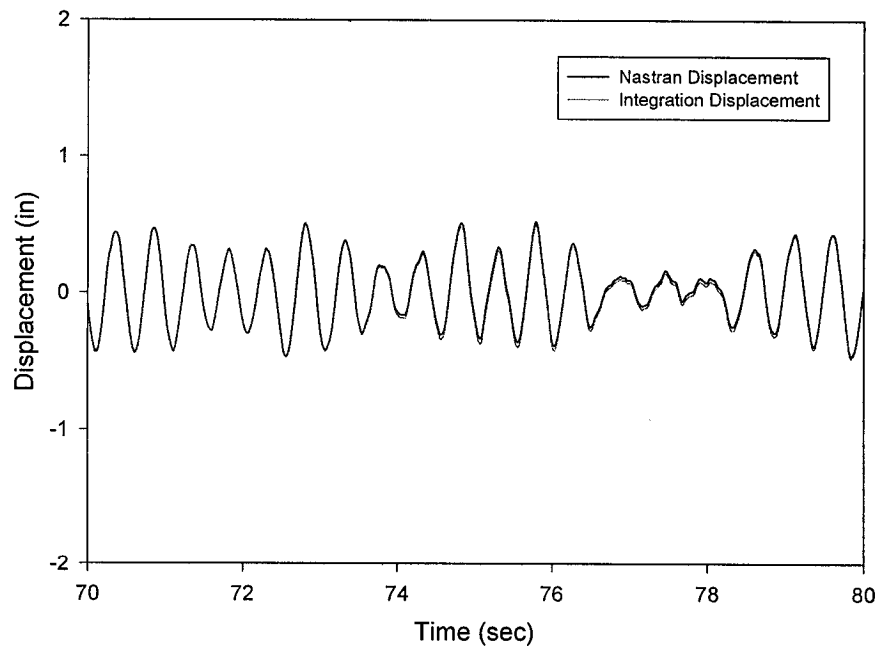
Figure 2.15: Close-up comparison output of double-integration of acceleration data (displacement) versus output of the FEM for the 4-mass system.

22

2.5 Laboratory Calibration of Integration Method

2.5.1 Introduction

The main objective of the following analysis is to validate the accuracy of the integration algorithm, and compare it to the output of a commonly used instrument, the Kinemetrics K-2, which was used in the data collection for the forced and ambient motions. The integrated acceleration will be compared to the corresponding measured displacement.

For a more realistic calibration study of the integration algorithm under discussion, a broad-band force-balance-accelerometer with a wide dynamic range was used to obtain acceleration measurements on a shaking table. A photograph of the sensor (K-2 accelerometer made by Kinemetrics) is shown in Figure 2.16. The K-2 utilizes 19-bits of resolution and a high dynamic range of 110 db. The internal sensor is an EpiSensor, a force-balance-accelerometer. Some of its important features are its low noise, and extended bandwidth from DC to 200Hz. The K-2 unit consists of three EpiSensor force-balance-accelerometer modules mounted orthogonally, with full scale recording ranges from +/- 0.25 to +/- 4 g as shown in Figure 2.17. It samples acceleration measurements at the rate of 200 Hz; hence, the data has a Nyquist frequency of 100 Hz, well beyond the 30 Hz cutoff frequency of interest in civil structures.

23
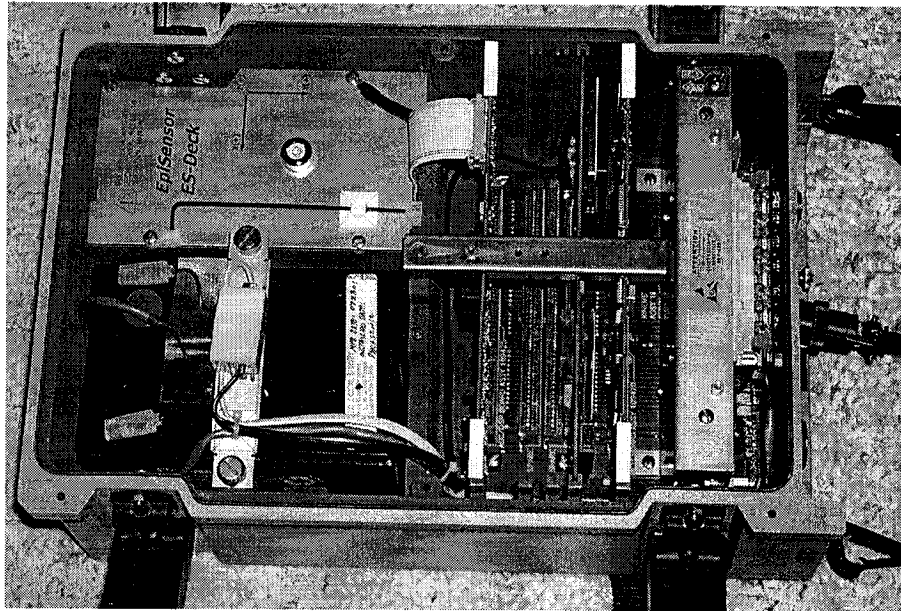
Figure 2.16: Photograph of K-2 instrument.
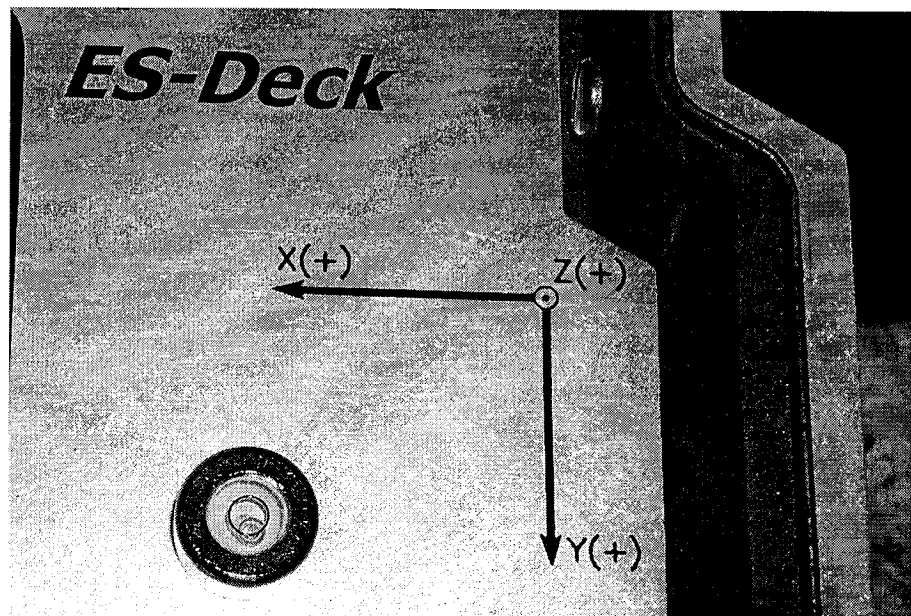
Figure 2.17: Close-up picture of the internal accelerometer of the K-2.

24

2.6   Data Acquisition

The K-2 device records the data on an internal PC card. The data is then transferred

to ASCII format. All data collected was in volts and had to be converted to

acceleration. The test set-up consisted of mounting the K-2 device on the University

of Southern California (USC) shake table as shown in the following figure.
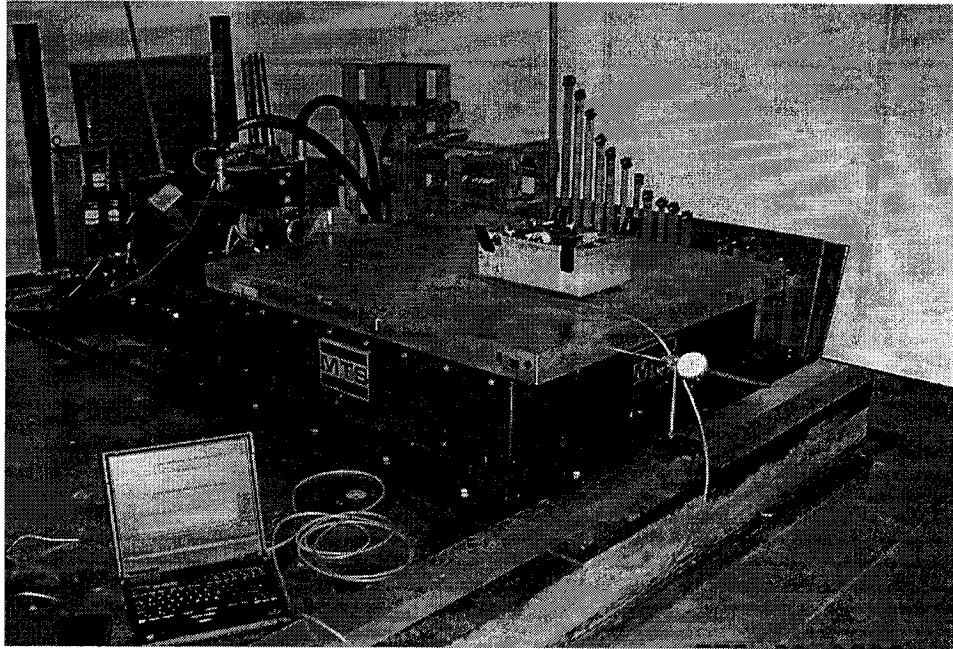
Figure 2.18: Calibration test set-up at the USC large shake table.

The test parameters were carefully determined prior to performing this study. The

following table shows the description of these tests:

25

Test Number	Frequency (Hz)	Disp. (in.) (+/-)	Sample Rate (sps)	Duration of Test (min.)
1	0.1	0.75	100	15
2	0.1	0.75	200	15
3	0.24	0.75	100	15
4	0.24	0.75	200	30
5	0.5	0.75	200	30
6	0.7	0.75	200	30

Table 2.1: Test set ups

2.7 Data Reduction

The recorded data from the K-2 was stored in an EVT proprietary compressed format. The K-2 data was converted to digital computer format by software provided by Kinemetrics. The digitization rate was at a rate of 100 and 200 equally spaced points per second, which resulted in a Nyquist frequency of 50 and 100 Hz respectively, which is well above the lowest frequencies being considered. The length of the records ranged from 900 seconds to 1800 seconds.

The integration algorithm was performed on all collected sets of data. This calibration method showed that the K-2 instrument was 100 percent accurate in relation to displacement.

26

2.8   Conclusion

This detailed study demonstrated both the validity of the integration algorithm and the accuracy of the measuring devices. The double integrated K-2 device acceleration data (displacement) resulted in excellent accuracy as compared to the linear variable-differential transformers (LVDT) measured displacement of +/- 0.75 inch from the shake table. A comparison of the measured shaker displacement obtained by means of LVDTs and the doubly-integrated acceleration record is shown in Figure 2.19. This again demonstrates the excellent accuracy of the integration algorithm under discussion.

Comparison of K-2 vs. LVDT
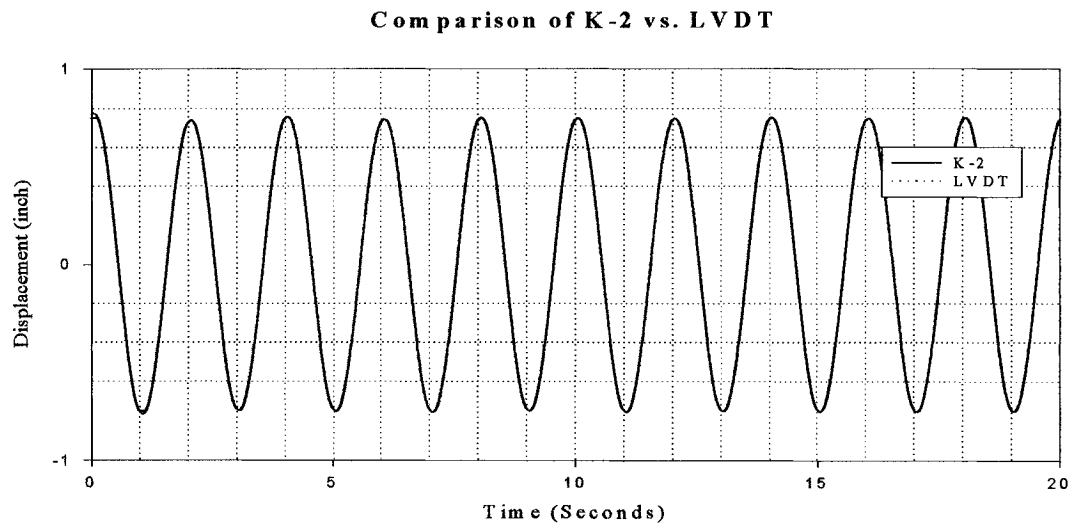
Figure 2.19: Comparison between the shaker table LVDT and integrated acceleration data from the K-2 instrument.

Chapter 3

A Vision-Based Approach for the Direct Measurement of Displacements in Vibrating Systems

3.1 Introduction

One of the main problems to be resolved, among the numerous practical issues in the field of SHM to be overcome, is the accurate measurement of the time history of the three-dimensional deformations of complex structures, such as flexible bridges, at many locations and orientations, in order to define the evolving (time varying) nature of the structural deformation field of the bridge and its sub-components (such as cable stays, etc). The increasing availability of high-performance vision-based systems, at affordable cost, provides the potential for developing an adaptable/re-configurable monitoring systems that serve a dual purpose: enhanced surveillance capabilities and high-fidelity monitoring of complex deformation field measured at selectable locations and orientations (Wahbeh et al, 2003).

The benefit of collecting ambient vibration data for determining the response of a large civil infrastructure is that this information can then be easily utilized in determining changes or damage which might occur to the structure, and hence improve the maintenance options. The ambient response data becomes the basis for an analysis of the performance of the structure via several system identification

28

methods. Methods of determining the displacement optically may be utilized either as a verification method or for direct measurements for further system identification techniques.

Structural response information due to the effects of dynamic loads on dispersed civil infrastructure systems is vital to accurately evaluating the structural integrity of such systems. Conventional monitoring instruments such as accelerometers, LVDTs, and global positioning systems (GPS) have various practical limitations in obtaining accurate data from the three-dimensional motions at many locations. However, vision-based methods have demonstrated promising results in both laboratory and field experiments. Vision-based approaches offer the potential of both high spatial and temporal resolution.

Notable contributions to research in the field of vision-based sensors include the work of Fraser and Riedel (1995), Olaszek (1999), and Woodhouse et al (1999), Fraser and Riedel (2000),who have demonstrated some of the capabilities of vision-based method in structural monitoring.

3.1.1 GPS-Based Monitoring Issues

Another method that holds promise in structural monitoring is the GPS. This method has also been the focus of research, including the monitoring of structural deformation at Pacoima Dam, California using continuous GPS (Behr et al, 1998,

Celebi 1999). Nakamura (2000) performed a study utilizing Global Positioning System (GPS) to measure displacement in a suspension bridge due to wind induced excitation. Roberts and Dodson (1998) performed a study to monitor the movement of the Humber Bridge, the third longest suspension bridge in the world. Hyzak et al (1997), Teague et al (1995) and Celebi and Sandli (2002) all studied the effects of utilizing GPS for measuring displacement on structures.

However the use of GPS to track displacements of dispersed civil infrastructures such as bridges has some limitations. The main concept behind GPS lies in computing the distance between the satellite and its receivers. Most of the published studies of GPS have shown that it has an accuracy of about +/- 1cm in the horizontal direction and +/- 2 cm in the vertical direction. The cost of high-accuracy and high sampling rate GPS-based tracking is significantly more than vision-based approaches. In addition it has been shown in a field study by Wieser and Brunner (2002), that GPS is not practical for measuring bridge deck movement due to the multi-passing and diffraction effects associated with cables, which could result in several centimeters of variance. It is also known that multi-path issues are the major source of error in GPS, and significant research is being focused on this area. Another area of limitation in GPS capability studied in the context of bridges is the effect of atmospheric phenomena. Research in this area has shown that, if the residual tropospheric delay is not properly modeled, it could introduce several centimeters of positioning error. Atmospheric effects, such as ionospheric delay, are the main impact factors when single frequency GPS receivers are used. Work on fast

30

integer ambiguity resolution is still in progress to further improve the accuracy and resolution of this method (Roberts and Dodson, 1998). Also it was noted that the visibility and geometry of the satellite constellation during the observation periods has a negative influence on the quality of measurements. This is a major concern regarding the use of GPS if the sky view of the sensors is obstructed by tall buildings, trees, or mountainous terrain (Knecht and Manetti, 2001).

3.1.2 Challenges in the Integration of Acceleration Signals

Furthermore, while in principle one can determine the time history of the displacements by double-integrating the corresponding accelerations (which can be conveniently measured by conventional accelerometers), careful studies have clearly established that there are some major pitfalls in various digital signal processing approaches that can cause significant distortion in the extracted time histories of the estimated displacements. Detailed discussions of some of these problems are documented in the work of Worden (1990) and the work of Smyth and Pei (2001). Consequently, it is essential to develop and calibrate robust procedures for processing acceleration measurements in order to obtain accurate displacement signals.

3.1.3 Objectives

The goal of this study was to evaluate the feasibility and determine practical implementation issues related to the deployment of a vision-based sensor system for

31

the direct measurement of displacement time histories of selected locations on a bridge undergoing ambient oscillations. Also investigated was a related issue concerning the development and evaluation of a protocol for processing acceleration measurements, containing very low frequency components typically encountered in dispersed civil infrastructure systems, to yield sufficiently accurate displacement data.

3.1.4 Scope

Section 3.2 deals with the architecture of the instrumentation system, Section 3.3 discusses the development and calibration of the integration procedure with synthetic data as well as laboratory measurements, and Section 3.4 presents the application of the optical measurement system, as well as the integration algorithm, to field measurements obtained from the Vincent Thomas Bridge in the metropolitan Los Angeles region. The advantages and limitations of the proposed system architecture are discussed in Section 3.5.

3.2   Optical Instrumentation System Architecture

A schematic diagram of the target bridge with the optical instrumentation mounted on it is shown in Figure 3.1. The general view shows the camera located at one of the bridge columns, while the optical target is located near the mid span of the bridge.

32

The detailed view shows that the two targets were placed under the bridge deck, and were attached to some of the support trusses.
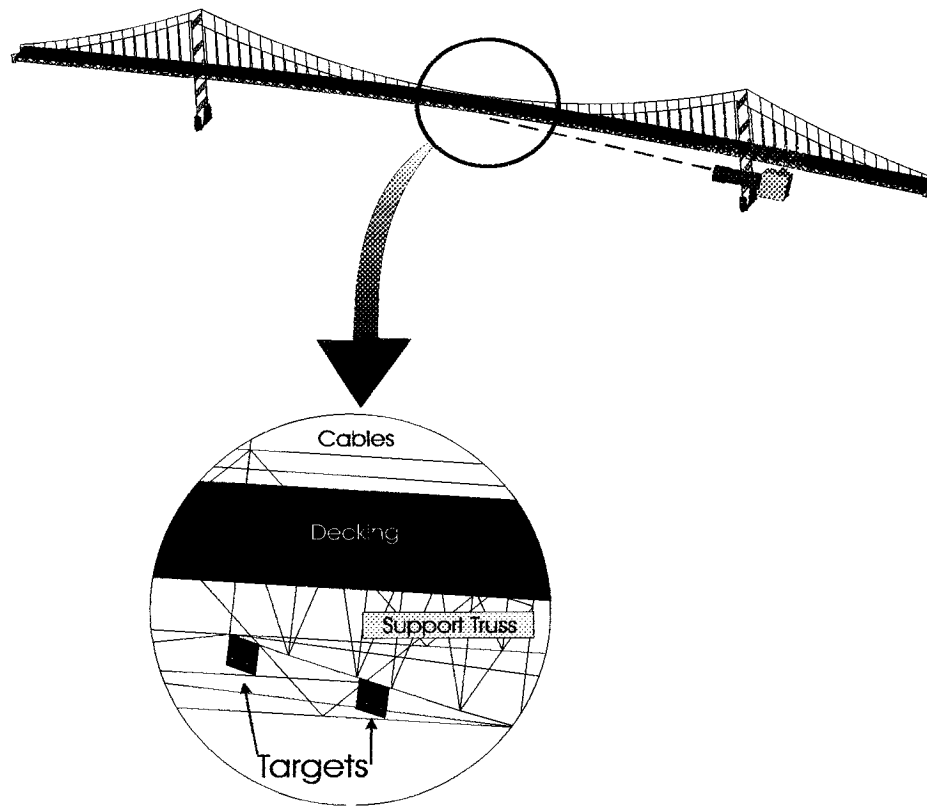
Figure 3.1: Schematic view of the test bridge optical instrumentation system.

The high fidelity video camera had a resolution of 520 lines and a capability of 450 digital zoom. The targets consisted of high-resolution low-power light-emitting-diodes (LED). Each target consisted of two LED's, spaced at a known distance, in order to calibrate the movement of the target. Both lights were lit for fifteen seconds at the beginning of the experiment, after which one light was left on for the remainder of the time. A schematic view of these lights is shown in Figure 3.2.

33
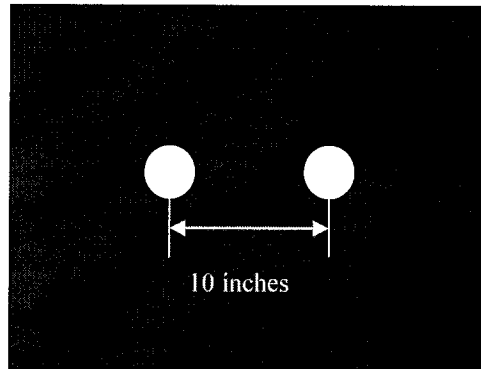
Figure 3.2: Schematic view of optical targets and placement of LED's on test bridge.

3.3 Field Measurements from Vincent Thomas Bridge

The Vincent Thomas Bridge is located in San Pedro, California, and is a major transportation artery connecting Los Angeles with its harbor. It is a cable-suspension bridge, approximately 1850 m long, consisting of a main span of approximately 457 m, two suspended side spans of 154 m each, and a ten-span approach of approximately 545m length on either end. The roadway accommodates four lanes of traffic. The bridge was completed in 1964, and in 1980 was instrumented with twenty-six accelerometers as part of a seismic upgrading project.

Currently, the sensor network is maintained by the State of California Department of Conservation (CDC), Office of Strong Motion Studies through California Strong Motion Instrumentation Program (CSMIP). Figure 3.3 shows the layout of the location of all 26 sensors mounted on the bridge. Notice that the eastern half of the bridge is more densely instrumented. This is because the analog recorder is housed in the eastern cable anchorage. Sixteen accelerometers are distributed at various

34

locations and in lateral, longitudinal and vertical directions about the superstructure itself.
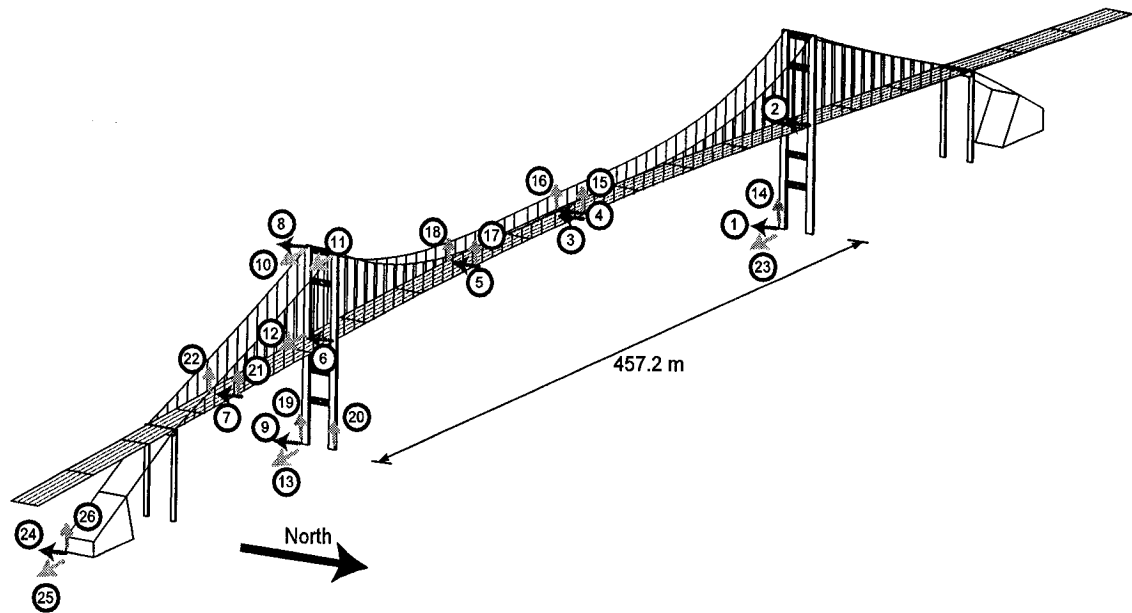
Figure 3.3: VTB sensor locations.

As part of the seismic retrofit program, the California Department of Transportation installed 36 large passive viscous dampers to mitigate the relative motion under strong shaking of the bridge roadway with respect to its piers. Since the condition assessment of these essential dampers is crucial to the safe operation of the bridge, it is necessary to accurately measure the time history of the relative displacement across the terminals of the dampers.

35

3.3.1 Optical Instrumentation

The high resolution digital camera discussed in Section 3.2 was mounted firmly at the center of the VTB west tower strut. Target frames were carefully designed in order to capture the motion of the target without influence from surrounding light noises. The targets consisted of black steel sheets 28 inches high by 32 inches wide, and two high-resolution red lights (LED) were mounted on these targets. Figure 3.4 shows the configuration of these targets.
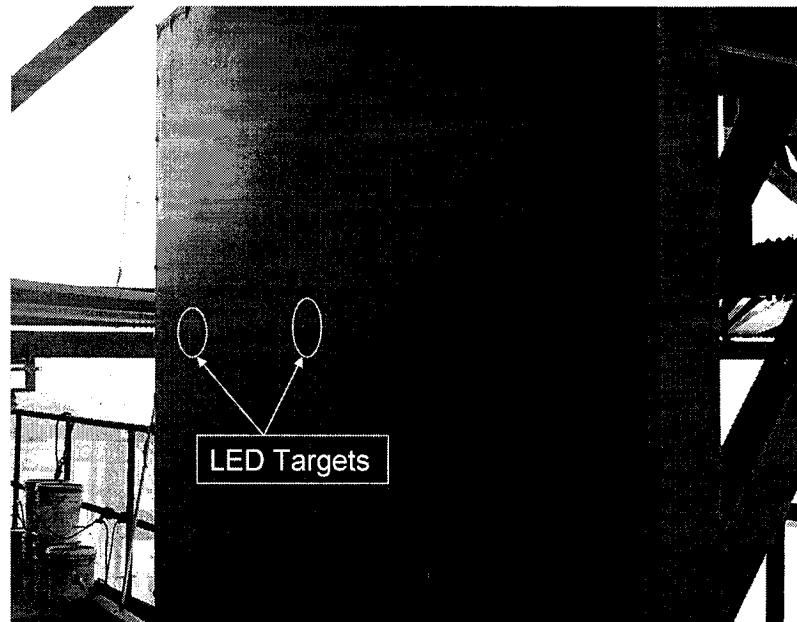
Figure 3.4: Close-up of targets used in the optical calibration study.

3.3.2 Optical Data Reduction

Optical data was transferred digitally to a PC at a rate of 30 frames per second. In order to determine the motion of the bridge, a software program was developed to

36

track the motion of each picture frame. The program consists of outlining the orbit of the red light and filtering the other colors with respect to red, in order to obtain the highest intensity of the red spot. The following details the data reduction algorithm.

The entire optically recorded data of 30 minutes was transferred to bitmap files by reading each frame into a separate file. Then each bitmap file was converted into a matrix A_{ij}, where i and j represent the horizontal and vertical pixel intensity of the file. A color mask was then applied to filter all non-red components of the light intensity. The A_{ij}'s are integers having a value ranging from 0- 255 representing the intensity of the resulting filtered intensity map. The area of interest, the center of the red spot for the first frame, was then identified by obtaining the highest value of A_{ij}'s, and a "bounding matrix" [B] was obtained, while ignoring the intensity terms of the surrounding sub-matrices [S]. The following equation represents the matrices selection:

$$[A] = \begin{pmatrix} [S_{11}] & [S_{12}] & [S_{13}] \\ [S_{21}] & [B] & [S_{23}] \\ [S_{31}] & [S_{32}] & [S_{33}] \end{pmatrix}$$
(3.1)

Since the camera used did not have a sufficiently high resolution, some of the recorded bitmap files contained what is known as fallouts of pixels in the video frame, where some elements of the bitmap file matrix [B] might have a significantly high readings. The following algorithm was applied in order to remove these pixel fallouts from the entire record.

37

$$\text{If} \qquad \left[B_{(i-1,j)}\right] \geq Il_{cutoff} \text{ and } \left[B_{(i+1,j)}\right] \geq Il_{cutoff} \qquad (3.2)$$

$$\text{then}$$

$$\left[B_{(i,j)}\right] = \frac{\left(\left[B_{(i-1,j)}\right] + \left[B_{(i+1,j)}\right]\right)}{2}$$

where: Il_{cutoff} is the specified lower cutoff parameter.

The next step was to compute the sub-matrix C_{ij} which included the nonzero components of A_{ij}, and apply a bounding frame of 25 x 25 pixels on the C_{ij}, zeroing the rest of the terms, and extracting the [C] matrix for further processing. This may be shown in matrix form as follows:

$$[B] = \begin{pmatrix} [0] & [0] & [0] \\ [0] & [C] & [0] \\ [0] & [0] & [0] \end{pmatrix} \qquad (3.3)$$

The above mentioned process was performed for the entire record including the calibration frames where two LED lights were lit; this was used in order to correlate the pixel number with the known distance between the two centers of the LED's and hence calibrating the movement of the target LED by developing a scaling factor to correlate the physical distance to pixel counts.

The next step was to perform a nonlinear Gaussian regression curve fit, in accordance with the following equation, which was subsequently utilized to determine the center of the high intensity red spot:

$$f = a \times e^{-\sqrt{\left[\frac{(x-x_0)^2}{b}\right] + \left[\frac{(y-y_0)^2}{c}\right]}} \qquad (3.4)$$

38

The Gaussian regression is to determine the values of a, b, and c. Then the program calculates the peak value of the curve for each frame, and develops a frame of 25 x 25 pixels around the red target. Figure 3.5 shows the result of the data processing for each frame.
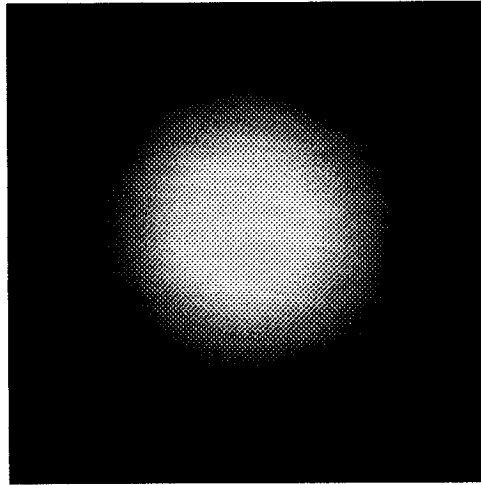
Figure 3.5: High intensity red light after filtering and processing.

The peak values resulting from the nonlinear Gaussian regression of each bitmap file were then extracted and stored in a file to be tracked as a function of time. The optical center area of interest was automatically updated for each frame utilizing Gaussian regression. This procedure was repeated for each frame, for the entire recorded data set. Upon completion, all the peaks of the Gaussian curve fits were stored in single file. The entire record was read and signal processing was performed in order to smooth the data. Figure 3.6 shows the 3-D plot of the Gaussian curve fit.

Gaussian Curve Fit of Red Light Intensity
Single Frame
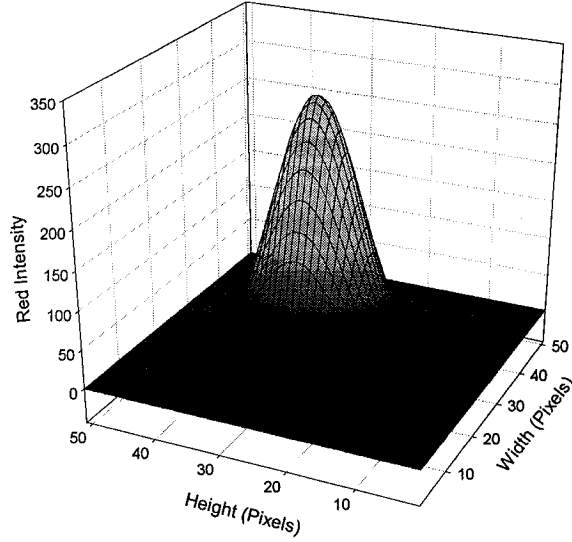
Figure 3.6: Nonlinear Guassian curve fit of high intensity red

The first signal processing step performed on the raw data mentioned above was to remove the mean utilizing the following equations:

$$\mu = \frac{1}{n}\sum_{i=1}^{n} x_i \qquad (3.5)$$

$$x_i = x_i - \mu \qquad (3.6)$$

where x_i represents the peak Gaussian value for each time step.

The next step was to digitally filter the de-meaned signal, x_i, using Fast Fourier Transform (FFT) techniques. A high-pass filter value of 0.01 Hz and a low-pass filter value of 5.0 Hz were used. Finally a cosine squared filter function was applied

40

to the leading and trailing portions of the signal in order to smooth the start and end

of the record as follows:

$$x(i) = \begin{cases} x(i)[1 - \cos\left(t_i * \dfrac{\pi}{2t_1}\right)^2, & t_i < t_1 \\ x(i)\left[1 - \cos\left((t_{max} - t_i) * \dfrac{\pi}{2(t_{max} - t_2)}\right)^2\right], & t_i > t_2 \\ x(i), & t_2 \le t_i \le t_1 \end{cases} \tag{3.7}$$

where: t_1 = lower time value cosine taper cutoff.

t_2 = upper time value cosine taper cutoff.

The program then stores the motion of each frame throughout the entire record. In

order to calibrate the movement of the target, a known distance between two red

lights was recorded at the beginning of each recording. The above-mentioned

procedures were performed for both red lights in one frame and the number of pixels

between those two lights were correlated to the known distance of these lights.

Figure 3.7 shows the frame of these two lights.
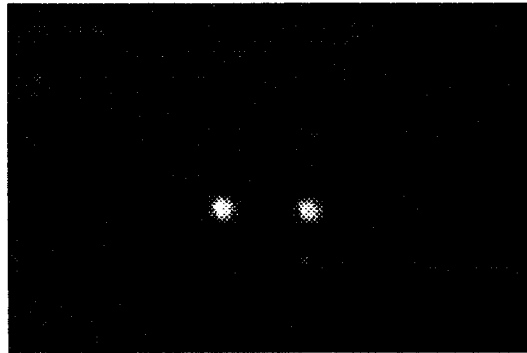
Figure 3.7: The two red calibration lights with pre-determined distance.

41

The following figures show the results of the data processing. Figure 3.8 shows the displacement time history record corresponding to the entire record of the optical center data after the signal processing. Note the displacement of the bridge ranged from 1.5 to 2.2 inch. This motion range is consistent with what other investigators have estimated for the ambient motion of VTB.

Center Displacement Time History
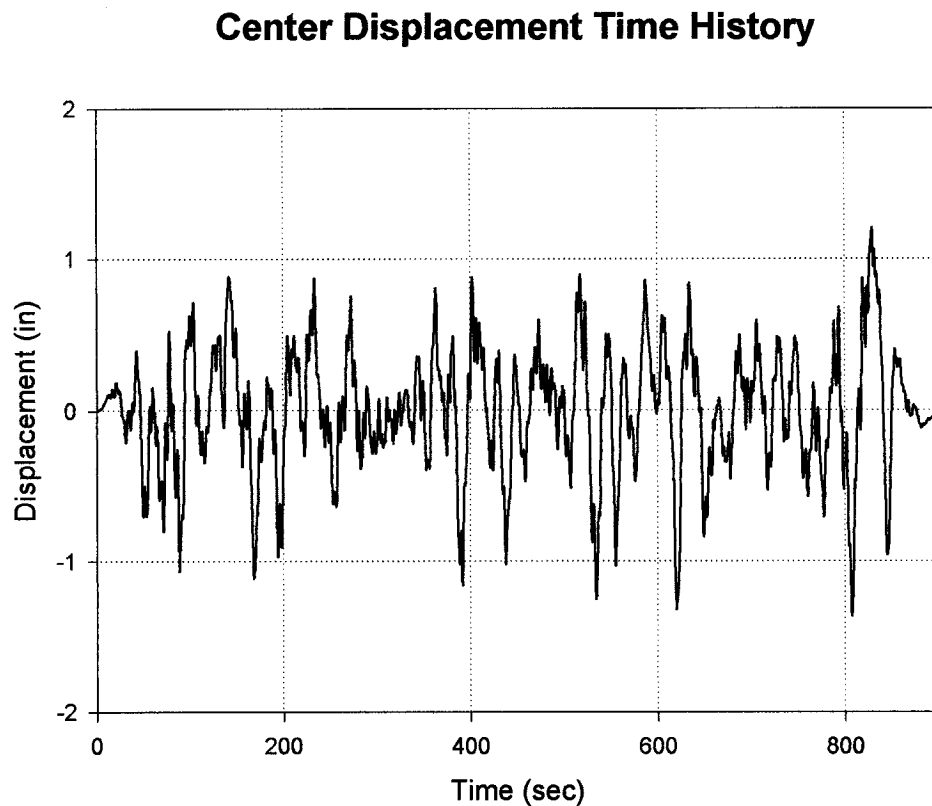
Figure 3.8: Displacement data of the center bridge optical data after signal processing.

Figure 3.9 shows the FFT of the entire record for the center measurement. It should be noted from this figure that the measurement detected the first two dominant modes of the bridge. The first mode is at 0.23 Hz and the second at 0.36 Hz. These

42

modes closely match those obtained by other studies using system identification techniques in conjunction with ambient vibration measurements from the sensor array discussed earlier.

**Center Location
FFT**
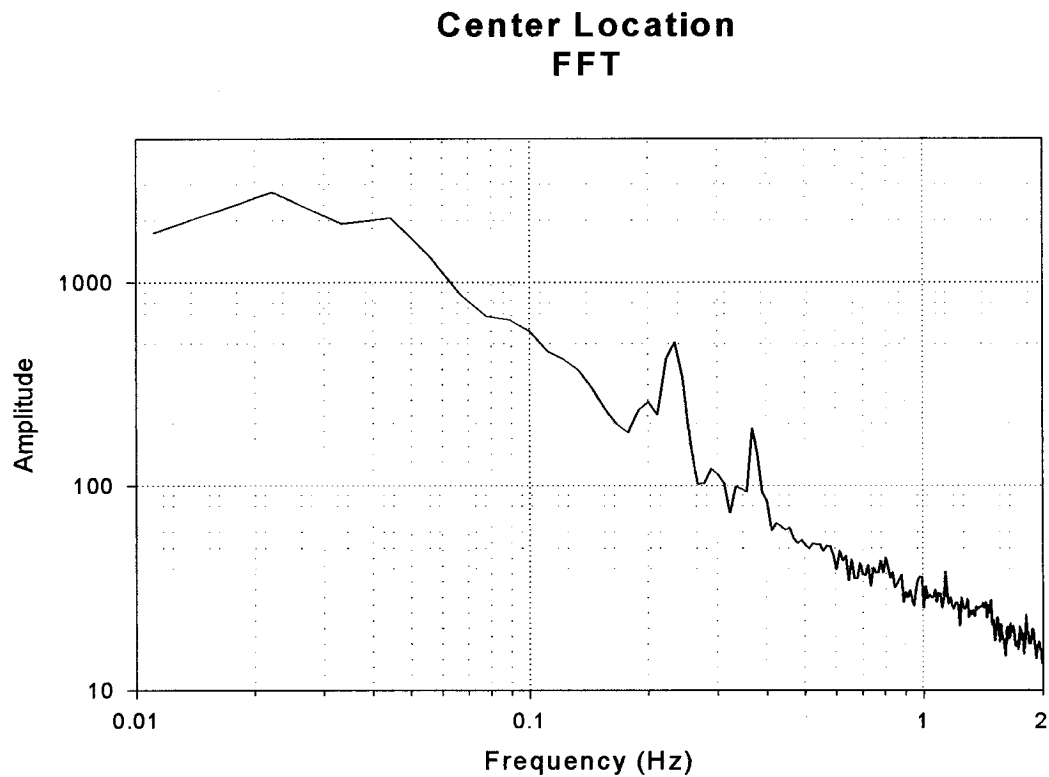
Figure 3.9: FFT of center optical data.

3.4   Discussion

This study has demonstrated the potential of vision-based approaches for the direct measurement of the time history of selected locations on a large civil infrastructure system. Some difficulties were encountered during the field experiment which will need to be addressed in the future. The mounting location of the video camera on the

43

bridge was not ideal. The camera was affected by the high frequency generated from the on-going traffic. A better rigid attachment location on ground level would optimize the picture quality and field of view. In addition the angular orientation of the camera with respect to the bridge was not addressed. This could be easily resolved if the camera is placed on the ground and triangulation calculation is performed in obtaining the bridge movement. Finally the camera used was a standard house-hold type of camera with high resolution. However, a professional video camera with a higher resolution could significantly improve the picture image. The targets were equipped with low-power LED's, which were initially battery operated. It will be necessary to experiment with different types of LED color and intensities. As previously indicated, this study used a pattern of red LED's with a black background; however, the ambient conditions in the vicinity of the Vincent Thomas Bridge such as rain, dust or light noise from the surroundings may dictate a different setup.

As pointed out in the Introduction, other methods such as GPS are being utilized to obtain direct displacement measurements. However, there are several technical difficulties with these methods. For example the GPS is highly regulated by government agencies, and there is considerable interference in highly congested urban areas (Celebi and Sanli 2002).

44

3.5 Summary and Conclusions

An overview is presented of an analytical and experimental study into the feasibility of a novel vision-based approach for obtaining direct measurements of the absolute displacement time history at selectable locations of dispersed civil infrastructure systems such as long-span bridges. The measurements were obtained using a highly accurate camera in conjunction with a laser tracking reference. Calibration of the vision system was conducted in the lab to establish performance envelopes and data processing algorithms (particularly integration-related issues) to extract the needed information from the captured vision scene. Subsequently, the monitoring apparatus was installed in the vicinity of the Vincent Thomas Bridge in the metropolitan Los Angeles region. This allowed the deployment of the instrumentation system under realistic conditions so as to determine field implementation issues that need to be addressed. It is shown that the proposed approach has the potential of leading to an economical and robust system for obtaining direct, simultaneous, measurements at several locations of the displacement time histories of realistic infrastructure systems undergoing complex three-dimensional deformations.

45

Chapter 4

Vibration-Based Signature Analysis of Dispersed Structures

4.1   Introduction

Performing large-scale dynamic experiments and analysis is considered the most accurate method of assessing the validity of the assumptions of any analytical model. Many assumptions and simplifications are made during the development of any analytical model, and due to the difficulties of performing a large-scale validation experiments, most models are not validated; hence most parameters for developing such a theory or model are not tested on large, complicated structures. Recently, this aspect of large-scale testing has become of more interest to civil engineering structures; however due to the logistics and complexity of such testing, most models are not tested. Large-scale testing is the only reliable way of determining the various dynamic parameters of interest to any structure. These parameters include natural frequencies, mode shapes, and damping.

Ambient vibration testing offers significant practical advantages to system identification approaches. One can rely on vibration generated from traffic or environment for analyzing large structures. However, in order to obtain meaningful data, the time history record must be long and relatively stationary. Most typical ambient vibration studies are conducted for several hours. Such long records are

46

needed to perform enough averaging. Another advantage of ambient vibration is the excitation level is relatively low and hence the behavior of the structure is mostly linear.

There have been numerous studies on identification methods; the following reference some of these studies, Rainer and Selst (1976). Abdel-Ghaffar and Housner (1977), Masri and Caughey (1979), Agbabian et al (1991), Masri (1994), Masri et al (1996), Farrar and Doebling (1997), Hanagud and Luo (1997), Park et al (1997), Farrar and Jauregui (1998), Farrar et al (1999, 2001), Lee and Liang (1999), Sohn et al (1999, 2001), Smyth et al (1999), Almalli and Cioara (2000), Gattuli and Romeo (2000), Marwala (2000), Masri et al (1984, 1987, 1993, 1998, 1999, 2000), Shinozuka et al (2000), Vanik et al (2000), Vestroni and Capechi (2000), Sohn and Farrar (2001), Sohn and Law (2001), Smyth and Masri (2001), Smyth et al (2002).

This chapter focuses on utilizing a large-scale structure, the Vincent Thomas Bridge, as the test bed for utilizing the multi-input-multi-output (MIMO) structural identification procedure. The MIMO procedure under discussion will be investigated with regard to its effectiveness in detecting structural changes.

4.2   Vincent Thomas Bridge Description and its Dynamic Monitoring System

The Vincent Thomas Bridge (VTB) in San Pedro, California supports the critical commercial traffic flow for the Los Angeles Harbor. The bridge is located in a

47

seismically active Southern California region, particularly because it saddles the Palos Verdes fault zone. VTB was constructed in the early 1960's across the main channel of Los Angeles Harbor and City of San Pedro to Terminal Island. The bridge consists of a suspended center span of 1500 feet long, and two 506.5 feet long suspended side spans, and a 52 feet wide four-lane roadway. Figure 4.1 shows a general view of the overall dimensions of the bridge.

The suspended structure has two stiffening trusses, floor trussed beams and a lower chord wind bracing of K-truss type. The two stiffening trusses are located at the outer edge of the deck. The lower chord bracing forms a box-like system, which has a high torsional rigidity of the structure. Transverse rolled-girders are utilized and supported by the transverse top chord of the floor trusses. The two towers have cruciform cross sections made of four welded box sections. The two main cables consist of 4,028 cold drawn, galvanized, 6 gage steel wires. These cables provide approximately 122 square inches cross sectional area of steel. The suspenders consist of small diameter of high strength wires.

In 1995 the California Department of Transportation started an extensive seismic retrofit of the bridge. Since then the bridge has been undergoing significant seismic retrofit. The work on the Vincent Thomas Bridge was completed May 2000.

4.2.1 Description of Sensor Locations

As mentioned previously, VTB was instrumented in 1980 with twenty-six accelerometers. The following figure depicts the schematic locations of these sensors. In addition, table 4.1 summarizes the location and measuring directions of each instrument. It should be noted the eastern half of the bridge has more sensors than the western half, due to the housing location of the analog recorder in the eastern cable anchorage. In addition, sixteen accelerometers are located at various locations at the bridge superstructure, while ten accelerometers are distributed at the substructure level.

49
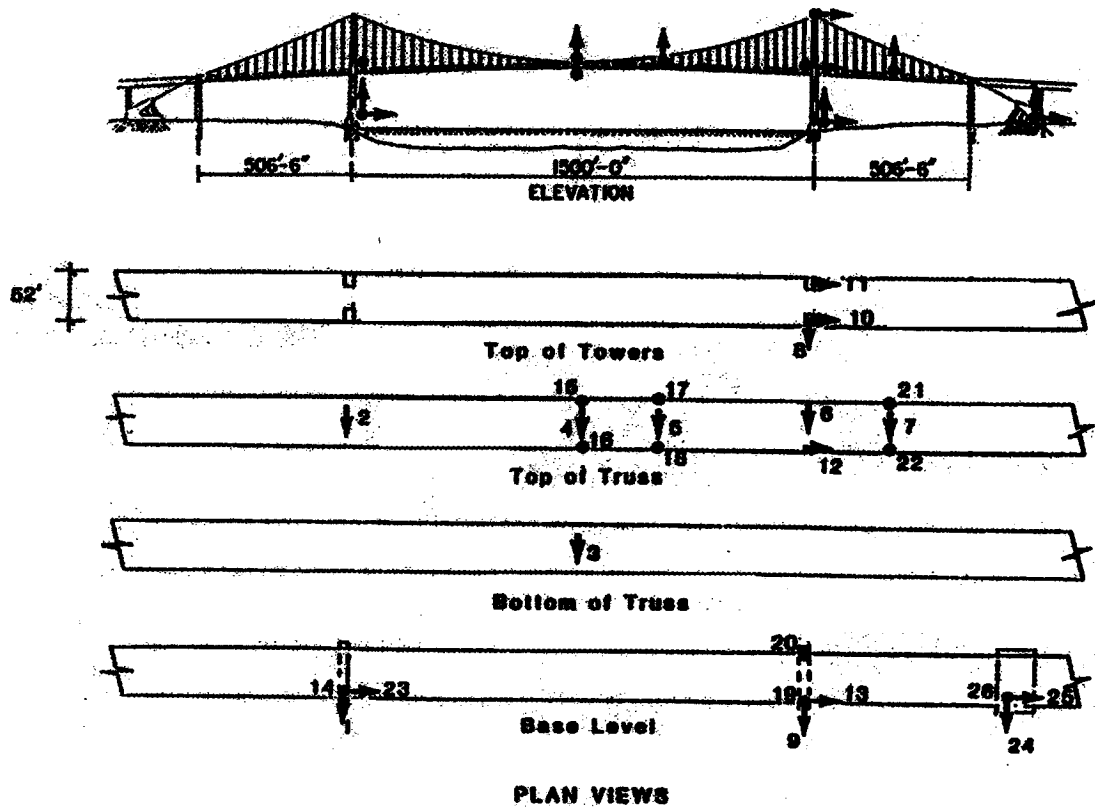
Figure 4.1: Schematic of sensor locations.

50

Sensor Number	Sensor Direction	Location on Bridge
1	Lateral	Base of South Column at West Tower.
2	Lateral	Top of deck truss at West Tower
3	Lateral	Bottom of deck truss at main span
4	Lateral	Top of deck truss at main span
5	Lateral	Top of deck truss at 1/3 way of main span
6	Lateral	Top of deck truss at East tower
7	Lateral	Top of deck truss at center of side span
8	Lateral	Top of South column at East tower
9	Lateral	Base of South column at East tower
10	Longitudinal	Top of South column at East tower
11	Longitudinal	Top of North column at East tower
12	Longitudinal	Top of deck truss at East tower
13	Longitudinal	Base of South column at East tower
14	Vertical	Base of South column at West tower
15	Vertical	North edge of deck at main span center
16	Vertical	South edge of deck at main span center
17	Vertical	North edge of deck at 1/3 way of main span
18	Vertical	South edge of deck at 1/3 way of main span
19	Vertical	Base of South column at East tower
20	Vertical	Base of North column at East tower
21	Vertical	North edge of deck at center of side span
22	Vertical	South edge of deck at center of side span
23	Longitudinal	Base of South column at West tower
24	Lateral	Base of East anchor
25	Longitudinal	Base of East anchor
26	Vertical	Base of East anchor

Table 4.1: Location and direction of instrumentation on the Vincent Thomas Bridge.

4.2.2 Retrofit of the Vincent Thomas Bridge

Shortly after the 1994 Northridge earthquake, the California Department of Transportation (Caltrans) deemed the bridge vulnerable to future earthquakes and hence implemented a comprehensive seismic retrofit of the bridge. The retrofit

51

program lasted from 1997 through 2000. During this program the structural characteristics of the bridge were enhanced by strengthening several critical components and by installing 36 large passive viscous dampers to mitigate the relative motion under strong shaking of the bridge roadway with respect to its piers.

4.2.3 Ambient Data and Real-Time Vibration Data Collection

During the retrofit modifications ambient data was collected. The data sets were collected during several phases of the retrofit of the bridge. In order to capture the ambient influence on the bridge, data was collected at different times throughout the day.

The data sets span a period of seven years from 1995 through 2002. The following summarizes the description of the data sets:

- Over 600 records have been collected ranging in size from 4 to 8 MB.
- The data collected channels range from 3 to 18 channels based on availability at time of recording.
- Each record length ranges from 800 to 1000 seconds
- Sample rates were either 100 or 200 samples per seconds.

In January 2003, a real-time structural health monitoring system was installed by University of Southern California (USC) research team at the VTB. The real time monitoring system distributes its data via the internet. The system connects to the

52

existing strong motion instrumentation. The data acquisition system (RTMS-2001R)

manufactured by *Digitexx Inc.* has several features which enables the acquisition of

long data records lasting several days, without interruptions. The data is sampled at

100 samples comparing to the existing strong motion data acquisition system. The

system utilizes 24-bits of resolution and a high dynamic range of 120 db.

Shortly after the real time monitoring system was installed, a small magnitude

earthquake struck Southern California on 22 of February, 2003 at 4:19:10 am (PST).

The earthquake magnitude was 5.4 with epicenter located near Big Bear city in

California. Both the California department of conversation (CDC) strong motion

instrument recording and the real-time monitoring system were triggered at the

bridge. A detailed analysis of the effects of this earthquake on the VTB is presented

later in this chapter.

4.2.4   Overview of Real-Time System Architecture

Much of the following material is based on information supplied by *Digitexx*

(Radulescu, 2003). The *Digitexx* system is based on a multithreaded software

design. This highly efficient software architecture allows the system to acquire data

on a high number of channels, monitor and condition this data, and distribute it, in

real-time, over the Internet to multiple remote locations.

The real-time specification here is each packet of data acquired should become available for distribution over the internet immediately after it becomes available from the system's acquisition loop, meaning that, the system acquires one packet every second. Every second, the system sends out a packet of data from all the channels in that acquisition pass. Now, at this point, data is being sent to the remote locations (the communication interface is discussed later) over the internet. The only time delay that can be encountered here is the transport time involved in carrying the packet over the Transmission Control Protocol (TCP) lines to remote locations. These times are usually in tens of milliseconds, and often considerably less.

The system is designed to send data as it is being acquired. Since this is the real-time specification that was adopted, during normal operation the system does not do any sort of buffering. The reason is as simple as it is obvious. First of all, a buffer here will throw off completely the real-time engine. If the data distribution loop is not synchronized with the acquisition loop, one of them will get out of synch. These two threads (distribution and acquisition) are always synchronized inside the system. This implies that, if at any moment one of them slows down, or stops, it will also slow down and stop the other one. This is why in the *Digitexx* system the acquisition thread is the driving engine, and all the others follow. This way the system will never loose any data in case of a major event. It should be kept in mind that this system is a full recorder, and it is monitoring and recording events locally just like a standard recorder, with all the associated features (pre/post event, triggering on 10 channels and so on).

54

Consider an example where somebody is monitoring a structure remotely, which is instrumented with one of the *Digitexx* systems. The system will feed all the channels to the remote client(s) as they are being acquired. However, if the client has a slow connection to the internet (less than 110Kb), it will not receive continuous data. Since the client is not able to digest data packets at the rate at which they are being acquired and sent out by the system, it will start loosing some packets. The client will receive data; however it will be sparse, because by the time it receives one packet of data, the system has already acquired another one or two and it is sending those out. The system will not wait for the recipient to control the traffic. Once again, this is all dictated by the real-time specification of the system.

The transmission control protocol/internet protocol (TCP/IP) data distribution interface of the system is designed around a publish/subscribe interface. It means that the system can send data of different types (publications) to different clients (subscriptions) requesting that specific type. For example, on a particular structure, one can group the sensors in different categories based on type, location orientation and so on. The system can make those separate types available for distribution in the same manner in which they were grouped. This way, remote clients can receive only the channels they are interested in. This optimizes communication and productivity. This is what is called "publishing". Now, the clients can subscribe to only the data they are interested in. The system will distribute to multiple clients for each subscription, meaning it can maintain multiple subscriptions per data type. More

55

than two clients can subscribe and receive data in real-time for each data type that exists on the system. Per each data type, the system will distribute the data to each client ("subscriber") in sequential order. The switching time is in the order of microseconds. The number of clients connected to the system and the number of data types specified are a measure directly proportional to the bandwidth available to the system.

4.2.4.1 Bandwidth

Bandwidth is a measure of data throughput over different data lines. In the present case, the discussion concerns bandwidth over TCP lines. Consider first a few interconnection scenarios. The type of connections the *Digitexx* system accepts can be multiple. The important parameter for the system is the up-link data rate of the connection. The system is *sending* high amounts of data on the line, which makes it different from the regular client browsing the web, generally *receiving* high amounts of data. One connection scenario is on a LAN layout. LAN speeds are usually 100 Mb and are usually symmetric (up-link throughput is equal to the downlink rate). Today's LAN speeds can reach up to Gigabits, which is very impressive. In such a setup the *Digitexx* system will perform at its best. Uplink rate is optimal, and the line symmetry makes data traffic very easy to handle. Another symmetric setup is also a T1 line offering 1.5 Mb symmetric connectivity. This is also a very suitable installation for the *Digitexx* systems since a 1.5 Mb uplink is more than enough to

56

satisfy 5 clients or more in real-time. The most common installation of such systems however, sits on Digital Subscribers Line (DSL) lines.

Speed (latency) and capacity (bandwidth) are two very separate things. The combination of latency and bandwidth give users the perception of how quickly a web page loads or a file is transferred.

The most commonly used example for comparing latency and bandwidth is the image of water running through a pipe; the pressure is latency, the width of the pipe is bandwidth. If one has a wide pipe but low pressure, one can move more water through the pipe but at a slower rate. On the other hand, if one has a narrow pipe but high pressure, one can move less water but at a faster rate.

4.2.4.2 Latency

Latency is normally expressed in milliseconds. One of the most common methods to measure the latency is the use of utility "ping." A small packet of data, typically 32 bytes, is sent to a host and the time is measured. Normally, the Round-Trip Time (RTT) for the packet to leave the source host, travel to the destination host, and return back to the source host is measured. Bandwidth is normally expressed in bits per second, the amount of data transferred during a second.

57

Internet Connection Type	Specification Comparison
Ethernet	0.3 μs
Analog Modem	100 - 200 μs
Integrated Services Digital Network (ISDN)	15 - 30 μs
DSL/Cable	10 - 20 μs
Stationary Satellite	> 500 μs, mostly due to high orbital elevation
DS1/T1	2 -5 μs

Table 4.2: Comparison between various internet connections.
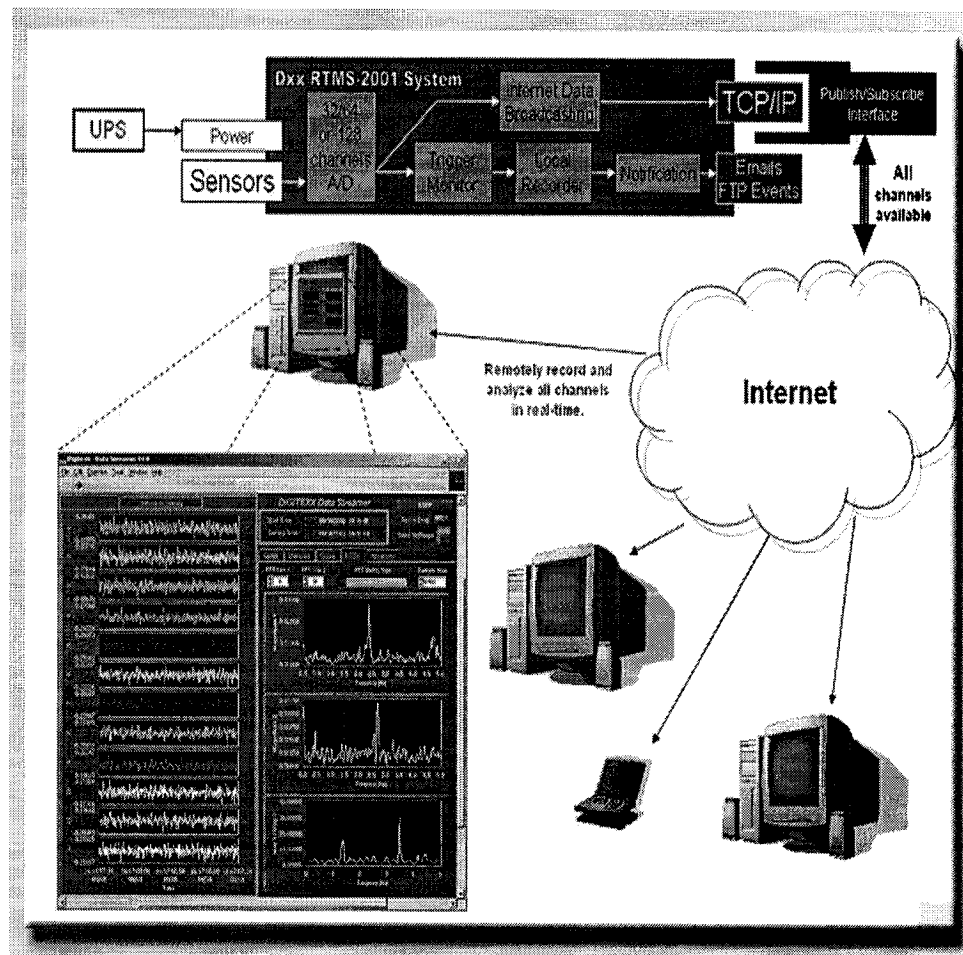
Figure 4.2: Real time monitoring system flow diagram

58

Bandwidth and latency are connected. If the bandwidth is saturated then congestion occurs and latency is increased. However, if the bandwidth of a circuit is not at peak, the latency will not decrease. Bandwidth can always be increased but latency cannot be decreased. Latency is the function of the electrical characteristics of the circuit.

Figure 4.2 shows a flow diagram of the *Digitexx* Real Time Monitoring System Model RTMS-2001RM. The following explanation provided by *Digitexx* and applies to this diagram.

4.2.5   Real-Time Server Software Description

The server software has three main threads. One is the local monitoring (recording) thread, another is the data distribution thread, and the third is the acquisition thread. They all revolve around a queue of limited size. Data from the acquisition thread goes into the queue. From here, each packet is analyzed for triggering conditions, and the same packet is being made available for distribution to the publishing communication interface. Each packet, based on its content (which data channels it contains), is routed to the corresponding publishing interface. Each interface has a number of subscriptions it maintains. Each subscription will receive a copy of the packet. For subscriptions, every time there is a change in the data stream, the protocol has to update its subscribers (as per the established real-time specifications).

59

Another important feature of the publish/subscribe interface is in case of a disconnect, the server retains the subscribers and when the connection is re-established, the server will start sending data to the subscribers without the need to restart the clients. The analogy to this situation is a TV set which is receiving a certain program. If the broadcasting station stops broadcasting for some reason, the TV will get static, and when the station starts broadcasting again, the TV gets the signal without being restarted. This is a useful feature for unattended operations.

4.2.6 Real-Time Data Monitoring and Distribution

The local monitoring (recording) thread, and the data distribution thread use exactly the same packet as input. The distribution thread takes the packet just as it was acquired and distributes it to the publishing interface. No conditioning of any sort is done to the data. The only signal processing applied to the data is scaling (conversion to cm/s/s if the sensors are accelerometers). The monitoring thread, on top of scaling, does signal conditioning for trigger monitoring, and local recording (eventually) with pre-event (user-specified). The local monitoring thread will record an event locally regardless of what happens to the data distribution thread. Once the event is recorded, it will try to notify a list of users (via email) and file transport protocol (FTP) the event to another site. If this process fails, the system will retry every 5 minutes until successful. The functionality of the server software (installed on the system on site) stops here (Radulescu, 2003).

60

Now, once the data is distributed to remote sites (clients), the data can be analyzed using a variety of approaches (some for "quick look" analysis, and others requiring an extensive amount of computational work) to obtain needed SHM indicators.

4.2.7 Sample Measurements through Streamer Software of Real-Time System

The real-time monitoring system discussed above was installed on VTB in early 2003. Sample measurements from the system are shown in Figures 4.3 and 4.4.
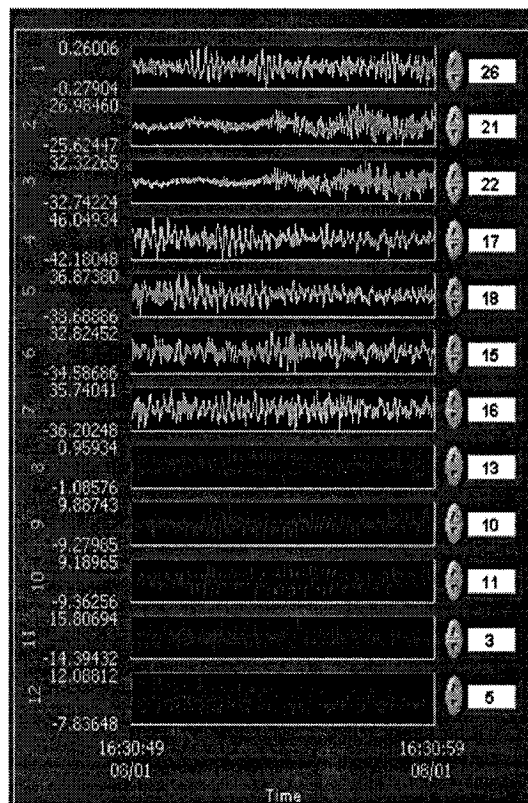
Figure 4.3: Acceleration screen
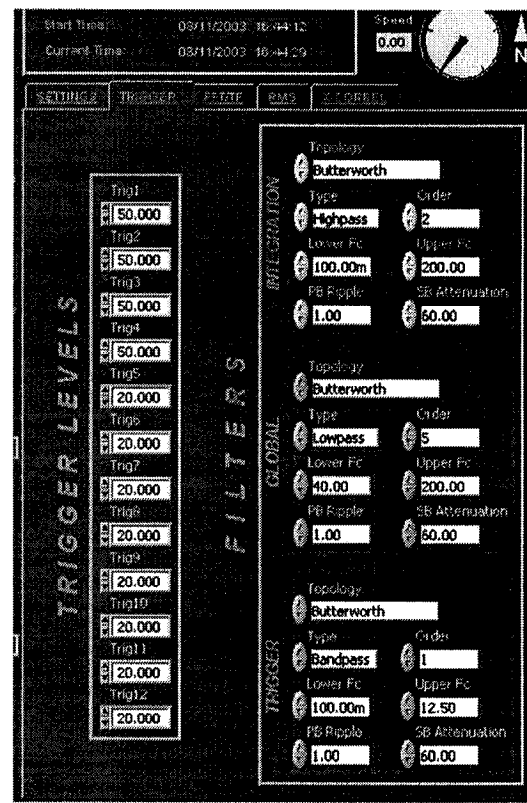
Figure 4.4: Trigger selection and filtering screen

The screen image shown in Figure 4.3 shows the time history of the "raw" sensor data (acceleration sensor measurement in the present example). The index of the displayed channel is shown on the left hand side of the panel, and the corresponding sensor index (as denoted in Fig 4.3) are shown on the right hand side of the panel. The displayed time history segment corresponds to a 10-second window. Automatic amplitude scaling is done for each displayed channel. Any arbitrary choice of channels can be displayed. To enhance ease of visual monitoring, data channels are color-coded so that sensors in the same direction of motion (bridge global x, y and z) are displayed with the same color.

The screen image shown in Figure 4.4 shows the settable parameters that can be used to select the physical quantities to be displayed (e.g., acceleration, velocity or displacement), the trigger level to start automatic recording of the sensor measurements.

Using the "quick analysis" capability of the real-time monitoring (RTM) system, various measures of the monitored system's response can be displayed in near real time, with the only delay (on the order of a few seconds) is due to filling data storage buffers needed to perform signal processing on a selectable time segment. The screen image shown in Figure 4.5a presents the FFT of any two arbitrary channel choices, and their transfer function. The screen in Figure 4.5b shows the short-term root-mean-square (rms) and long-term rms of one selectable channel. The short-term window displays the updated channel rms level once per second, while the long-term

62

window has settable averaging time so as to show the moving average rms of the

same channel.
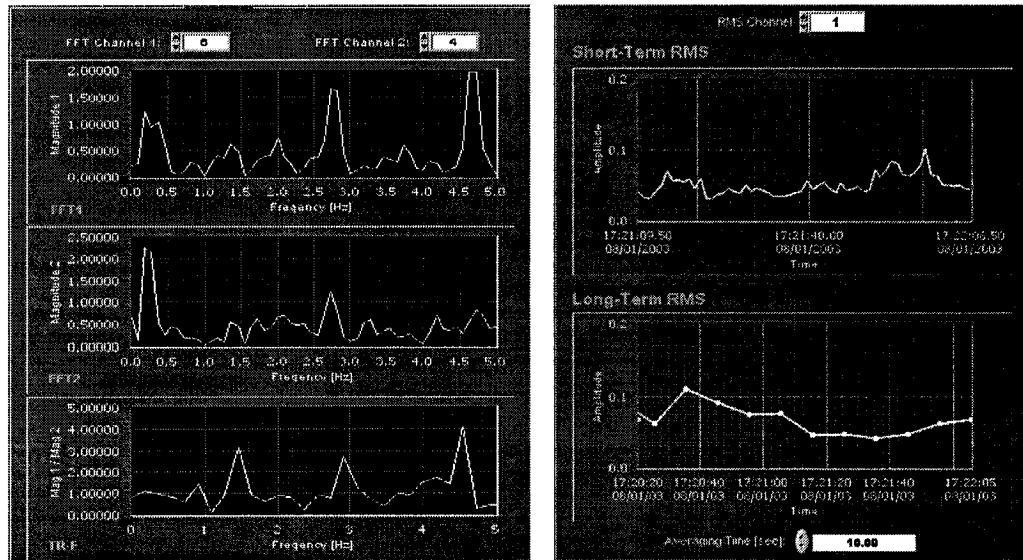
Figure 4.5a,b: (a) FFT of channels 15 and 17 and transfer function between 15 and
17. (b) Showing short-term and long-term rms levels of selected channels.

Another choice of the quick analysis conveniently displayed is the cross correlation

between any two channels. The screen image in Fig 4.6 shows the cross correlation

between channel 15 and 17, both on the bridge deck, with orientation in the vertical

direction. This plot contains a significant amount of useful information about the

interaction between the dynamic loads on the bridge and its modal characteristics.
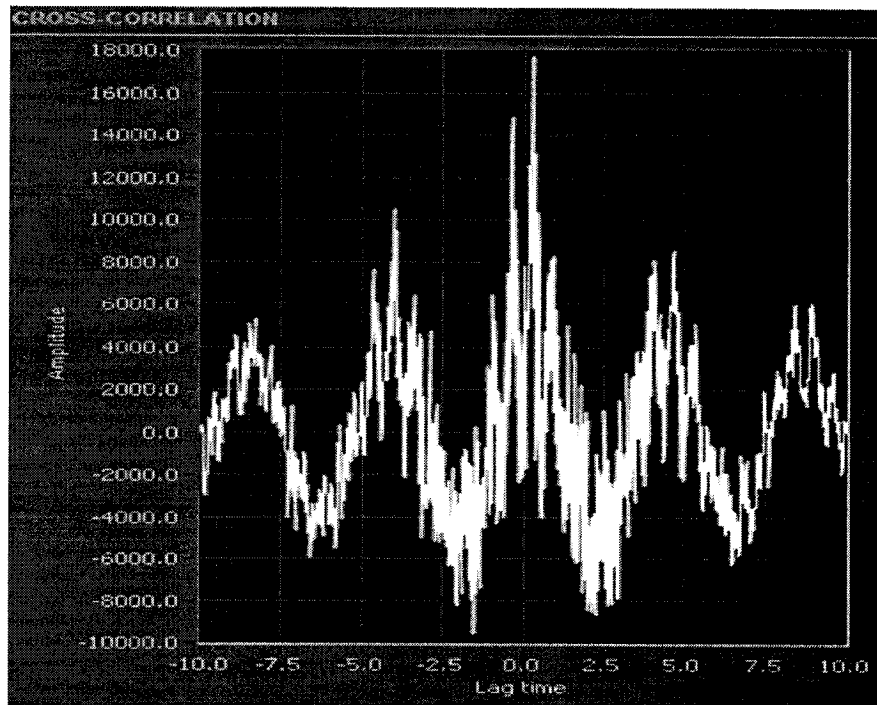
Figure 4.6: Sample Quick Analysis Results showing cross-correlation function between two data channels 15 and 17.

4.3   Analysis of Earthquake Data Collected through RTM

4.3.1   Measurement of 22 February 2003 Earthquake Response

In the early morning of 22 February 2003, a relatively small earthquake occurred in the vicinity of Big Bear city, California. Big Bear earthquake epicenter was 3.1 miles North of Big Bear city. The earthquake struck at 04:19:10 a.m. PST with magnitude 5.4M at N34.31 W116.85 with depth of 1.2 km. Figure 4.7 shows the location relative to the VTB vicinity.

64
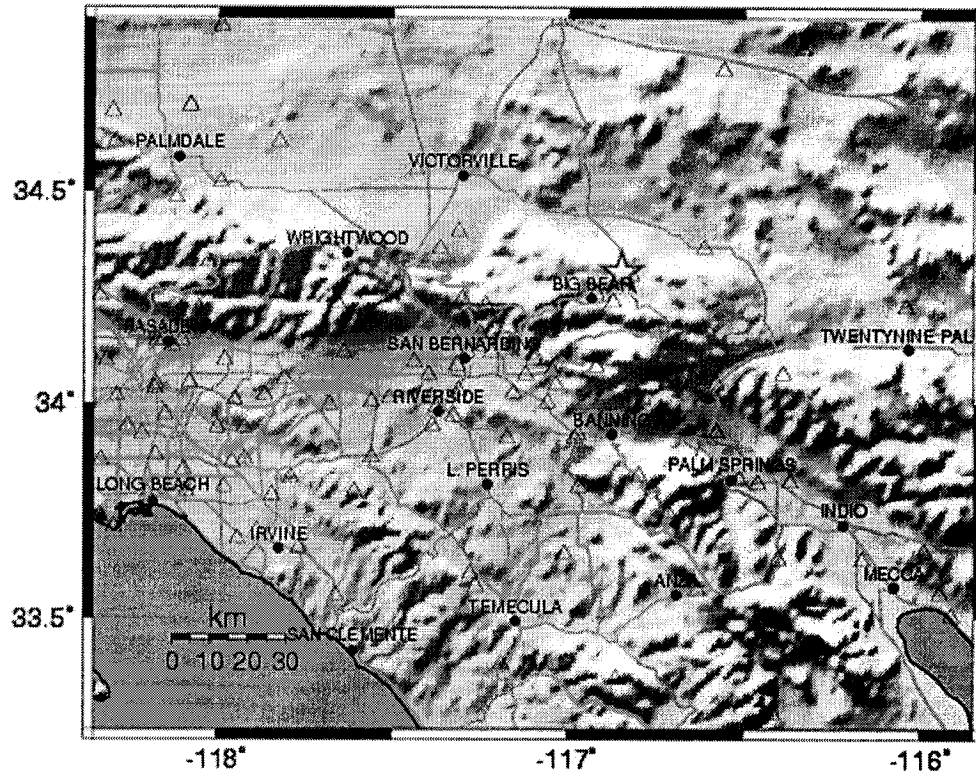
Figure 4.7: Geographical location of Big Bear Earthquake epicenter with respect to
Long Beach where VTB is located.

This location is approximately 180 km. from the position of the Vincent Thomas

Bridge. All acceleration channels were triggered on the VTB and a complete data set

comprising a total of 26 channels was obtained by the RTM system.

The collection of all 26 acceleration records obtained during this earthquake are

shown in Figures (4.8 a, b) using different amplitude scale for each component, in

order to enhance resolution. It should be noted that channel 4 is out of order. It can

be seen that the channel had relatively the same amplitude before and after the

earthquake as compared to the rest of the channels.

65
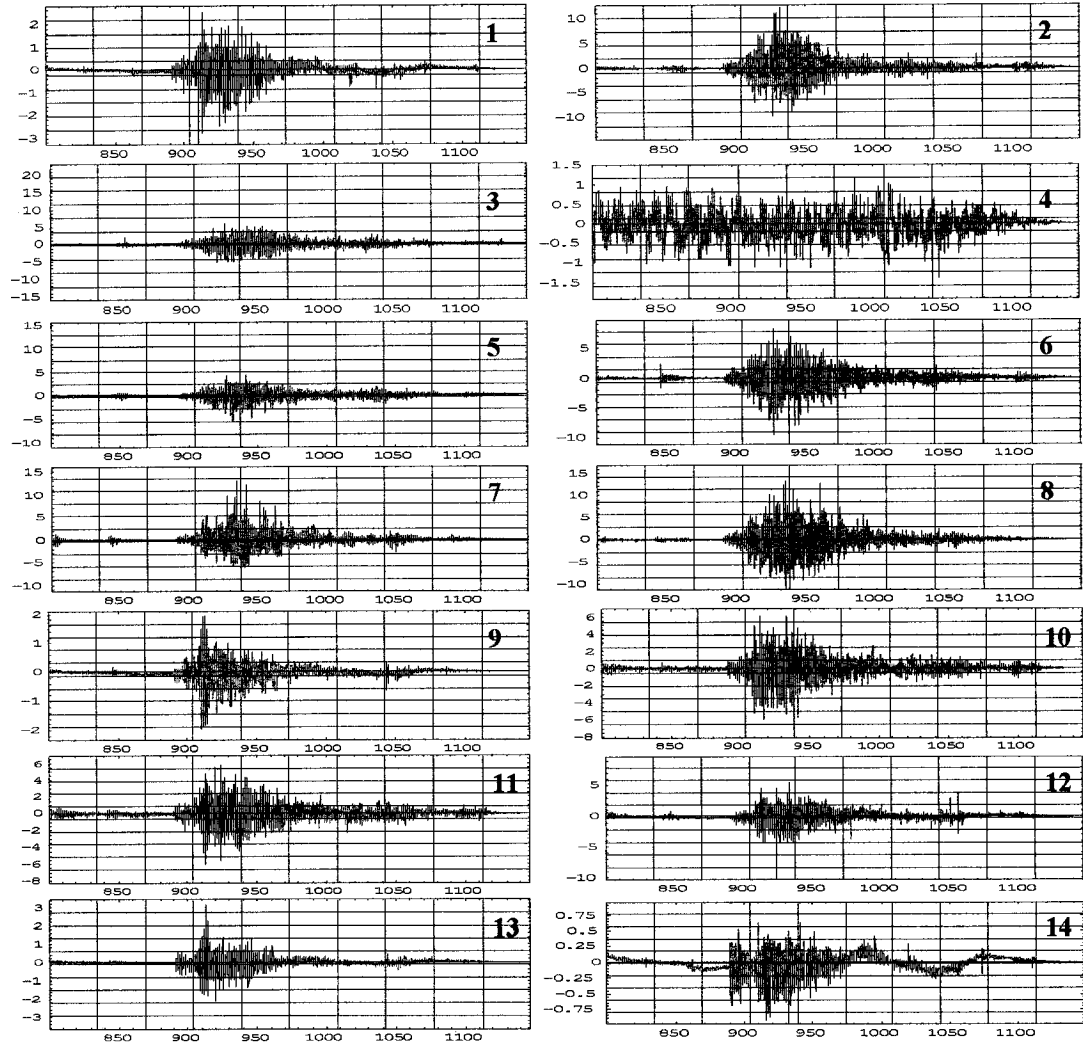
Figure 4.8a: Acceleration time histories of all 26 data channels recorded during the 22 Feb 2003 earthquake (only channels 1 through 14 shown in this figure).

66
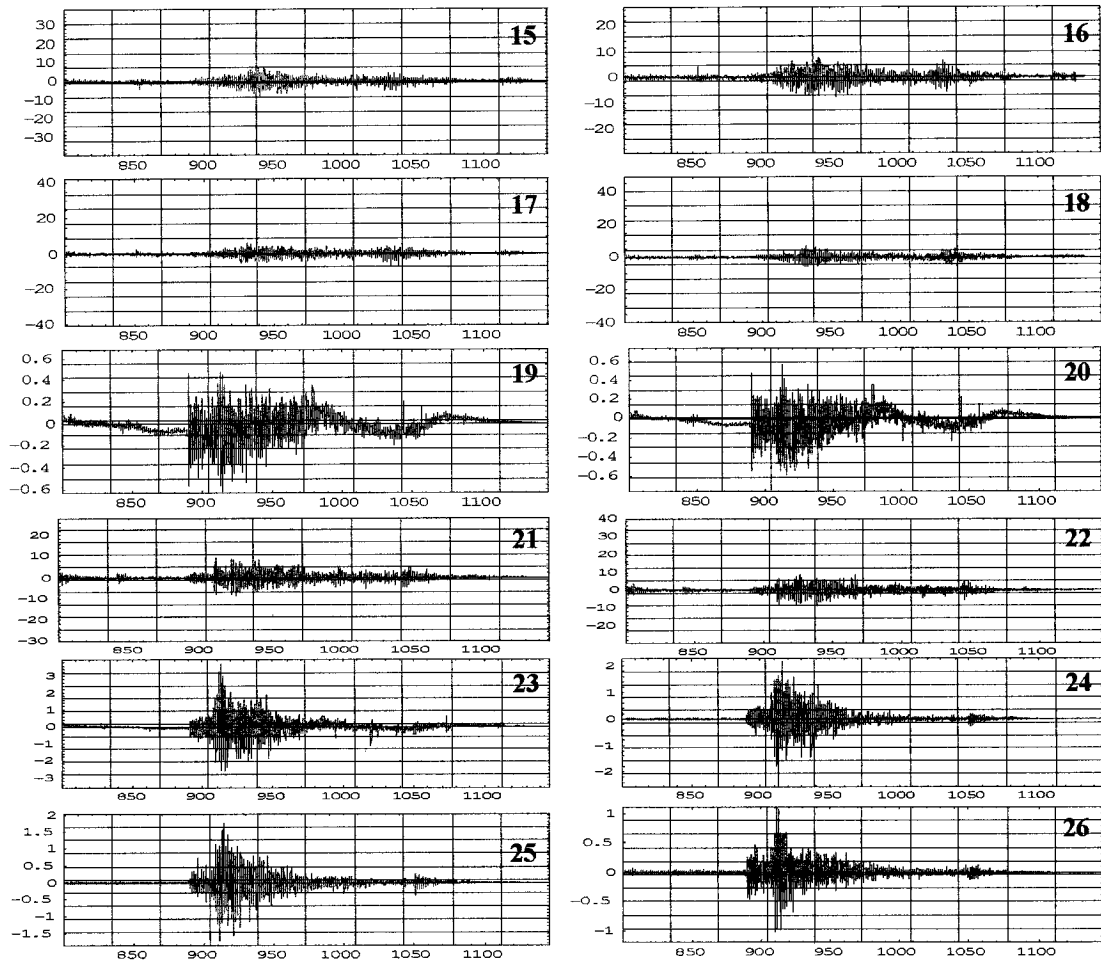
Figure 4.8b: Acceleration time histories of all 26 data channels recorded during the 22 Feb 2003 earthquake, (the remaining channels 15 through 26 are shown in this figure).

A sample of three acceleration components at the base of VTB (channels 1, 23 and 14, corresponding to the lateral, longitudinal and vertical components, respectively) as well as three response components on the bridge deck (channels 5, 12, and 17, corresponding to a lateral, longitudinal and vertical components, respectively) are shown in Figure 4.9.
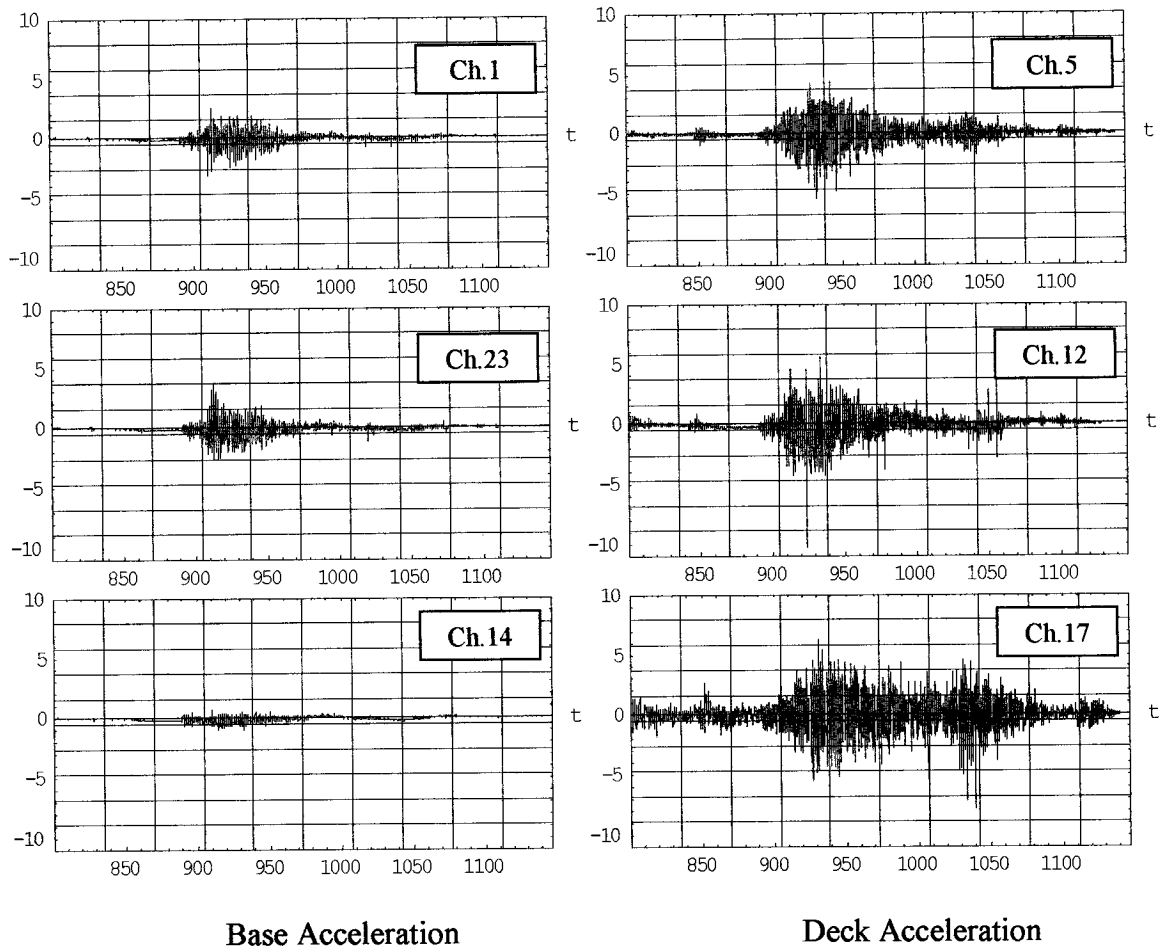
Figure 4.9: Sample acceleration records measured at VTB base (LHS) column and its deck (RHS column) during the 22 Feb 2003 earthquake. Plot units are (cm/s^2).

The recorded accelerations were subsequently processed to obtain the corresponding velocities and displacements for all the channels. The resulting velocity and displacement time histories for all the channels are displayed in Figures 4.10a, b and 4.11a, b.

68

Channel 4 was
Out-of-order
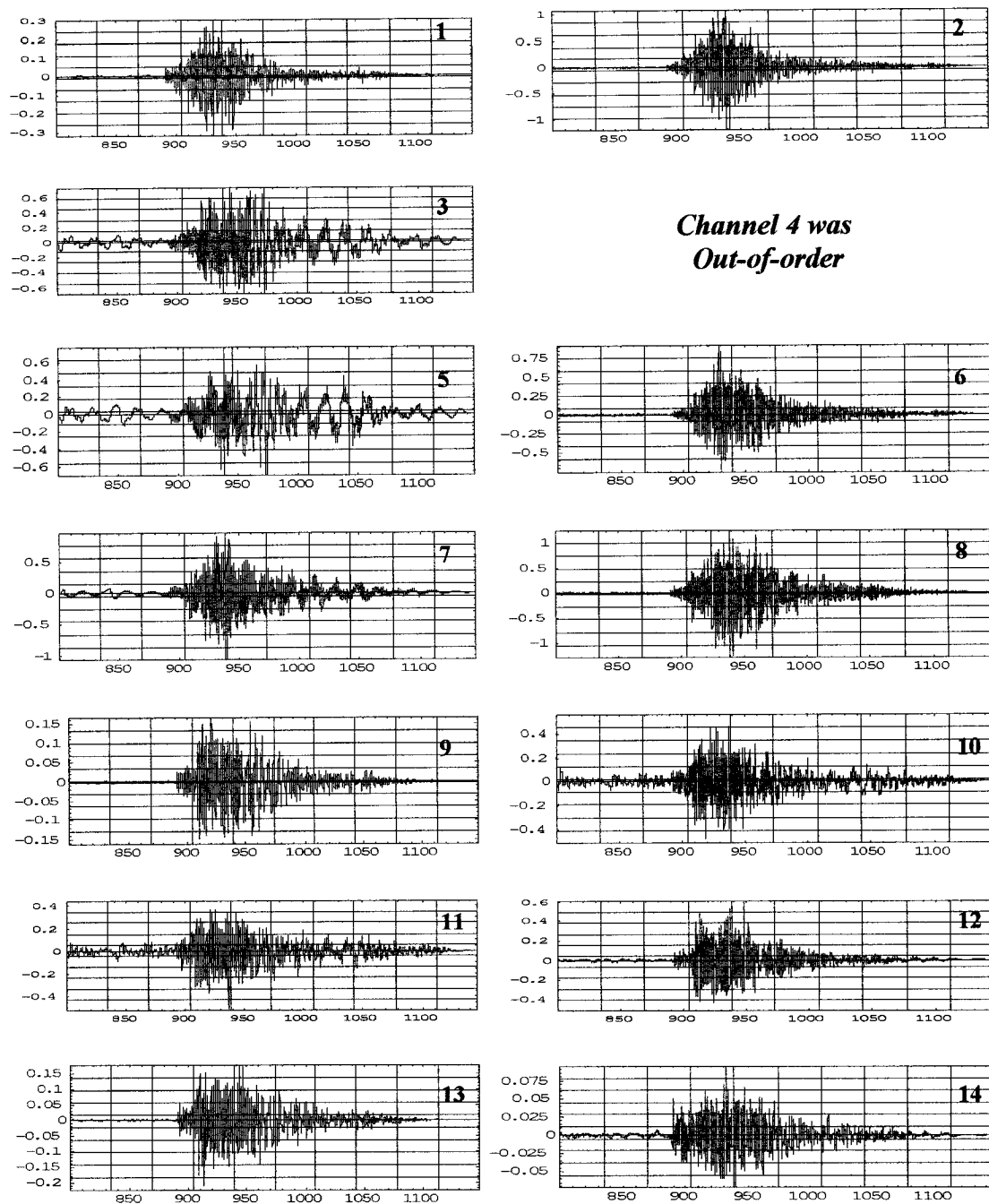
Figure 4.10a: Velocity time histories of all 26 data channels recorded during the 22 Feb 2003 earthquake (only channels 1 through 14 are shown in this figure).

69
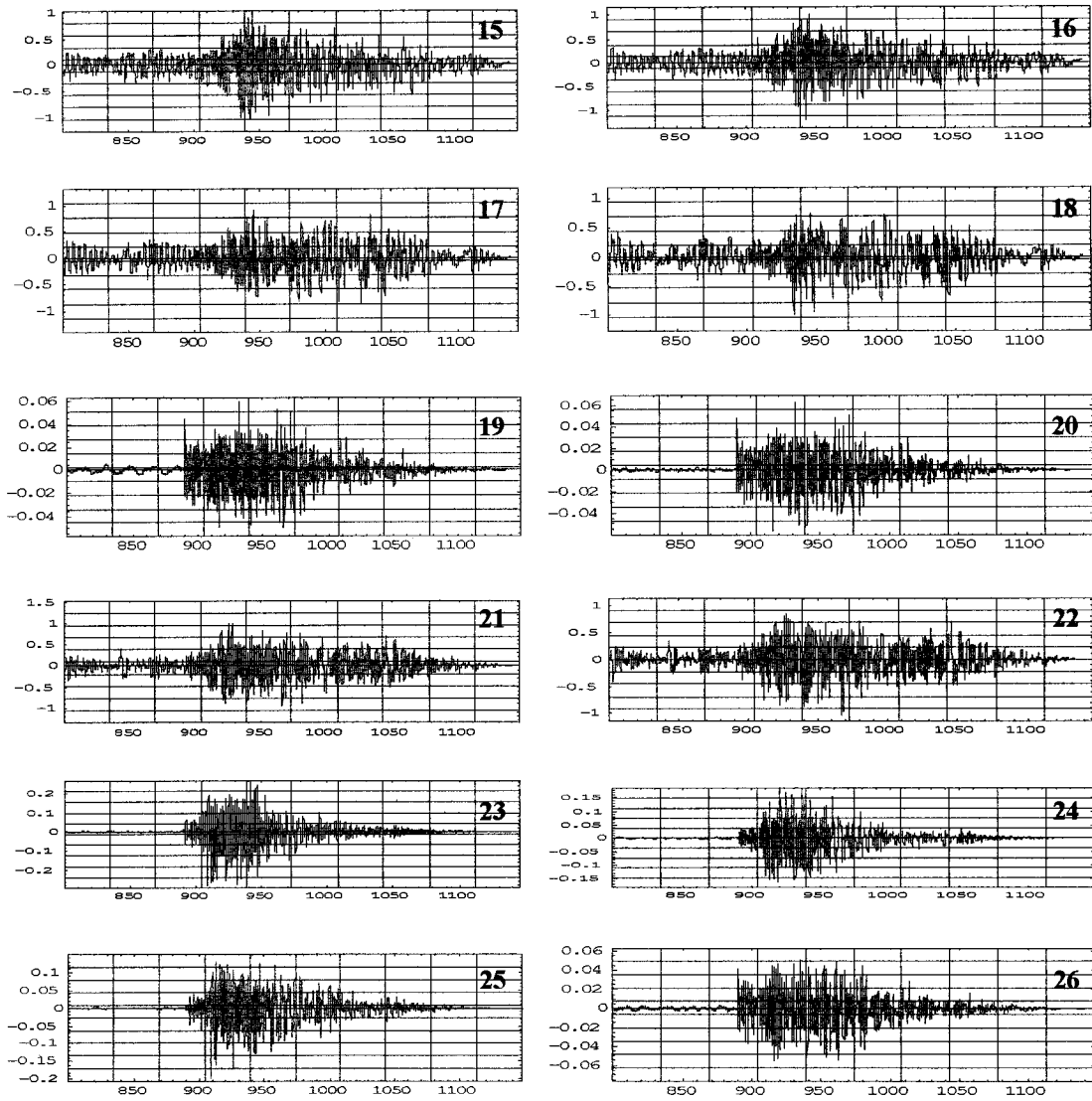
Figure 4.10b: Velocity time histories of all 26 data channels recorded during the 22 Feb 2003 earthquake (the remaining channels are shown in this figure, channels 15 through 26).

70
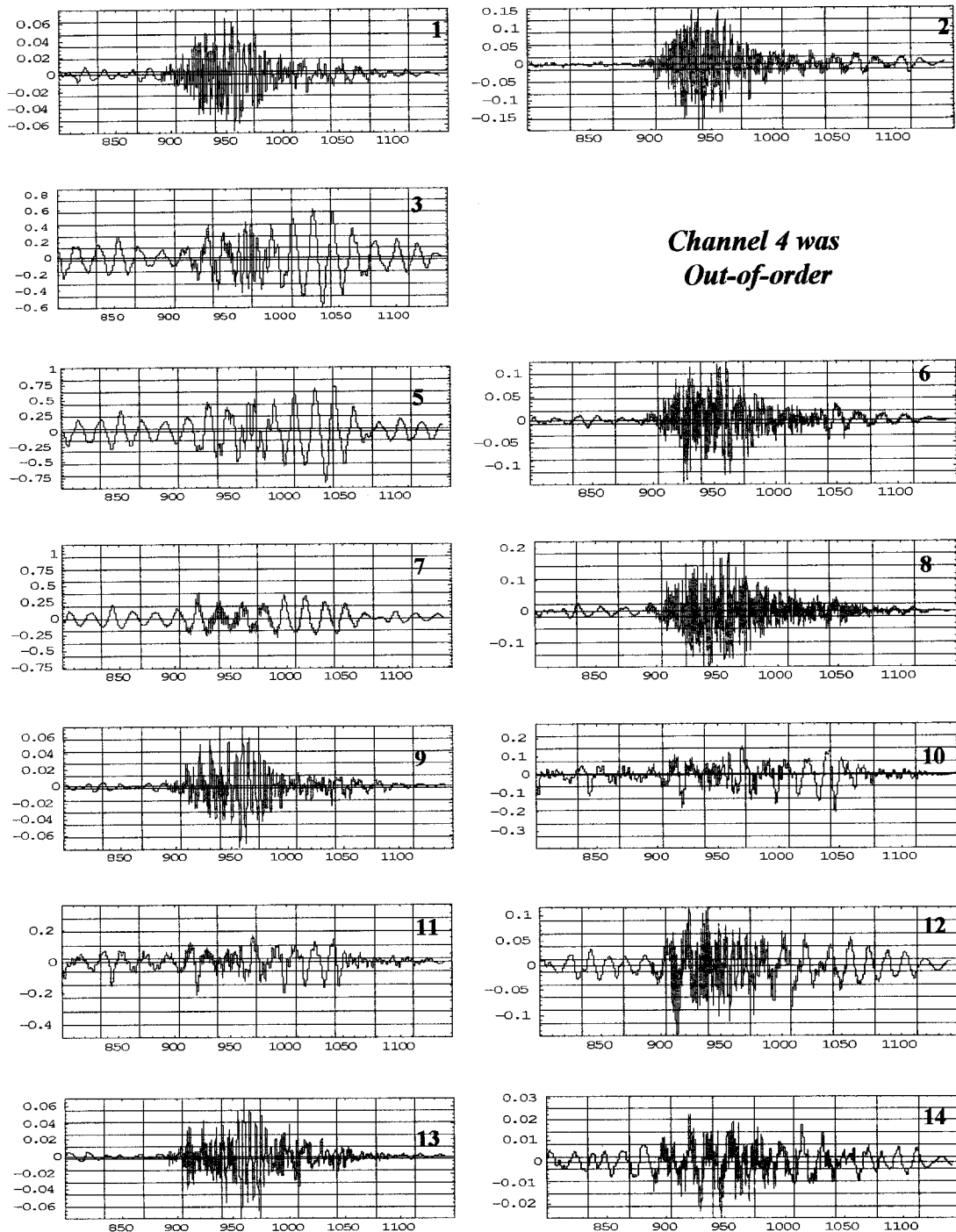
Figure 4.11a: Displacement time histories of all 26 data channels recorded during the 22 Feb 2003 earthquake (only channels 1 through 14 are shown in this figure).

71
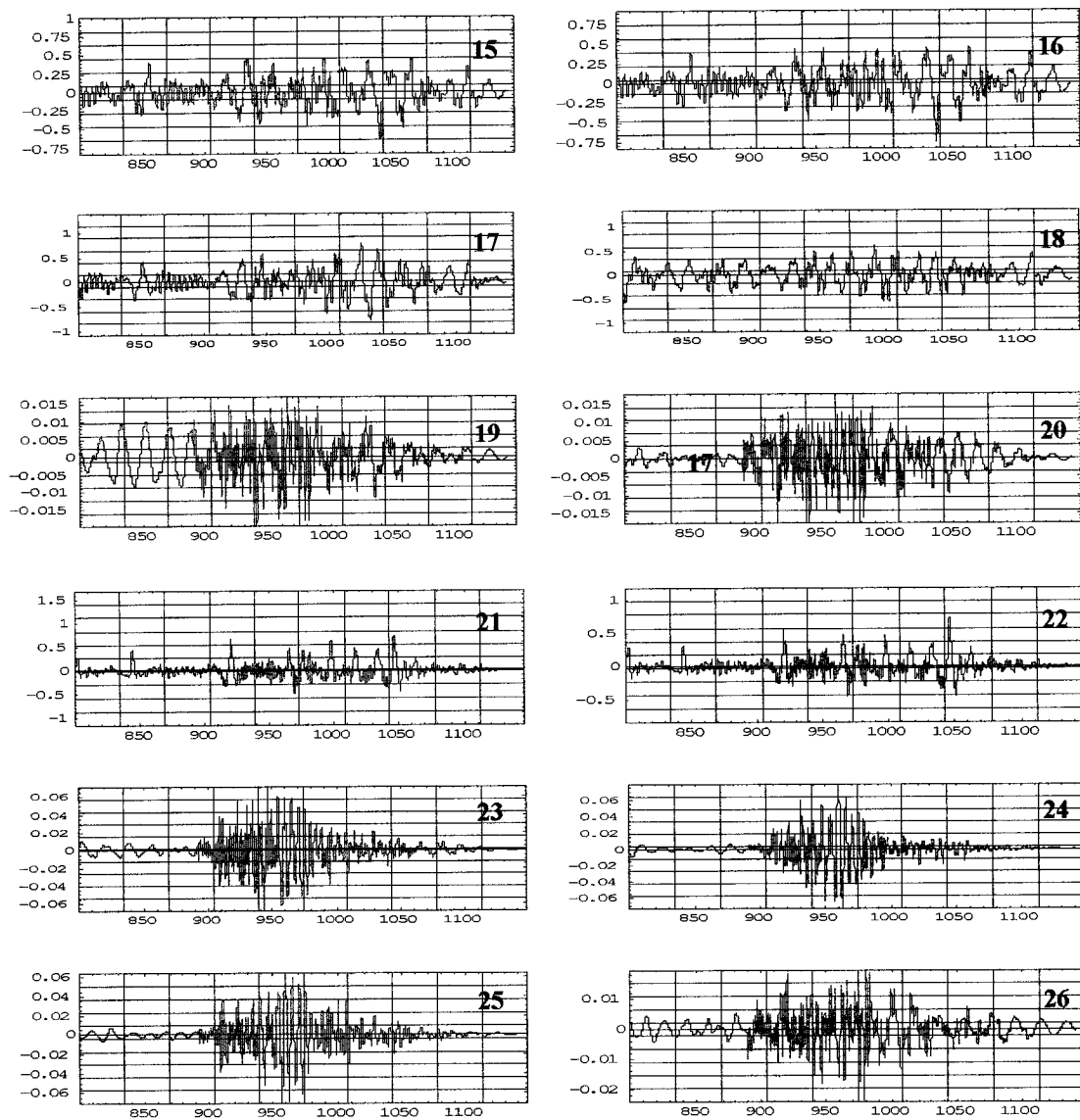
Figure 4.11b: Displacement time histories of all 26 data channels recorded during the 22 Feb 2003 earthquake (the remaining channels 15 through 26 are shown in this figure).

72

Sample input and response velocities obtained by integrating and processing the recorded accelerations are shown in Figure 4.12. The corresponding bridge displacement time histories were also obtained through double-integrating the accelerations, and sample displacement time history results are shown in Figure 4.12.

Base Velocity   Deck Velocity
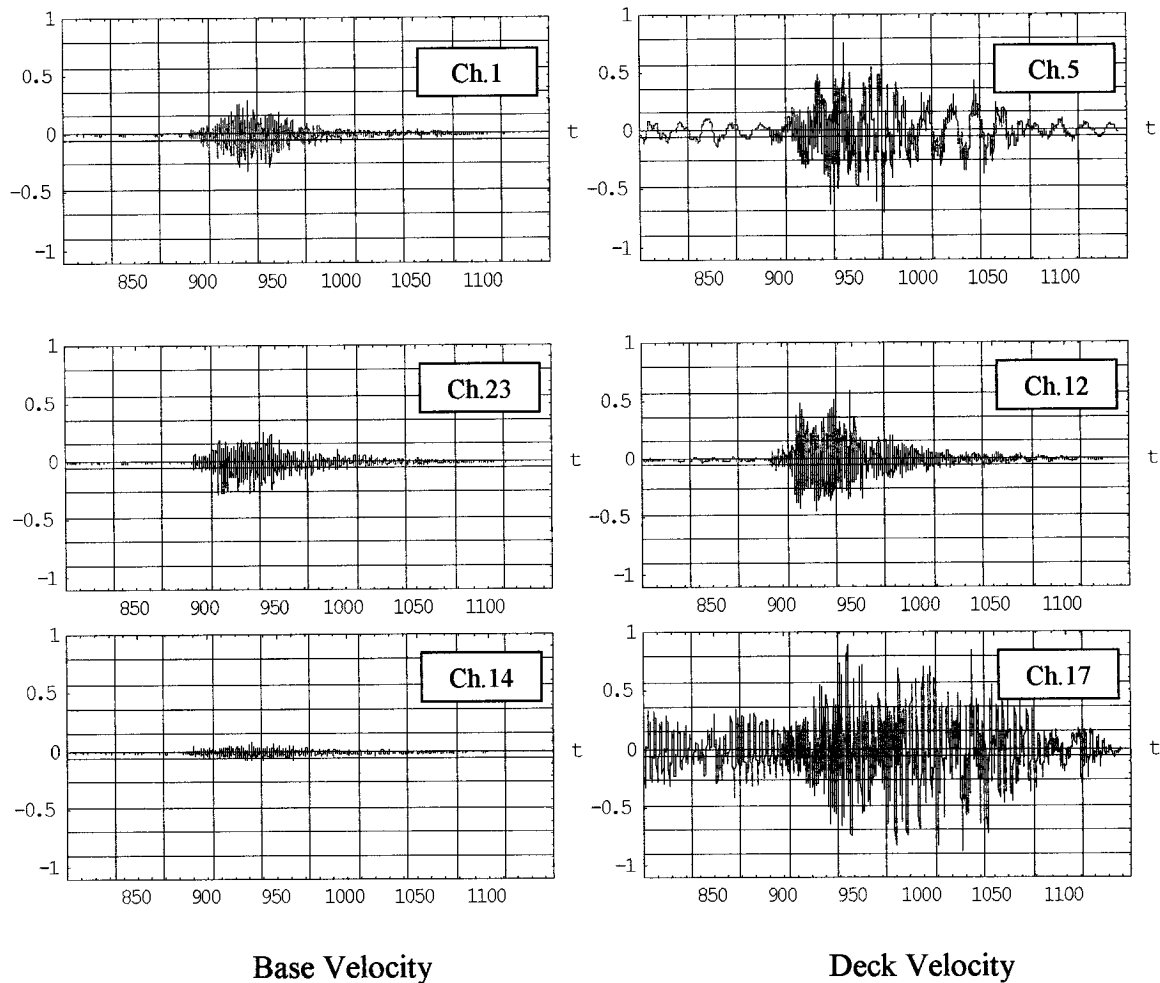
Figure 4.12: Comparison of velocities between base and deck locations. Time (Seconds) versus Velocity (cm/Sec).

73
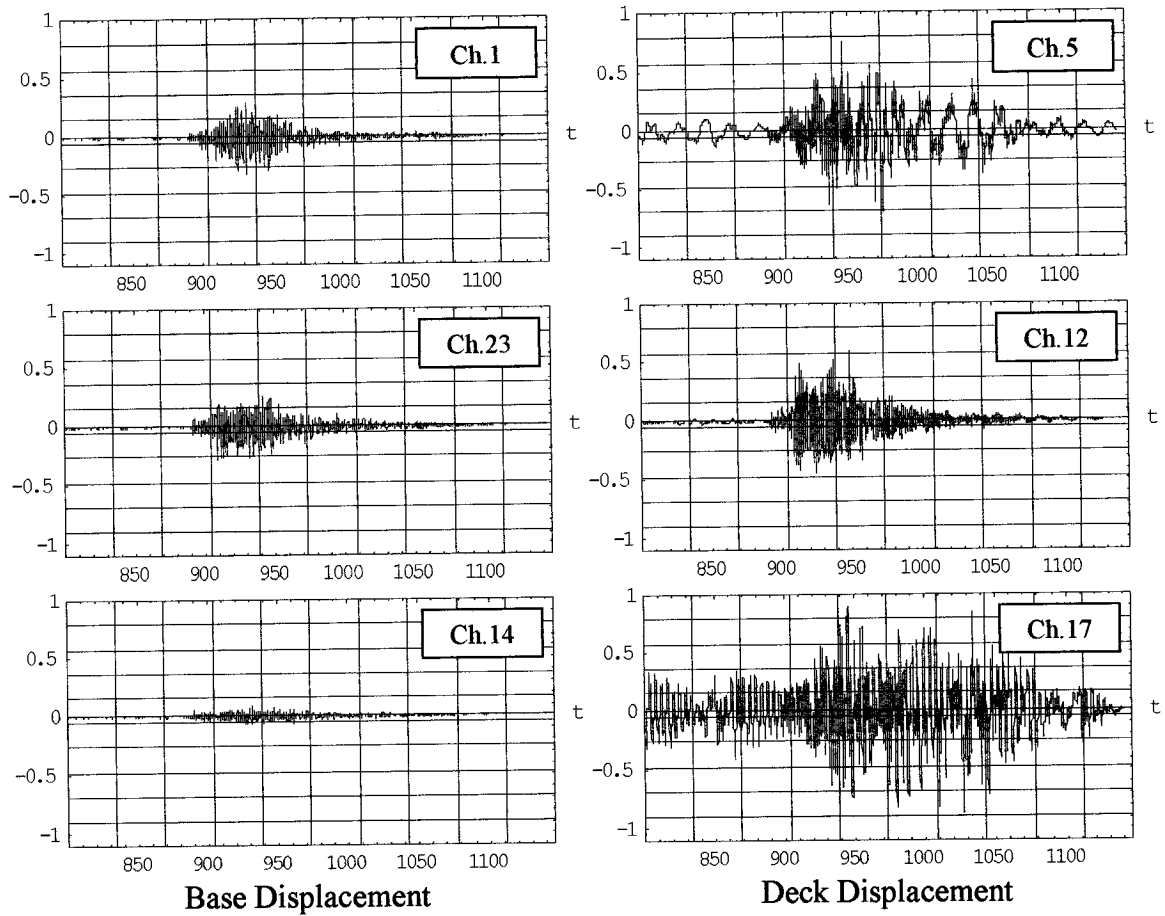
Figure 4.13: Comparison of displacements between base and deck locations. Time (Seconds) versus Displacement (cm).

It is worth noting that particular care is needed to use suitable digital signal processing approaches to obtain correct values of the time histories of the system velocities and displacements from the measured accelerations. As mentioned in chapter 2, there are potential problems and serious computational pitfalls encountered by using naïve data processing approaches to integrate acceleration measurements.

74

FFT of acc[i]

Base FFT of acceleration   Deck FFT of acceleration
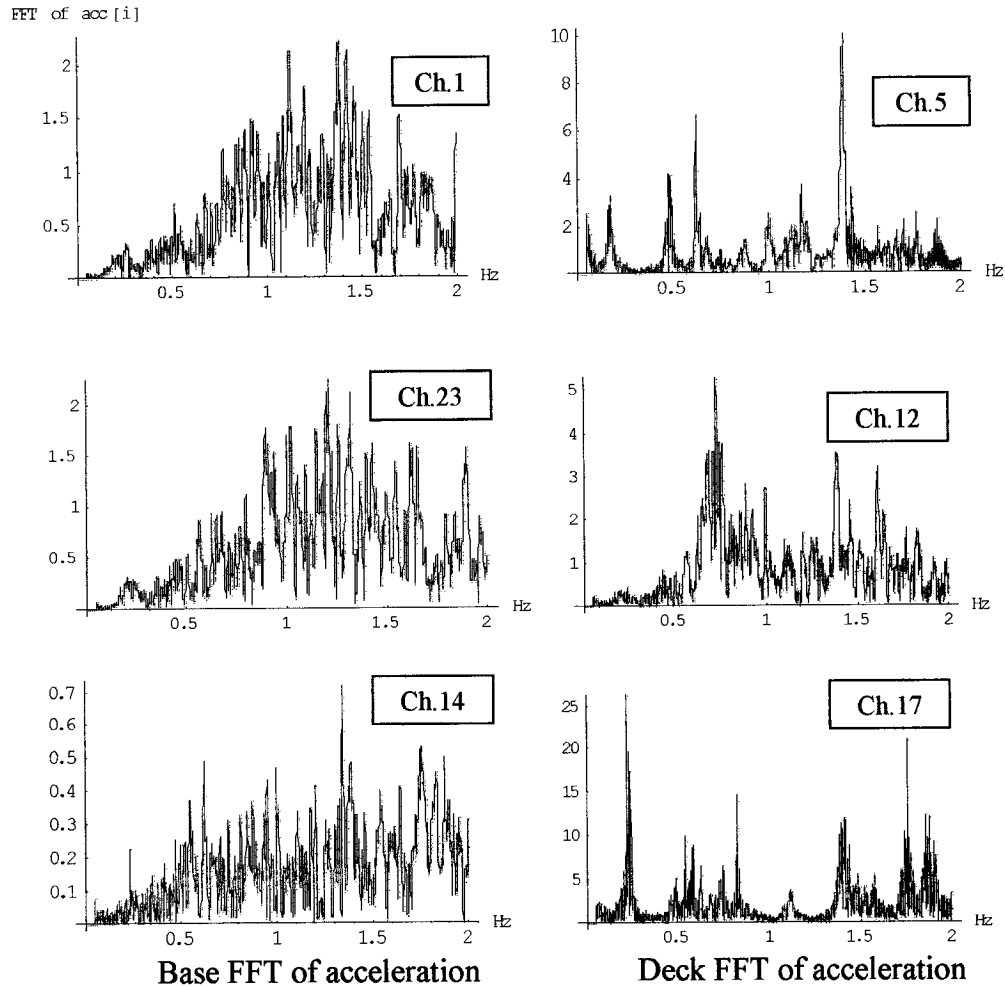
Figure 4.14: FFT of Acceleration for the VTB base vs. deck.

Comparison of the dynamic environment acting on the VTB during the subject

earthquake shows there is a drastic difference in the measured accelerations at the

bridge base (on the order of milli-g's) as compared to the response on the bridge

deck. Note that, for convenience, identical amplitude scales are used in Figures 4.9,

4.12 and 4.13 for similar types of response measures. It is also worth noting the

75

drastic change in the spectral content of the motion at the base and deck of the bridge.

Figure 4.14 shows the FFT of the acceleration time history records shown in Figure 4.9. Notice the input records have a relatively small amplitude, but a broad-band nature, while the bridge response records have a much higher amplitude level as well as behaving as a low-pass filter. As will be shown in the following section, the response peaks are directly correlated with the dominant (identified) system natural frequencies.

4.4   Multi-Input-Multi-Output (MIMO) System Identification Technique

This section explores the potential use of a time-domain identification method to detect changes in structural systems on basis of noise-polluted measurements. This method requires the use of excitation and acceleration response records. The basis of this method consists of developing a reduced order mathematical model that has the same equivalent number of degree of freedom as the number of sensors.

System identification techniques can be classified into the two broad categories of parametric and non-parametric depending on the level of prior knowledge of the structural system that requires the system identification (Masri, 1994).

76

Parametric identification methods assume the mathematical structure of the model is known from theoretical consideration, apart from some unknown parameters. They provide the estimated system parameters that can easily be associated with identified system parameters such as stiffness and damping. Therefore, deviations in the identified model parameters can be traced to actual changes in the system being estimated.

The nonparametric methods refer to techniques that require little or no theoretical knowledge of the structure. These techniques can be viewed as an approach to evaluate a "black box" system representation. Information regarding the system excitation and relevant output data are fed into a variety of analytical tools to yield the internal system characteristics.

One proposed system identification method for this type of large complicated structure that can capture the time-domain based identification in a reduced order model, would utilize a hybrid parametric and nonparametric approach. The approach will be utilized in a two-stage method. The first step is to identify a linear model, and then treat the un-modeled response as a nonlinear dynamic rather than an error (Smyth et al 2000).

The first step of this approach involves the identification of an equivalent linear model of the structural system. This will be dependent on the amount of responses from the structure. For example if the structure has a known amount of instruments

77

that will produce a response with a known input, the model will have the same number of degrees of freedoms (DOF) and input. Therefore the equation of motion for such a system when pre-multiplied by $M^{-1}{}_{11}$ becomes:

$$M_{11}^{-1}C_{11}\dot{x}_1(t)+M_{11}^{-1}K_{11}x_1(t)+M_{11}^{-1}M_{10}\ddot{x}_0(t)+M_{11}^{-1}C_{10}\dot{x}_0(t)+M_{11}^{-1}K_{10}x_0(t)=-I\ddot{x}_1(t_1)$$

(4.1)

where:

M_{11}, C_{11} and K_{11} are the typical mass, damping and stiffness matrices, which characterize the forces associated with the unconstrained DOF of the system. Each of these is an $n_1 \times n_1$ matrix.

M_{10}, C_{10} and K_{10} are constant matrices, which are associated with support or input motions.

$x_1(t)$ is a vector of order n_1 of the active degree of freedom (measured response) displacement, velocity and acceleration, respectively

$$x_1(t)=[x_{11}(t),\cdots,x_{1n1}(t)]^T$$
$$\dot{x}_1(t)=[\dot{x}_{11}(t),\cdots,\dot{x}_{1n1}(t)]^T$$
$$\ddot{x}_1(t)=[\ddot{x}_{11}(t),\cdots,\ddot{x}_{1n1}(t)]^T$$

(4.2)

and $x_0(t)$ is a vector of n_0 order of the support displacement, velocity and acceleration, respectively.

78

$$x_0(t) = [x_{01}(t), \cdots, x_{0n0}(t)]^T$$

$$\dot{x}_0(t) = [\dot{x}_{01}(t), \cdots, \dot{x}_{0n0}(t)]^T \qquad\qquad (4.3)$$

$$\ddot{x}_0(t) = [\ddot{x}_{01}(t), \cdots, \ddot{x}_{0n0}(t)]^T$$

These system matrices and their shorthand notations and dimensions are summarized as follows:

Matrix product	$M_{11}^{-1}C_{11}$	$M_{11}^{-1}K_{11}$	$M_{11}^{-1}M_{11}$	$M_{11}^{-1}C_{10}$	$M_{11}^{-1}K_{10}$
Shorthand notation	^2A	^3A	^4A	^5A	^6A
Dimension	$(n_1 \times n_1)$	$(n_1 \times n_1)$	$(n_1 \times n_0)$	$(n_1 \times n_0)$	$(n_1 \times n_0)$

Table 4.3: Summary of shorthand notations for the identified system matrices.

The parameters of the above-mentioned matrices can be obtained by setting the problem as a series of over determined equations and then getting the unknown parameters by utilizing the least-square solution method. This is done by writing each row of these matrices of the above-mentioned equation of motions at every discrete time-step, $t = [t_1, \ldots, t_N]$, where N is the time step index, yields parallel matrix equations as follows:

$$M_{11}^{-1}C_{11}\dot{x}_1(t_1) + M_{11}^{-1}K_{11}x_1(t_1) + M_{11}^{-1}M_{10}\ddot{x}_0(t_1) + M_{11}^{-1}C_{10}\dot{x}_0(t_1) + M_{11}^{-1}K_{10}x_0(t_1) = -I\ddot{x}_1(t_1)$$

$$(4.4)$$

$$\vdots$$

$$M_{11}^{-1}C_{11}\dot{x}_1(t_N) + M_{11}^{-1}K_{11}x_1(t_N) + M_{11}^{-1}M_{10}\ddot{x}_0(t_N) + M_{11}^{-1}C_{10}\dot{x}_0(t_N) + M_{11}^{-1}K_{10}x_0(t_N) = -I\ddot{x}_1(t_N)$$

$$(4.5)$$

79

Therefore the above equations could be represented by the following equation assuming that mass, damping and stiffness are the unknowns.

$$\hat{R}\hat{a} = \hat{b} \tag{4.6}$$

where $\hat{R}$ is a block diagonal matrix whose diagonal elements are equal to R,

$\hat{\alpha} = \left[\alpha_1^T, \alpha_2^T, \alpha_3^T, \ldots, \alpha_v^T\right]^T$ and $\hat{b}$ is the corresponding vector of excitation

measurements. Keep in mind that $\hat{R}$ is of order $m \times n$ where $m = Nn_1$ and $n = 3n_1$

$(n_1 + n_0)$. This can be shown as follows:

$$\hat{R} \equiv \begin{bmatrix} R & 0 & \ldots & 0 \\ 0 & R & & \\ \vdots & & \ddots & \\ 0 & & & R \end{bmatrix} \qquad \hat{a} \equiv \begin{Bmatrix} a_1 \\ a_2 \\ \cdot \\ \cdot \\ \cdot \\ a_{nl} \end{Bmatrix} \qquad \hat{b} \equiv \begin{Bmatrix} b_1 \\ b_2 \\ \cdot \\ \cdot \\ \cdot \\ b_{nl} \end{Bmatrix}$$

$$\underbrace{\qquad}_{n_1 Nby n_1(2n_1 + 3n_0)} \qquad\qquad \underset{n_1(2n_1 + 3n_0)by1}{} \qquad \underset{n_1 Nby1}{}$$

The above equation could be formulated in several ways depending upon the assumptions, which are made upon a priori knowledge of certain parameters in the system matrices (Masri et al., 1987). In this research we will assume there is no a priori knowledge, and the $\hat{a}$ parameter vector is assumed to either contain coefficients of symmetric or asymmetric system matrices. In the case of symmetric conditions, the $\hat{a}$ vector has fewer parameters, and the $\hat{R}$ matrix must be constructed in a very particular order. However the asymmetric case is quite simple to present. Equation (4.6) can be decomposed into:

80

$$Ra_i = b_i \qquad i = 1, n_i \qquad\qquad\qquad (4.7)$$

For clarity of the parameters, let the following matrices in equation 5.1 $M^{-1}_{11} C_{11}$,

$M_{11}^{-1} K_{11}$, $M_{11}^{-1} M_{10}$, $M_{11}^{-1} C_{10}$, $M_{11}^{-1} K_{10}$ be denoted by ^2A, ^3A, ^4A, ^5A, ^6A

respectively. Also let $<^jA_i> = i^{th}$ row of generic matrix ^jA. Therefore α_I is

represented as follows:

$$a_i = \left[\left\langle ^2A_i \right\rangle, \left\langle ^3A_i \right\rangle, \left\langle ^4A_i \right\rangle, \left\langle ^5A_i \right\rangle, \left\langle ^6A_i \right\rangle \right]^T \qquad (4.8)$$

$$b_i = \left[-\ddot{X}_{1i}(t_1), -\ddot{X}_{1i}(t_2), -\ddot{X}_{1i}(t_3), \dots, -\ddot{X}_{1i}(t_N) \right]^T \quad i = 1, n_I$$

$$(4.9)$$

In combination with either equation 4.6 or 4.7, one can solve for the unknown

parameter vectors $\overset{\wedge}{\alpha}$ or the α_i's by determining the pseudo-inverse of $\hat{R}$ or R

matrices. This can be written as follows:

$$\alpha = \hat{R}^\dagger b \quad \text{or} \quad \alpha_i = R^\dagger b_i \qquad\qquad\qquad (4.10)$$

where $\hat{R}^\dagger$ stands for the pseudo-inverse of matrix $\hat{R}$ (Golub and Van Loan, 1983).

The unknown matrix coefficients can now be determined by inserting the pseudo-

inverse into either equation 4.6 or 4.7, which yields an estimated b vector (b_{est}). This

vector simply contains estimates of the accelerations of the active degree of freedom.

Instead of treating the difference between b and b_{est} ($b-b_{est}$) as a molding error, one

can treat it as a nonlinear residual (b_{nl}) to be modeled (Smyth, 1998). In this research

a nonparametric technique is used to model this nonlinear residual.

4.4.1 Modal frequencies, damping and mode shapes

The identified matrices $M^{-1}{}_{11} C_{11}$ and $M_{11}{}^{-1} K_{11}$ can be utilized to obtain the modal frequencies, modal damping coefficients and mode shape. It should be noted however that there is an inherent error since the M_{11} matrix is not known. However the model solution could be derived from these identified matrices by following a standard eigenvalue solution as follows (Inman, 1994):

$$Az = \lambda z \tag{4.11}$$

$$A = \begin{bmatrix} 0 & I \\ -M_{11}^{-1}K_{11} & -M_{11}^{-1}C_{11} \end{bmatrix} \tag{4.12}$$

Since both $M_{11}^{-1}C_{11}$ and $M_{11}^{-1}K_{11}$ are identified through the above mentioned method, at the matrix A is also identified. It has a dimension of $2n_1$ by $2n_1$. Hence the eigenvalue λ_k $(k = 1, 2, ..., 2n_1)$ or $2n_1$ numbers may be complex valued. Therefore the eigenvector Z_k $(k = 1, 2, ..., 2n_1)$ of $2n_1$ number with a dimension of $2n_1$ each, may be complex valued. These complex eigenvalues come in complex conjugate pairs, where n_1 is the physical modal frequencies, w_i, and modal damping coefficient, E_i are related to λ_k by:

$$\omega = \sqrt{\mathrm{Re}(\lambda_{2i-1})^2 + \mathrm{Im}(\lambda_{2i-1})^2} = \sqrt{\mathrm{Re}(\lambda_{2i})^2 + \mathrm{Im}(\lambda_{2i})^2} \qquad i = 1,...,n_1 \tag{4.13}$$

$$\xi_i = \frac{-\mathrm{Re}(\lambda_{2i-1})}{\sqrt{\mathrm{Re}(\lambda_{2i-1})^2 + \mathrm{Im}(\lambda_{2i-1})^2}} = \frac{-\mathrm{Re}(\lambda_{2i})}{\sqrt{\mathrm{Re}(\lambda_{2i})^2 + \mathrm{Im}(\lambda_{2i})^2}} \qquad i = 1,\cdots,n_1 \tag{4.14}$$

In addition the $2n_l$ dimension complex eigenvectors Z_k $(k = 1, 2, ..., 2n_{1j}$ of $2n_l$

numbers also come in complex conjugate pairs. These conjugates are related to the

n_1 dimension complex mode shapes $u_i = a_i + b_{ij}(i = 1, 2, ..., n_i, j = \sqrt{-1})$ in the

following manner:

$$z_{2i-1} = \begin{bmatrix} u_i \\ \lambda_{2i-1} u_i \end{bmatrix}, \quad i = 1, ..., n_1 \tag{4.15}$$

$$z_{2i} = \begin{bmatrix} Conj(u_i) \\ \lambda_{2i} Conj(u_i) \end{bmatrix}, \quad i = 1, ..., n_1 \tag{4.16}$$

It should be noted that the first n_l, rows of the eigenvectors with odd subscript form

the n_l dimension complex mode shapes $u_i = (i = 1, 2, ..., n_l)$.

4.4.2 System Identification of VTB from Big Bear Real-Time data system

As previously mentioned, there are 26 sensors (strong-motion accelerometers)

mounted on the bridge deck, and 10 sensors at its base. However, measurements

from sensor number 14 were not available due to instrumentation problems.

Consequently, for the purposes of the present analysis, the model to be identified will

be considered as having $n_0=10$ inputs and $n_1=15$ outputs. Hence, the order of the

system matrices to be identified is 15 by 15 for $M_{11}^{-1}C_{11}$, and $M_{11}^{-1}K_{11}$, while it is 15

by 10 for $M_{11}^{-1}M_{10}$, $M_{11}^{-1}C_{10}$, and $M_{11}^{-1}K_{10}$. For illustration, the elements of matrix

$M_{11}^{-1}C_{11}$ are shown in Table 4.4 and those for $M_{11}^{-1}K_{11}$ are shown in Table 4.5

Since both $M_{11}^{-1}K_{11}$ and $M_{11}^{-1}C_{11}$ are obtained as a by-product of this identification technique, one can obtain not only the classical normal modes from the solution of the eigenvalue problem associated with $M_{11}^{-1}K_{11}$, but also the damped natural frequencies and corresponding ratios of critical damping which is furnished by knowing $M_{11}^{-1}K_{11}$ as well as $M_{11}^{-1}C_{11}$ (dominant) modal frequencies and damping ratios obtained through the solution of the underlying eigenvalue problem. Notice the method under discussion does not assume anything (or restrict the nature of) about the damping mechanism (whether it is of the "proportional" or non-proportional type).

-0.07	0.10	-0.58	0.28	-0.17	0.43	-0.09	-0.14	0.40	0.24	-0.24	0.16	-0.16	0.33	-0.38
0.58	-0.17	0.30	-0.275	-0.08	-0.36	-0.70	0.55	0.47	-0.30	0.20	0.00	0.12	0.01	-0.02
0.20	-0.14	-0.01	-0.24	-0.72	0.68	0.76	-0.51	-0.35	0.14	-0.26	0.06	0.00	0.25	-0.32
-0.45	0.08	0.23	0.45	0.20	-0.31	1.14	-1.28	-0.83	0.08	0.04	-0.02	-0.08	-0.27	0.24
0.91	-0.31	0.75	-3.25	-0.14	0.33	-1.02	1.36	-1.32	-0.15	0.08	0.20	-0.19	0.29	-0.28
-0.87	0.17	-0.69	1.18	0.21	-0.26	1.50	-0.12	-0.45	-0.10	-0.03	0.13	-0.15	-0.06	0.26
0.09	0.11	-0.39	0.38	0.44	-0.48	-1.32	1.69	0.11	-0.09	0.12	-0.15	0.15	0.20	-0.09
0.01	-0.05	0.05	1.04	-0.12	-0.37	-1.68	1.08	0.62	0.02	0.05	-0.12	0.14	0.11	-0.29
-0.43	-0.20	0.11	0.66	0.45	0.01	0.37	-0.69	0.13	0.01	0.02	-0.05	0.04	-0.10	0.05
-0.78	-0.42	1.1110	-0.58	0.00	0.70	1.08	-1.77	0.21	-0.20	0.13	0.41	-0.31	-0.21	0.10
0.18	-0.94	2.12	-0.57	0.12	0.22	-2.29	0.97	1.10	-0.21	0.26	-0.19	0.25	0.11	-0.26
-1.29	-1.40	0.88	0.72	-0.89	0.15	0.48	-0.16	0.30	-0.39	0.16	-0.08	0.21	-0.02	-0.04
-0.24	-0.88	0.74	0.20	0.46	-0.65	-0.96	-0.09	-0.30	-0.10	0.20	-0.14	0.15	-0.27	0.14
-0.44	-0.13	0.06	-0.19	-0.11	0.13	-1.31	0.38	0.28	0.00	0.03	-0.16	0.18	0.11	-0.20
-0.27	-0.82	0.86	-0.44	-0.11	0.30	0.33	0.63	-0.59	-0.07	0.12	-0.07	-0.02	0.01	0.07

Table 4.4: Sample output of M^{-1}_{11} C_{11} matrix (15 by 15).

84

32.81	-0.62	0.22	-15.57	-0.67	2.17	5.04	-3.80	-2.52	1.81	-1.86	0.25	0.14	0.00	0.46
-9.00	1.14	-0.07	-5.44	0.26	1.57	-1.25	1.58	0.79	-4.53	4.26	0.19	-0.10	-0.08	0.32
6.22	-0.14	0.30	-1.35	0.34	-4.35	-3.29	3.73	-0.28	0.30	-0.26	0.15	-0.08	0.74	-0.73
-7.55	0.13	-0.20	22.04	-0.04	1.75	1.43	-4.12	0.33	1.14	-1.15	-0.14	0.02	-1.56	0.71
1.64	-0.17	0.06	0.76	1.12	-1.25	-5.77	5.73	-1.46	0.07	0.02	-0.04	-0.01	0.30	-0.52
-4.31	-0.28	0.04	-8.58	-1.15	33.41	6.07	-8.96	0.51	0.36	-0.73	0.19	-0.01	-0.72	-0.06
1.31	0.28	0.14	-1.50	-0.80	0.08	10.75	-9.75	0.98	-0.30	0.36	-0.01	-0.02	-0.37	0.61
-0.55	-0.24	0.02	0.25	1.13	-0.48	-7.39	8.76	1.71	-0.20	0.26	-0.13	0.08	-0.45	0.61
-1.36	0.03	0.19	-0.47	-0.13	0.81	1.63	-1.62	5.23	-0.07	0.17	-0.19	0.22	-0.28	0.43
7.14	-2.53	0.36	-1.00	0.10	-2.18	1.36	-1.14	-0.89	12.37	-10.14	-0.28	0.08	-0.50	0.57
-1.29	2.57	-0.30	-7.42	-0.20	2.61	-1.22	1.26	0.77	-13.32	13.78	0.83	-0.29	0.94	-0.64
4.67	0.05	-0.26	-3.33	0.36	0.03	-8.98	7.05	0.63	-0.73	1.06	1.52	-0.33	1.14	-1.60
-3.33	0.57	-0.16	4.78	-0.71	-0.39	7.51	-10.03	1.01	-0.73	1.04	0.25	0.65	-1.78	1.44
-0.69	0.42	-0.63	-3.88	-2.86	-0.14	0.41	3.91	-1.26	-1.29	1.34	0.11	-0.37	10.63	-8.90
-0.90	-0.35	0.41	-0.89	3.15	-0.01	11.60	-1.09	-2.47	1.03	-0.91	-0.24	-0.12	-10.62	16.10

Table 4.5: Sample output of M^{-1}_{11} K_{11} matrix (15 by 15).

Therefore for the reduced order modeling procedure used on the VTB, the corresponding number of degree-of-freedom is 15 in this case. Hence, only 15 modal frequencies can be identified by the reduced-order identification procedure. It should be noted that this is the first time that USC research time has been able to get raw data. As discussed earlier in Chapter 2 the integration of acceleration data is very complicated as to what cut-off frequency is needed for different type of structure. The detailed calibration method used in chapter 2 becomes very important in analyzing earthquake data. It was determined a cut-off frequency of 0.05 Hz. was the appropriate frequency that matches both the optical measurements obtained from the VTB as shown in Chapter 3.

Based on research of how the earthquake data is processed by the California Department of Conservation (CDC), it was determined CDC applies corrections to

85

collected earthquake acceleration. The baseline corrections consist of applying both low and high-pass filters. The low-pass filter is set at a default of 45 Hz, while the corner high-pass filter is set at a default of 0.12 Hz. Therefore, for corrected acceleration data provided by CDC, the low frequencies can not be identified from pervious earthquake records. For comparison purposes table 4.6 shows the results obtained from this earthquake as compared with other frequency estimates by other investigators who studied the behavior of this bridge.

Smyth et al. Dominant Modes (All directions)		Lus et al. (1999) Vertical Composition Modes		Masri (2003) Dominant Modes (All directions)
Whittier	*Northridge*	*Whittier*	*Northridge*	*Big Bear 2003*
0.212	0.225	0.234	0.225	0.078
0.242	0.240	0.388	0.304	0.084
0.317	0.358	0.464	0.459	0.121
0.531	0.390	0.576	0.533	0.127
0.570	0.448	0.617	0.600	0.163

Table 4.6: Comparison between other research studies for earthquake records.

There is a clear, significant dynamic behavior of the bridge, not considered in the dynamic analysis of previous earthquakes and hence emphasizing the need of accurate dynamic analysis which involves calibration of the integration, and determining the proper data reduction procedure and the analysis method. The following table demonstrates the varying results on the first 15 frequencies of applying different cut-off (high-pass filters) on the Big Bear 2003 earthquake record.

86

Frequency Index Number	Cut-off frequency of 0.05 Hz	Cut-off frequency of 0.1 Hz	Cut-off frequency of 0.15 Hz	Cut-off frequency of 0.20 Hz
1	0.0777	0.1889	0.1944	0.2402
2	0.0837	0.2069	0.2340	0.2938
3	0.1210	0.2315	0.2827	0.4080
4	0.1274	0.2596	0.3605	0.4734
5	0.1626	0.3248	0.5151	0.6596
6	0.1755	0.3800	0.6413	0.6759
7	0.1998	0.5151	0.6791	0.7293
8	0.2883	0.5504	0.7158	0.8516
9	0.3631	0.7171	0.8914	0.9479
10	0.6173	0.8143	0.9160	1.0516
11	0.6811	0.9631	1.0439	1.1016
12	0.7549	1.0696	1.2064	1.2391
13	0.8394	1.1458	1.2415	1.2959
14	0.9087	1.3714	1.4886	1.5691
15	1.0103	1.4599	1.8051	1.9856

Table 4.7: Comparison of effects of different frequency cut-off of the Big Bear 2003 earthquake record.

Table 4.8 shows comparison results of ambient vibration analyses of the first ten frequencies identified by other studies of the VTB. The identified frequencies from these studies are very close to each other, and it should be noted neither study detected the lower frequencies. This could be contributed to several factors one being the range set for the high-pass filter of the corrected earthquake acceleration data.

87

Frequency Index	Abdel-Ghaffar (1977)	Pridham et al. (2001)
1	0.168	0.155
2	0.216	0.220
3	0.234	0.232
4	0.366	0.368
5	0.487	0.477
6	0.494	0.531
7	0.542	0.571
8	0.623	0.618
9	0.678	0.633
10	0.740	0.687

Table 4.8: Comparison research studies of ambient vibration records.

Further details regarding the use of this approach to model nonlinear MIMO technique systems are available in the work of Masri et al (1987a, 1987b). The application of this approach to the analysis of strong earthquake motion recorded in previous earthquakes at the Vincent Thomas Bridge is reported in the work of Smyth et al (2003), where significant nonlinear contributions from the bridge response were detected and modeled with fairly good accuracy by using the identification procedure under discussion.

4.4.3 Statistical analysis of Ambient Data

At this point, the structural identification procedure can be used to identify the system matrices corresponding to M, C and K. By repeatedly applying the same structural identification method to different time segments of the data, an ensemble of matrices will be identified. Then the statistical analysis will yield the important statistical measures such as mean, variance, and probability density function (*pdf*).

88

This method could be applied to specified ensemble data sets corresponding to distinct non-overlapping time segments. The results are then used to calculate the mean, standard deviation, and the *pdf* associated with each element of matrices C and K.

This method has been validated on a small scale simulation model. The following figure shows the results of a study done by Agbabian et al., 1990, on a three degree-of-freedom system with 5% noise. The ensemble consisted of 600 non-overlapping data sets. The dashed lines correspond to the estimated *pdf* for each indicated stiffness element while the solid lines correspond to the *pdf* of a data set having the same mean and variance but with exact Gaussian distribution.
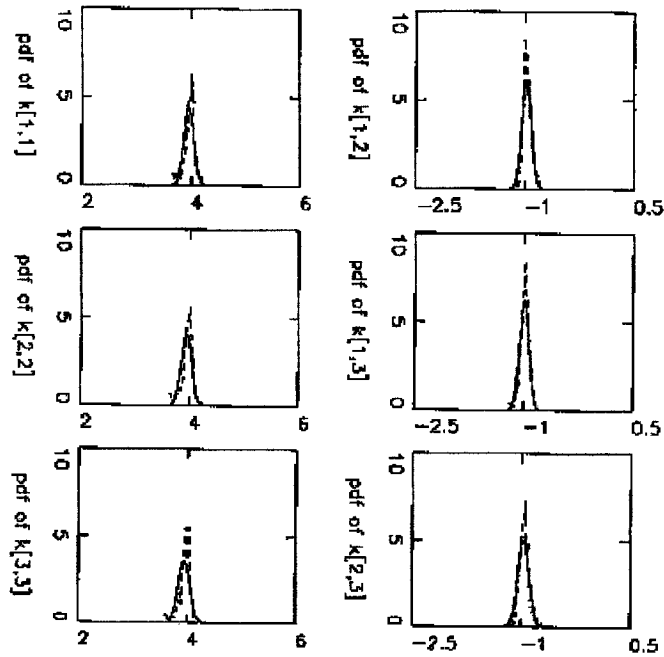
Figure 4.15: Identification Results, *pdf* of 5% Noise-Pollution Level, dotted line is estimated *pdf*, solid line exact Gaussian distribution (Agbabian et al, 1990).

The next step of the algorithm is to calculate the percentage error corresponding to each element of the stiffness matrix. An exact solution is referred to as the reference solution while the changed solutions are used for comparison. In the bridge, data the reference cases will be picked based on relevant information from the bridge. The information will be discussed in detail as the data will be presented later on for discussion. The corresponding dimensionless error is calculated as follows:

$$e_{ij} = \frac{(\bar{k}_{ij} - k_{ij}^*)}{k_{ij}^*}$$ (4.17)

where:

e is the element in the matrix corresponding to the error between the identified mean value and the exact value.

$\bar{k}_{ij}$ is the matrix element corresponding to the mean value of the identified matrix

k_{ij}^* is the exact or reference matrix element.

$$r_{ij} = \frac{(\bar{k}_{ij} - \bar{k}_{ij}^{(0)})}{\bar{k}_{ij}^{(0)}}$$ (4.18)

where:

r_{ij} is the matrix whose element corresponds to the change in the mean values of the identified results.

$\bar{k}_{ij}^{(0)}$ is the reference matrix element.

90

$$d_{ij} = \frac{(\overline{k}_{ij} - \overline{k}_{ij}^{(0)})}{s_{ij}}$$

(4.19)

where:

d_{ij} is the element of the matrix that corresponds to the change in K with

respect to the reference case with respect to the standard deviation.

s_{ij} is the standard deviation element.

The confidence level of the detected changes can be identified by an analysis of

matrix D, whose entries represent the quantitative change in K relative to the

reference K that is expressed as a fraction of the standard deviation of the

corresponding element. The following figure shows the *pdf* plots of the case study

by Agbabian for 5% noise level.
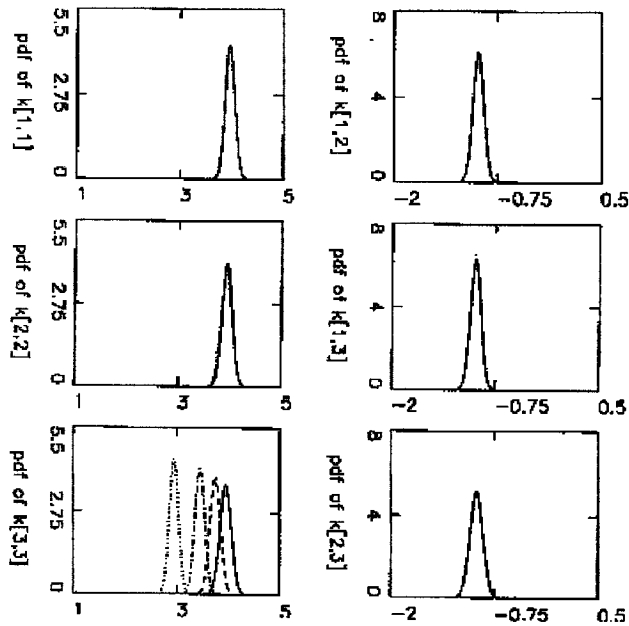
Figure 4.16: Comparison of k_{ij} *pdf* at 5% noise, solid line indicates nominal value, dashed line 10% reduction, dot-dash line 25%, dotted line 50% reduction in k5 (Agbabian, 1990).

91

The following was noted in the Agbabian study:

- The percentage error in the mean value of the identification results corresponds to the dominant diagonal terms of the global stiffness matrix as the noise level changes.

- The dispersions of the statistical variation, for a given noise level, in the estimates of k's are about the same for all elements.

- Increasing the noise pollution by a factor of 4 increased the standard deviation by the same factor.

- Superimposing the *pdf* plots from different tests for elements of the stiffness matrix shows the severity as well as the location of the damage.

- The shift of the superimposed *pdf* curves for the k elements was substantially more than the scatter in the *pdf* curves due to noise-pollution effects.

- Small changes in the structural parameters could lead to a detectable variation in the *pdf* curves.

By utilizing the changes from the R and D matrices, confidence limits may be established on observed changes in the system parameters.

92

4.5   Ambient Vibration Identification of Vincent Thomas Bridge

As noted earlier in order for ambient vibration analysis to be meaningful, the time history record must be long. Therefore to validate the reduced-order discrete system on a large-scale project (MIMO identification procedure), the Vincent Thomas Bridge (VTB) was chosen to be the test bed. In addition, the study utilized the recently installed real-time monitoring system discussed earlier in this chapter, and collected continuous ambient data from the bridge for several days without any interruptions in the data collected. The following section will discuss the analysis and results for these data sets.

In this study, the VTB structural system is analyzed as a reduced order discrete system based on the 15 structural response locations corresponding to the number of operating sensors located on the superstructure. The base input in not considered in ambient vibration analysis. Therefore the analysis parameters value used in this study were $n_1 = 15$ and $n_0 = 0$.

The recorded data from the real-time monitoring system did not have any signal processing. Therefore before performing any system identification analysis, the supplied data was further processed to obtain the displacements and velocities corresponding to the available acceleration records. These algorithms have been validated in previous chapters. Then the MIMO identification procedure was utilized in order to identify the system matrices.

93

4.5.1 Shifted Window Identification

It is reasonable to assume that during ambient vibration, the system is mostly linear. Hence identification may be performed on various time windows of the recorded measurements. The identification procedure can be performed over these selected windows and then each window is shifted by a small amount until the end of the record is reached. The results can then be compiled to track any structural changes. Statistical results from the shifted response segments can be analyzed for any indication of changes in the structural dynamics of the system.

There are various factors that affect the ambient dynamics of a monitored system such as traffic, ambient temperature, wind, and rain. In order to capture the variation effects in the system identification results, one must have a continuous record spanning an extensive period of time. Only then can the small changes reliably can be detected. Therefore, in order to determine the appropriate length of the record needed for the MIMO technique to work, a long record for several days was obtained from the VTB. The recorded time history was one-hour long for a total of 97-hours.

The analysis of the data was then performed in accordance with the above mentioned approach, utilizing a shifted window method where the record was divided into several segments of equal length and the system identification was performed in order to obtain the system matrices. The algorithm repeats the process for each segment, and generates the corresponding $M_{11}^{-1} C_{11}$, $M_{11}^{-1} K_{11}$, natural frequencies,

94

eigenvectors, and damping coefficients. Statistical analyses are then performed in order to detect any pattern changes.

In order to detect changes in the system, the identified matrices must exhibit a statistically significant change. The purpose of this study is to determine the required length of data collected where the output of the method becomes stable. Therefore 97 continuous hours of ambient recording were procured and the statistical implications of the results were analyzed. The averages for each hour of the 97 hours were plotted and compared for both $M^{-1}_{11} C_{11}$ and $M_{11}^{-1} K_{11}$. In order to choose the most critical component of the matrices the averages were normalized with respect to the total mean of all 97-hours in accordance with the following equation:

$$\Delta_{norm} = \frac{(\mu_i - \mu_{all})}{\mu_{all}}$$ (4.18)

where:

Δ_{norm}:   Normalized mean difference.

μ_i: Mean for hour i.

μ_{all}:   Mean for all recorded data.

In addition the covariance was calculated and plotted for the most similar hour in accordance with the following equation. The following figure shows the normalized mean difference and covariance for both $M^{-1}_{11} C_{11}$ and $M_{11}^{-1} K_{11}$ matrices.

95

$$Cov = \frac{\mu_i - \sigma_i}{\sigma_i} \qquad (4.19)$$

where:

Cov: Covariance.

μ_i: Mean for hour i.

σ: Standard deviation for hour *i*.

The 3-D bar plots of the symmetrical sample recorded hour for $M^{-1}{}_{11}\, C_{11}$ and

$M_{11}{}^{-1}\, K_{11}$ matrices are represented by the following figures. The height of each bar

simply represents the magnitude of each matrix coefficients. It can be clearly seen

that both of these matrices are un-symmetric.

96

Normalized Mean Value - M^{-1} K
April 11, 2003

Normalized Mean Value - M^{-1} C
April 11, 2003
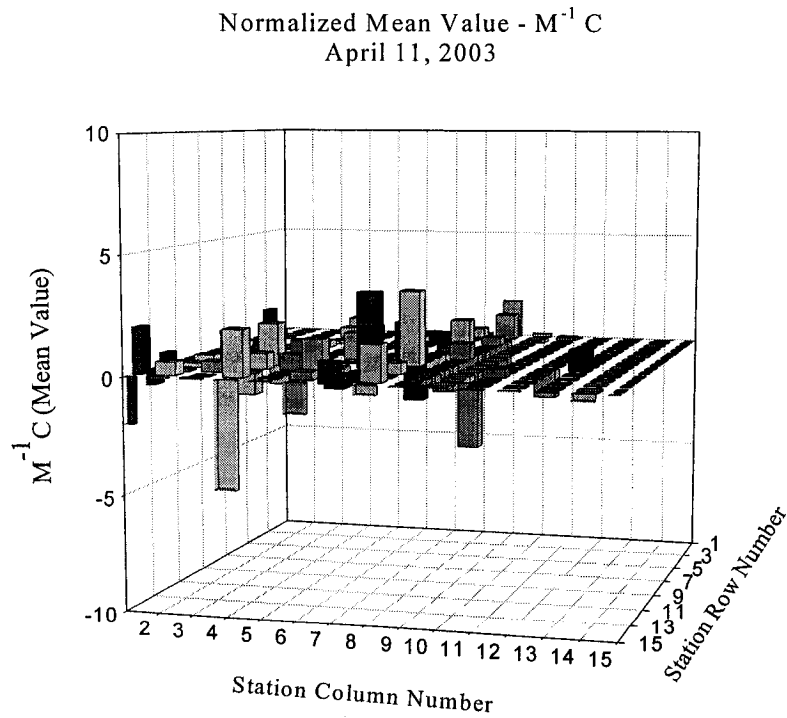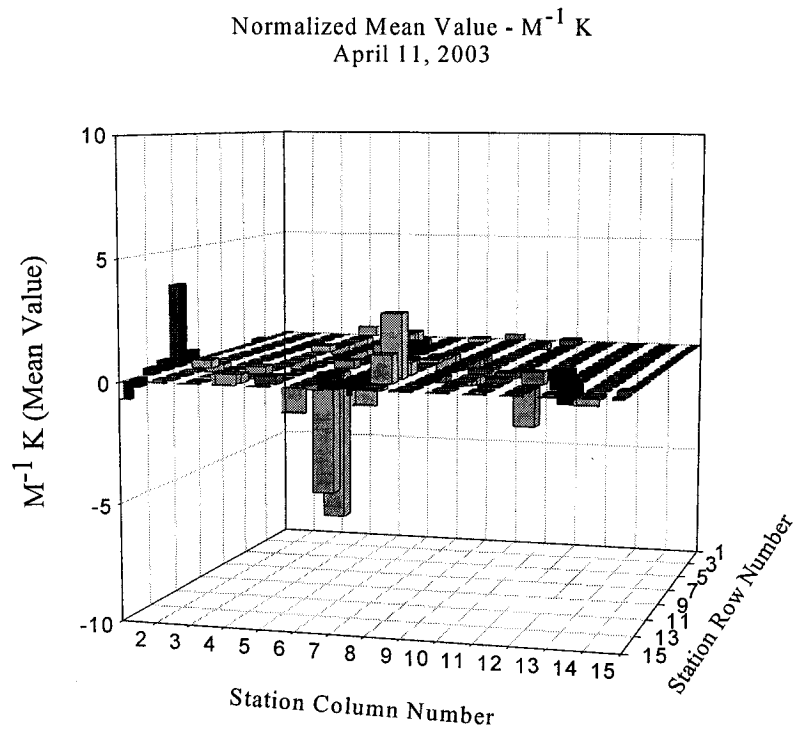
Figure 4.17: Comparison between the normalized first recorded hour of all element of $M^{-1}{}_{11}$ C_{11} and $M_{11}{}^{-1}$ K_{11} matrices with respect to the entire recorded data.

97

Covariance Value - M^{-1} K
April 11, 2003
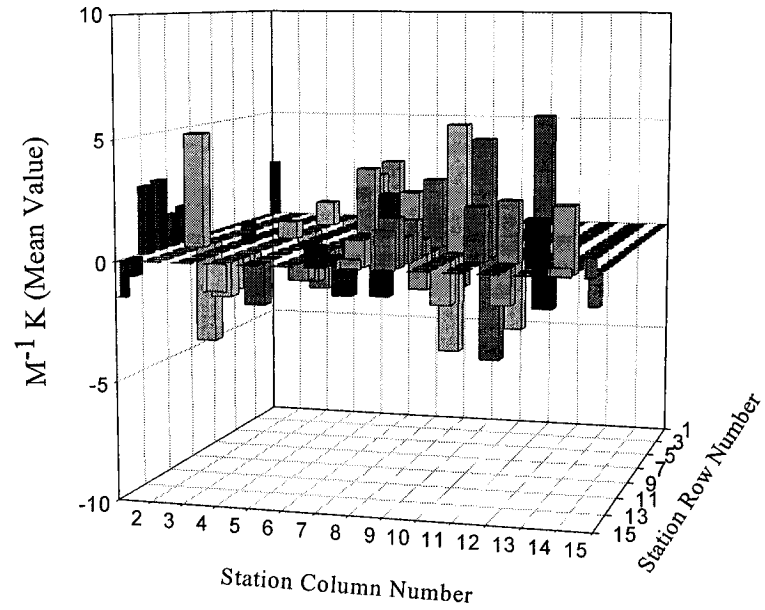
Covariance - M^{-1} C
April 11, 2003
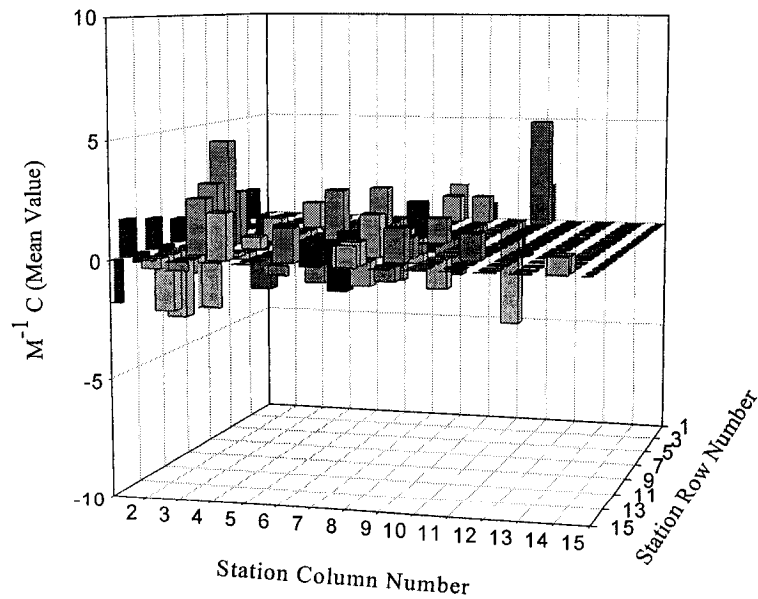
Figure 4.18: Comparison between the normalized first recorded hour of all element of M^{-1}_{11} C_{11} and M_{11}^{-1} K_{11} matrices with respect to the entire recorded data.

98

Based on the analysis of both $M^{-1}{}_{II} C_{II}$ and $M_{II}{}^{-1} K_{II}$ for several recorded hours, three representative elements were selected for further analysis; these elements were K[6,6], K[12,6], and K[13,13].

4.5.2 Probability Density Functions:

Statistical averaging is utilized in order to get a sense of the probability distribution of the system matrix coefficients. This approach could be utilized to assess and calibrate the sensitivity of identification approaches to detect, locate and quantify levels of structural changes. The averaging for these 97 hours was conducted using 69 time-history windows, of one hour length (60,000 points) each, staggered by ten minutes (6000 points) each. The identification procedure under discussion was repeated over for each analysis period.

In order to determine if the a Gaussian distribution is a good estimate of the collected data, a histogram with 100 equal spaced 100 bins was performed on the collected data. It can been depicted in the following figure that the one-hour record shows a crude fit of corresponding *pdf* with the same mean and variance, however for the 97-hour plot it can been seem that fit is much improved. Therefore, the use of Gaussian *pdf* is an applicable estimate for comparison of analyzed data. This emphasizes the need of having very long records for a better estimation of the *pdf*.
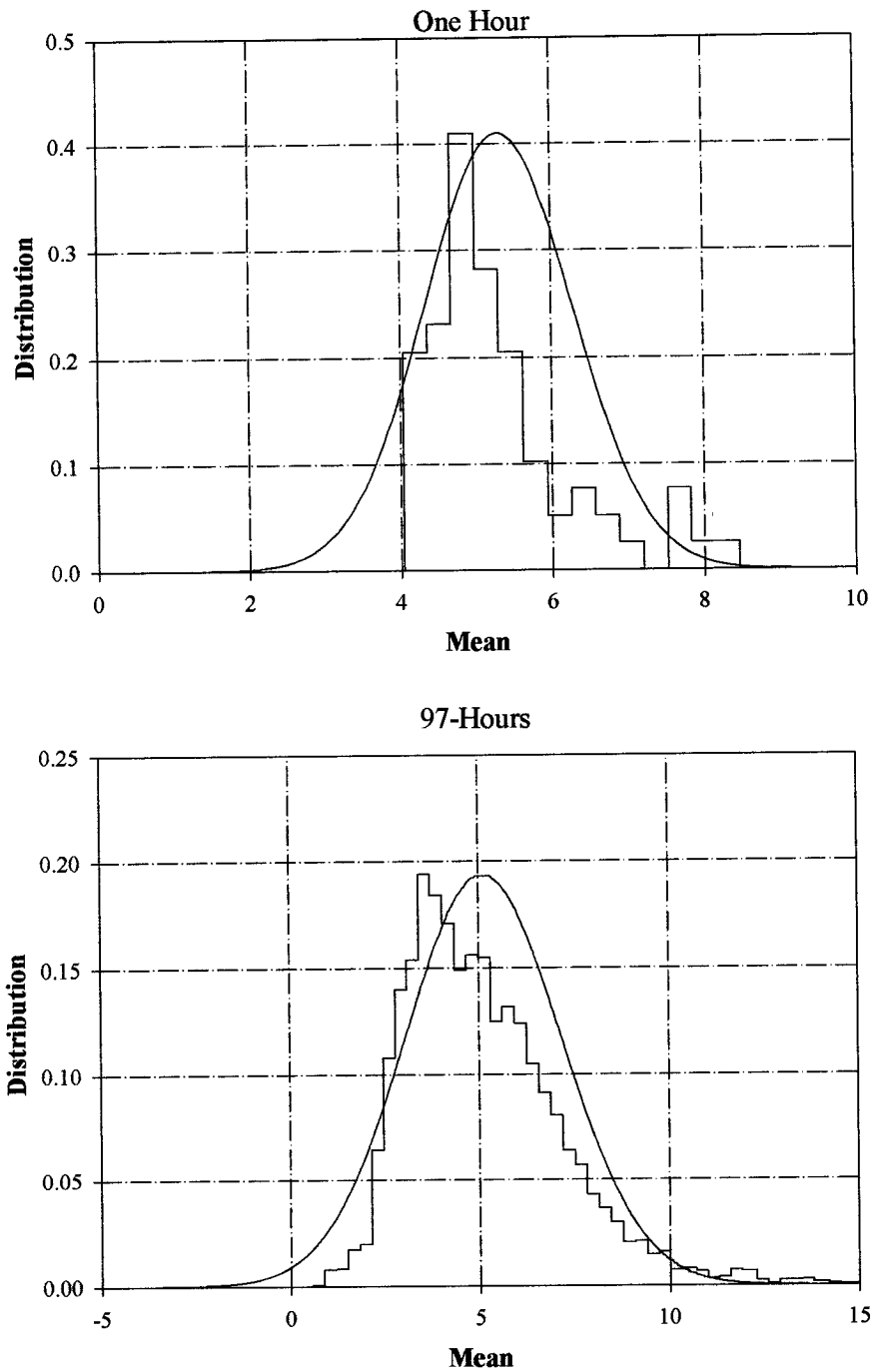
Figure 4.19: Comparison between histograms and corresponding *pdf* with the same mean and variance for 1-hour and 97-hour.

100

4.5.3 Identification Results of $M_{11}^{-1} K_{11}$ and $M_{11}^{-1} C_{11}$ Matrices

The identification of both damping and stiffness matrices C_{11}, K_{11} enables a direct dynamic evaluation of the structure. However, it should be noted from the formulation of the MIMO procedure under discussion that both matrices are pre-multiplied by M_{11}^{-1} hence adding several complicating factors in the evaluation of such matrices. For example, if the mass is very small for an element, one can potentially predict a significant structural change to that element, even though such an element is very minor in nature.

Utilizing the 97-hour recorded data, and 3-D plots of both stiffness and damping matrices shown in figures 4.17 and 4.18, three elements were selected for further analysis. The main focus was to determine at what point the variation of the data is minimal, assuming that it is known that no change has occurred in the bridge structural characteristics during the recorded data. The following figures show a comparison between the estimated *pdf*'s for varying selected periods for the three selected elements, the range of comparisons, ranging from several hours to several days, for both stiffness and damping matrices.
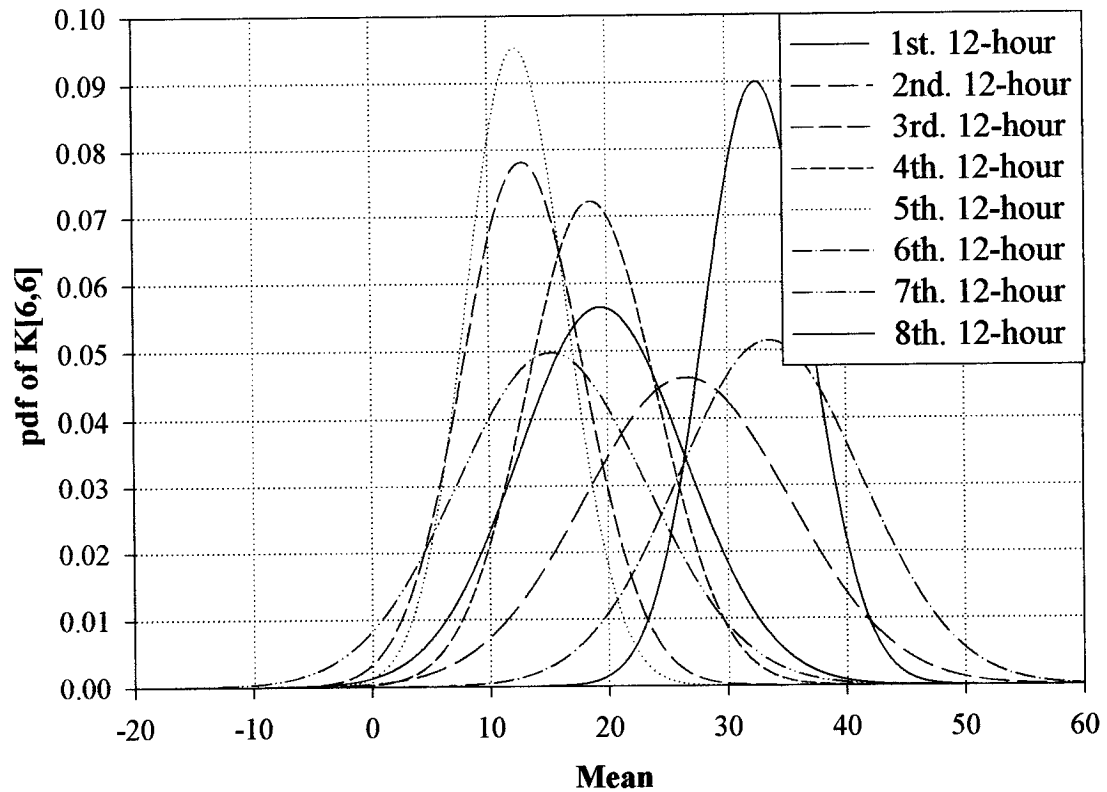
Figure 4.20: Comparison between the *pdf*s for 12-hour selected periods.

It should noted from the above shown figure that for stiffness element K[6,6] a 12 hours comparison periods of the *pdf*'s is a very crude estimate, and one can not make any estimation of structural changes for such element. Therefore, an increase in the record is a must. The following figures show the comparison of one day and two days records.

102
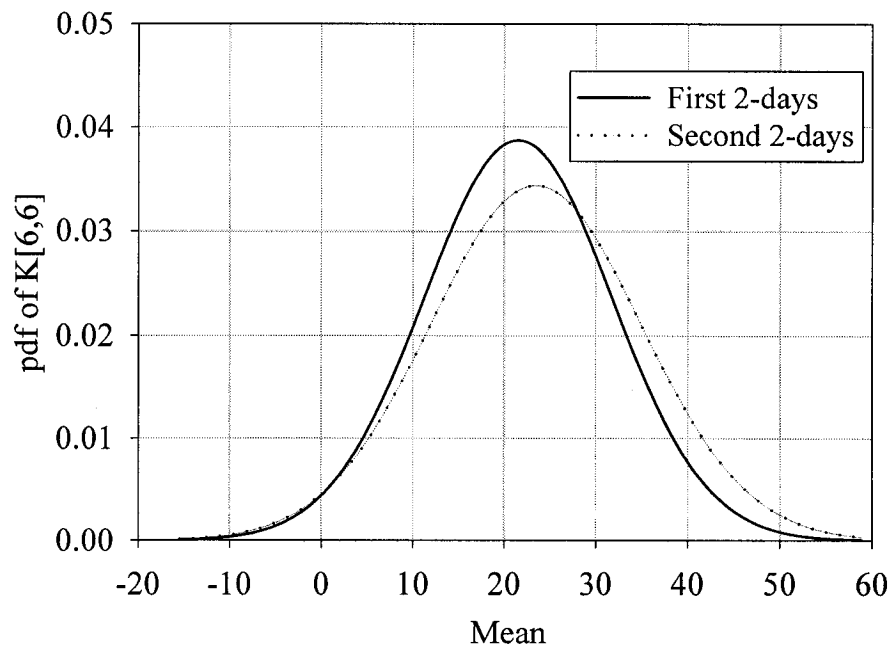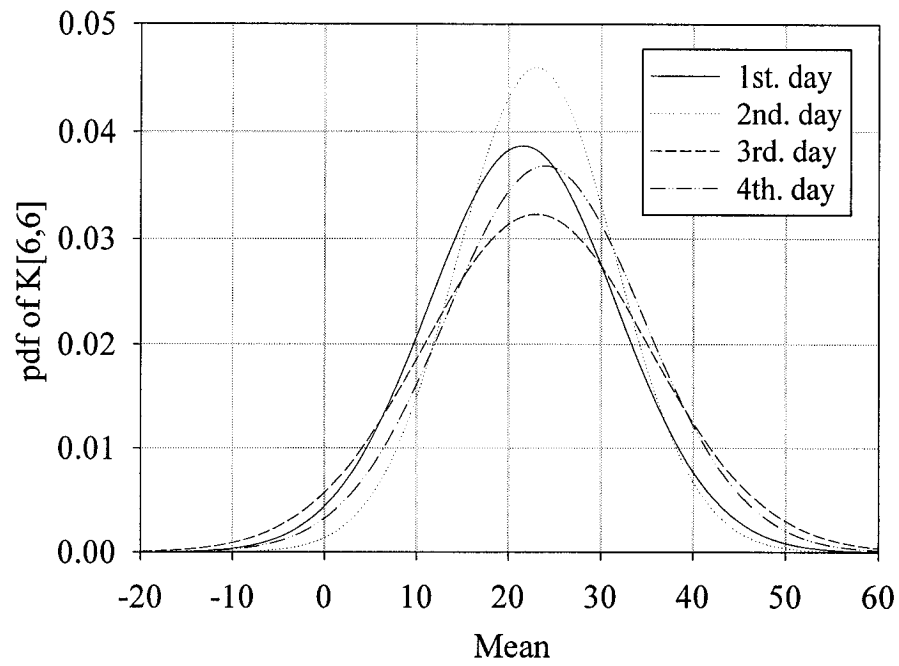
Figure 4.21: Comparison of *pdf* for element $M^{-1}K[6,6]$ of different length of 24 and 48 hours.

103
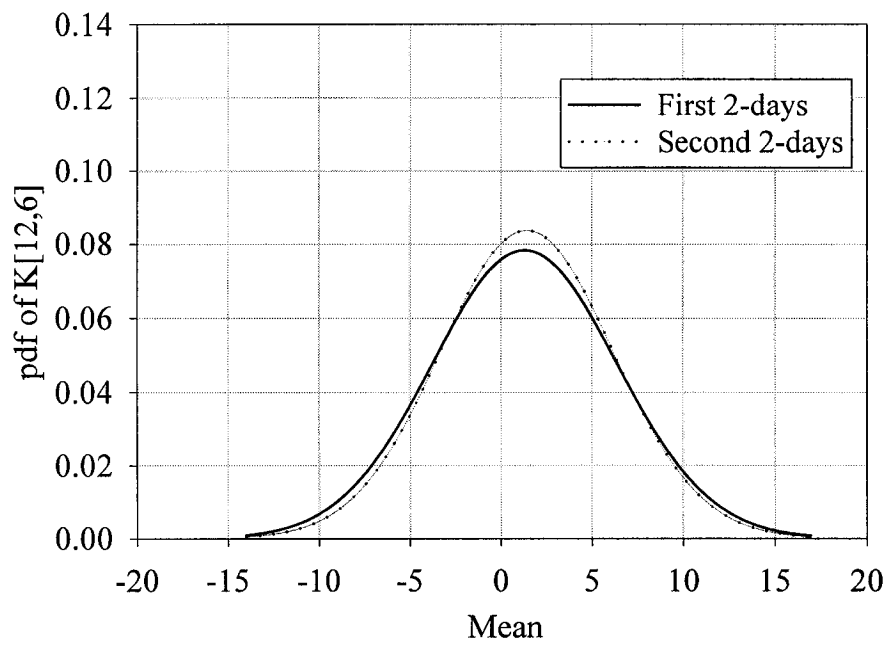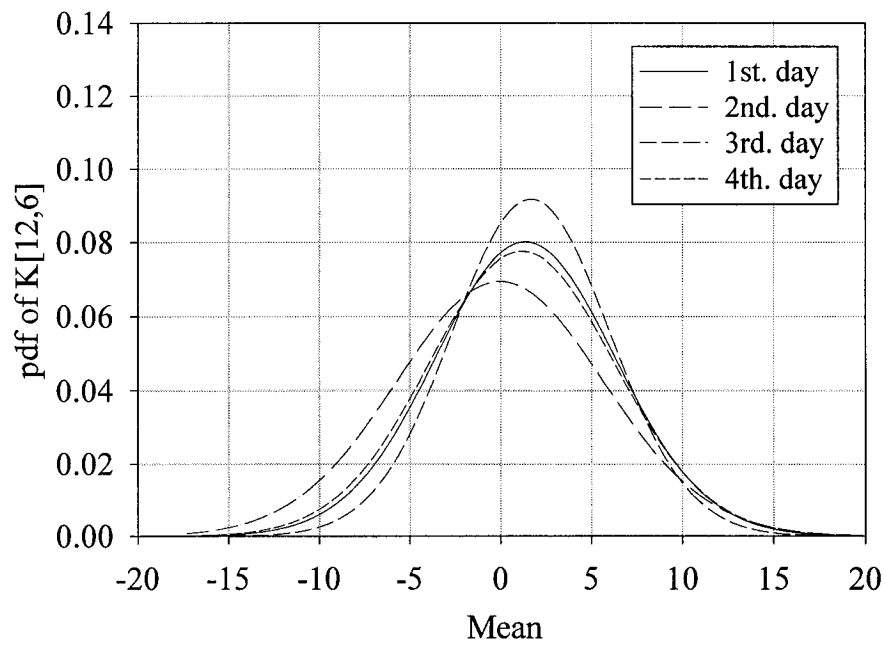
Figure 4.22: Comparison of *pdf* for element $M^{-1}K[12,6]$ of different length of 24 and 48 hours.
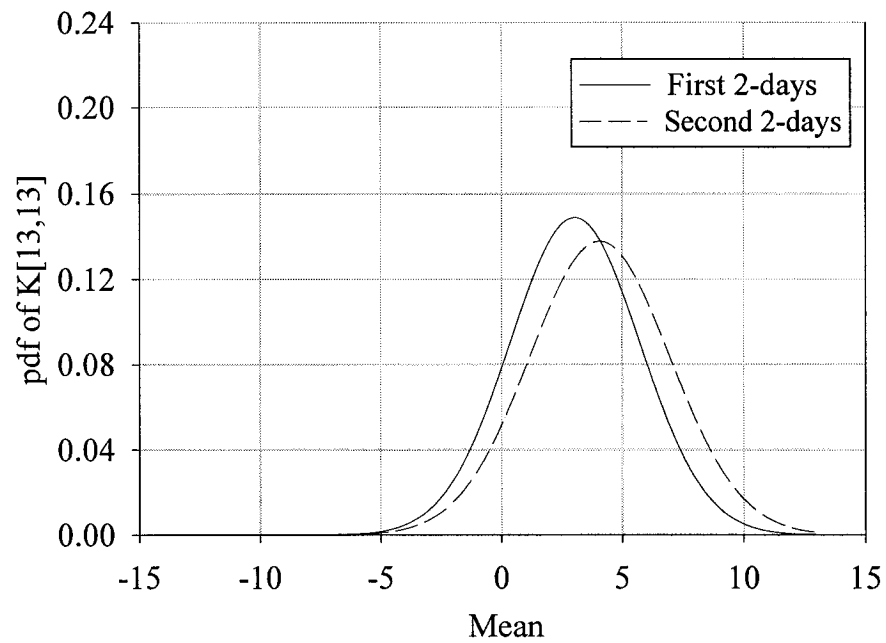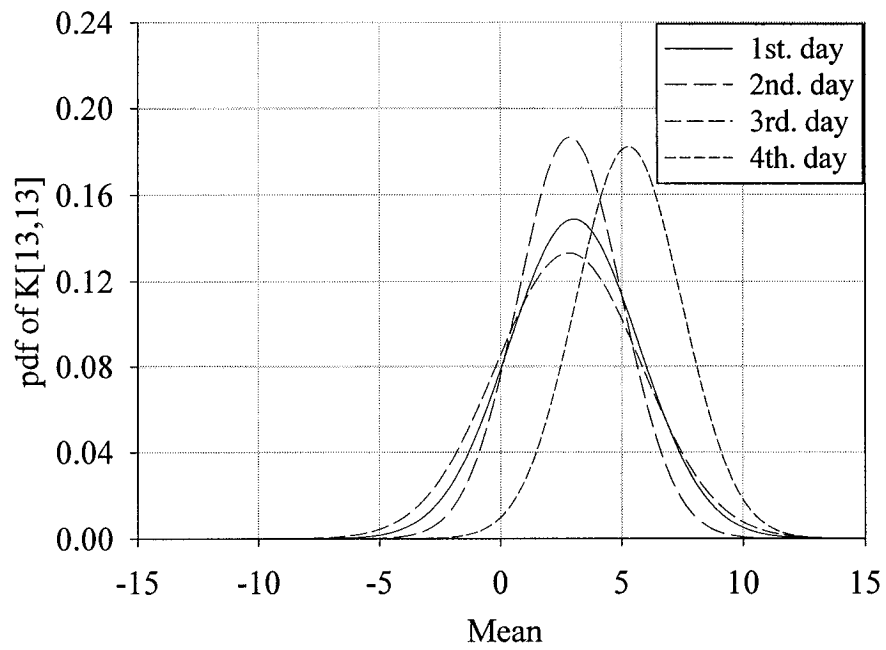
Figure 4.23: Comparison of *pdf* for element $M^{-1}K[13,13]$ of different length of 24 and 48 hours.
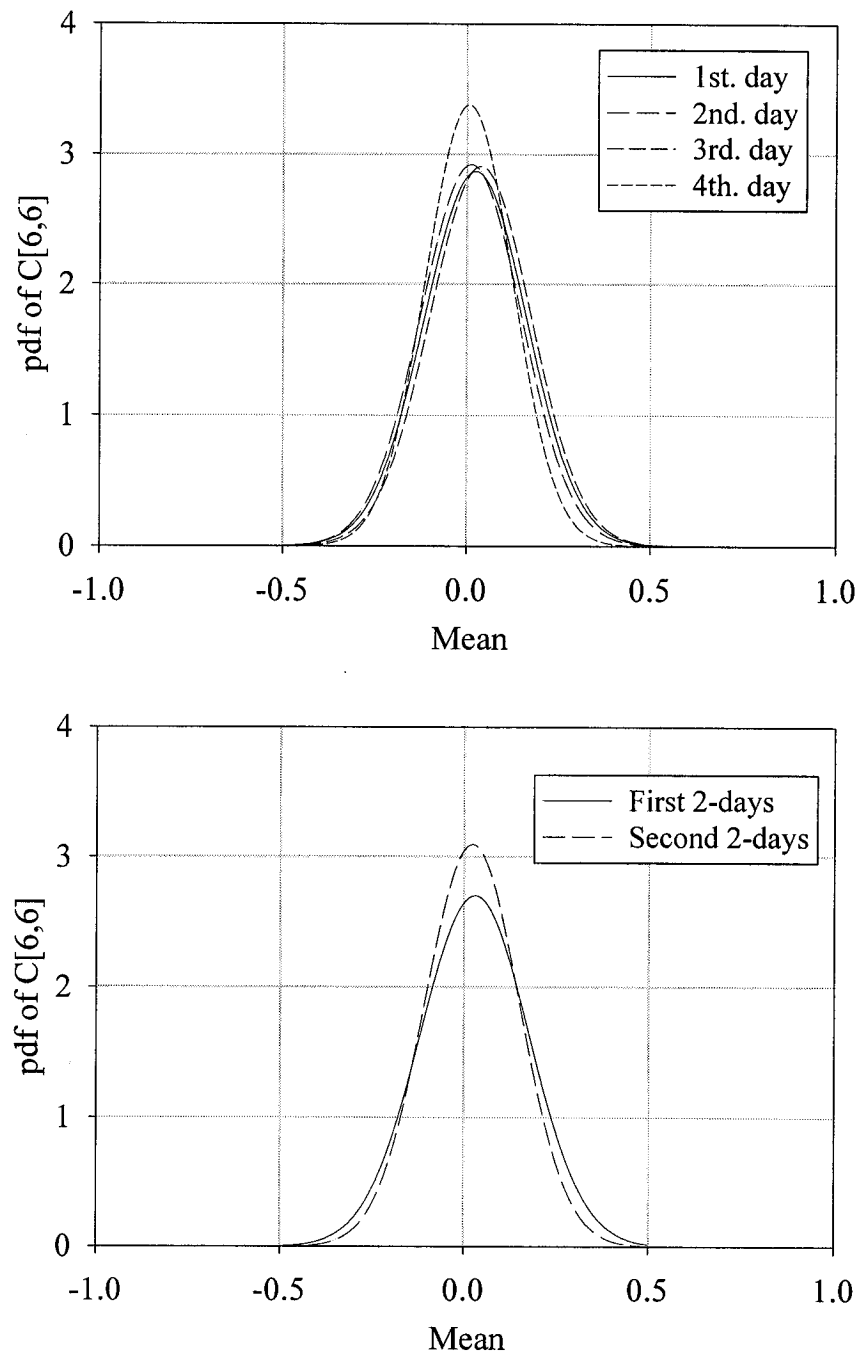
Figure 4.24: Comparison of *pdf* of element M^{-1} C[6,6] for 24-hour and 48-hour.

106
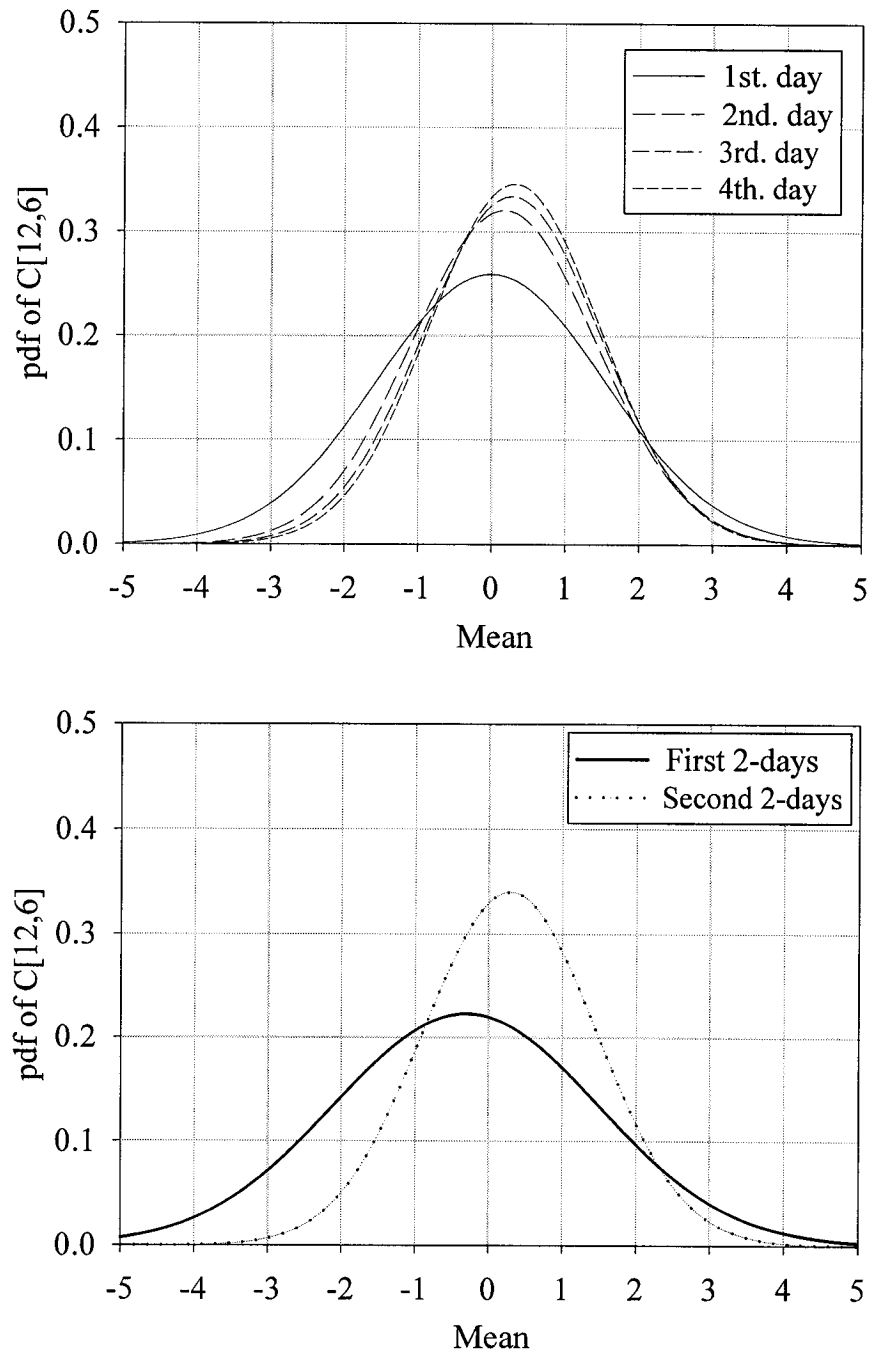
Figure 4.25: Comparison of *pdf* of element M^{-1} C[12,6] for 24-hour and 48-hour.
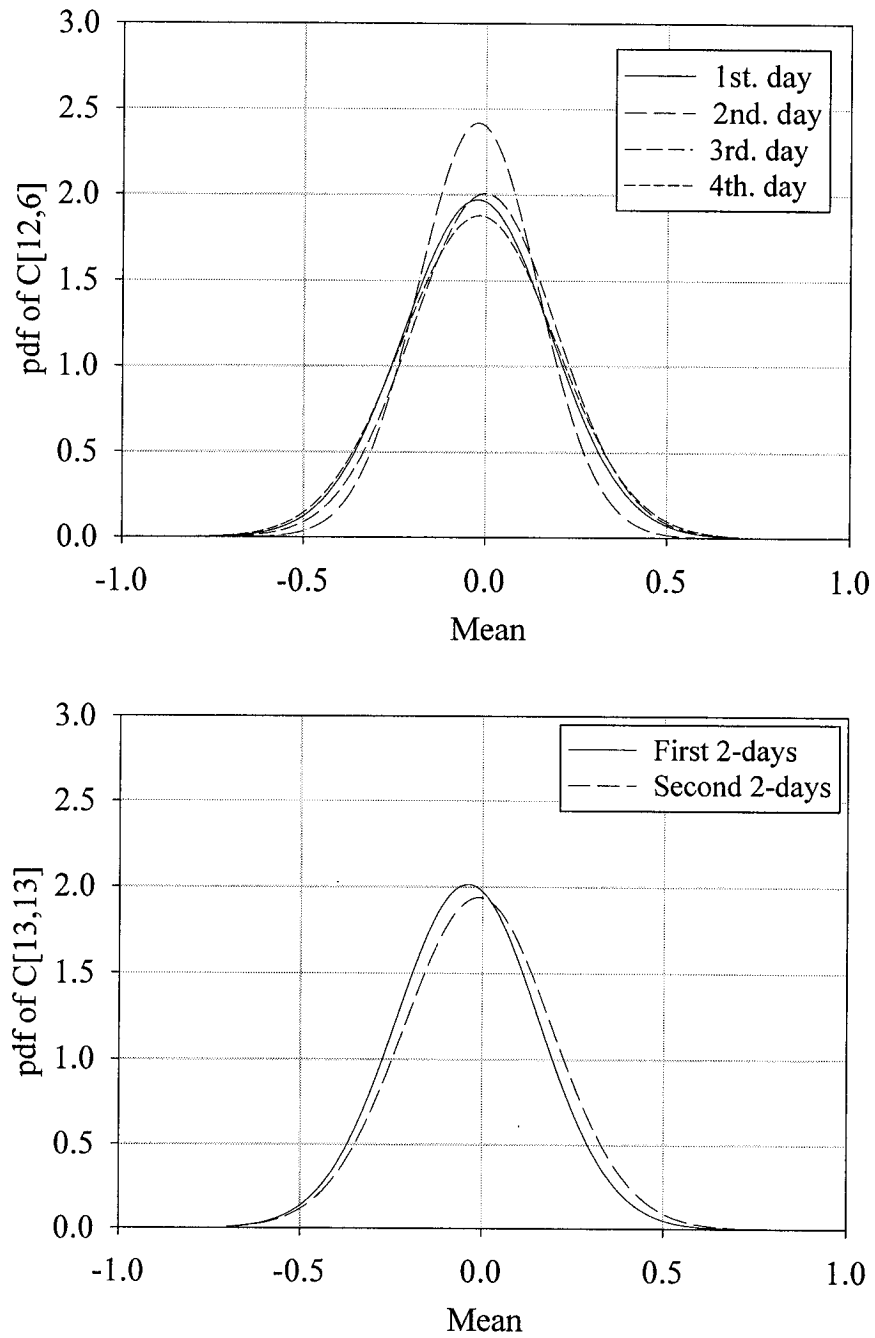
Figure 4.26: Comparison of *pdf* of element M^{-1} C[13,13] for 24-hour and 48-hour.

108

The *pdf* curves clearly demonstrated that the 1/2-day (12-hour) averaging is insufficient since the curves show such significant variance. The one-day (24-hour) averaging shows some stabilization but the variation is still significant. At 2-days (48-hour) averaging, the stiffness matrix indicates minimal variation; therefore based on the limited study reported here at least several days of averaging is needed for a meaningful damage detection analysis.

4.5.4 Mode Shapes Analysis

Another important feature of the reduced order method MIMO procedure under discussion is the extraction of the modal frequencies. In this study, the modal frequencies are actually computed indirectly after the complete reduced-order system matrices are identified. This identification method does not make any assumptions regarding the modal characteristics associated with the identified matrices.

In the reduced-order model of the Vincent Thomas Bridge, the number of degree-of-freedom is 15 which corresponds to the number of sensors on the superstructure. Hence, only up to 15 modal frequencies can be identified for each time-history window. The reduced-order analysis was performed, as mentioned previously, over several windows with lengths of 60,000 data points (i.e, about 120 fundamental periods). The eigenvalues and comparing eigenvectors for each segment are then computed.

109

The mean values for the identified frequencies are quite similar. One must analyze data carefully when using the type of mode-number frequency statistics presented. Since the total number of modes determined by this method depends on the same number of active degrees of freedom (n_l), and therefore is quite possible for a system of a higher order, which the MIMO technique will identify n_l modes which are not the same as the n_l modes in the next window. The least-squares based approach, on which this method is based, will identify the n_l order system that yields the dominant motion, for the particular response time interval. This feature is common to all methods which obtain a second order model with physically meaningful parameters based on discrete location measurements, with no additional *a priori* information on the system dynamics. Therefore, conclusions cannot be drawn from the variation over time of a given mode-number, and the possibility remains of tracking a particular mode by its mode shape and frequency.

In a linear system, mode shapes are used as a time-invariant basis for the displacement profile. Therefore for a system with n_l degrees of freedom, the absolute displacement x (as a function of time t) can be expressed as follows (Crandall and Mark, 1963):

$$x(t) = \sum_{i=1}^{n_l} c_i(t) u_i e^{(-\zeta_i \omega_i \sqrt{1-\zeta_i^2} j)t}$$
(4.20)

where:

c_i's :   mode shape coefficients.

u_i: mode shapes.

110

ξ_i: modal damping coefficients.

ω_i: modal frequencies.

The mode shapes are derived as previously shown in the MIMO formulation approach. For any selected window, a set of mode shapes can be generated. These mode shapes represent the displacement profile at $n_l=15$ stations for a total of $n_l=15$ mode shapes that correspond to the specific window. Each mode shape is composed of $n_l=15$ discrete points showing the relative displacement at the 15 sensor locations. It should be noted that in this study all recorded acceleration measurements have the same unit of translational movement. Each plotted mode shape vector is normalized to have a Euclidian norm of one.

In order to capture a feel for these mode shapes, a 3-D bridge-like model was developed. However, since most of the instruments are located on the eastern half of the bridge, only a half bridge model was developed. The depicted mode shapes use only experimental measurements, no assumptions about the overall response of the bridge, where no sensors are available, were made. The reason for that is if interpolating was implemented for the other half of the bridge one can not exactly determine if the interpolated mode is a symmetric or anti-symmetric. Therefore, the presented mode shapes in this study are only representing were actual sensor data were collected.

111

In order to maximize the possible structural behavior of the bridge, three different time periods were selected to be analyzed. It was decided to pick two rush-hour time periods, since the traffic will be the heaviest, and at least one time of the day when traffic is expected to be slow. It was decided to select 8 a.m. and 5 p.m. as representatives of rush hour traffic, and noon would as an example of less traffic. The following figures depict the first identified 15 modes for the aforementioned three different time periods.

112

North

Mode 1 Lateral   Mode 2 Lateral   Mode 3 Lateral

Mode 4 Vertical   Mode 5 Vertical   Mode 6 Vertical

Mode 7 Vertical   Mode 8 Lateral   Mode 9 Torsion

Mode 10 Torsion   Mode 11 Torsion   Mode 12 Torsion

Mode 13 Torsion   Mode 14 Torsion   Mode 15 Torsion
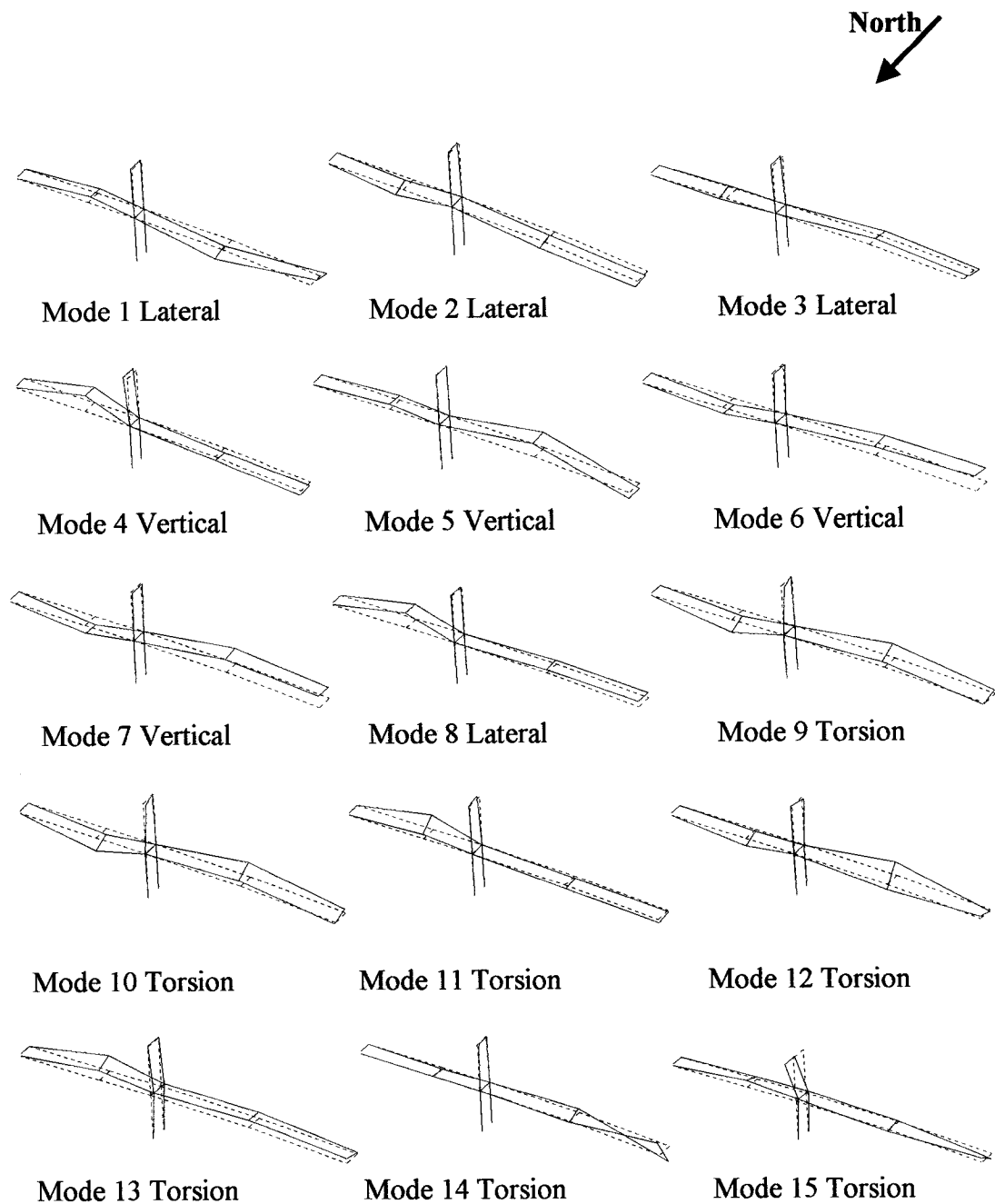
Figure 4.27: The identified mode shapes results for 07:45 a.m. until 08:45 a.m.

113

North

Mode 1 Lateral   Mode 2 Lateral   Mode 3 Lateral

Mode 4 Vertical   Mode 5 Vertical   Mode 6 Vertical

Mode 7 Vertical   Mode 8 Vertical   Mode 9 Torsion

Mode 10 Torsion   Mode11 Torsion   Mode 12 Torsion

Mode 13 Torsion   Mode 14 Torsion   Mode 15 Torsion
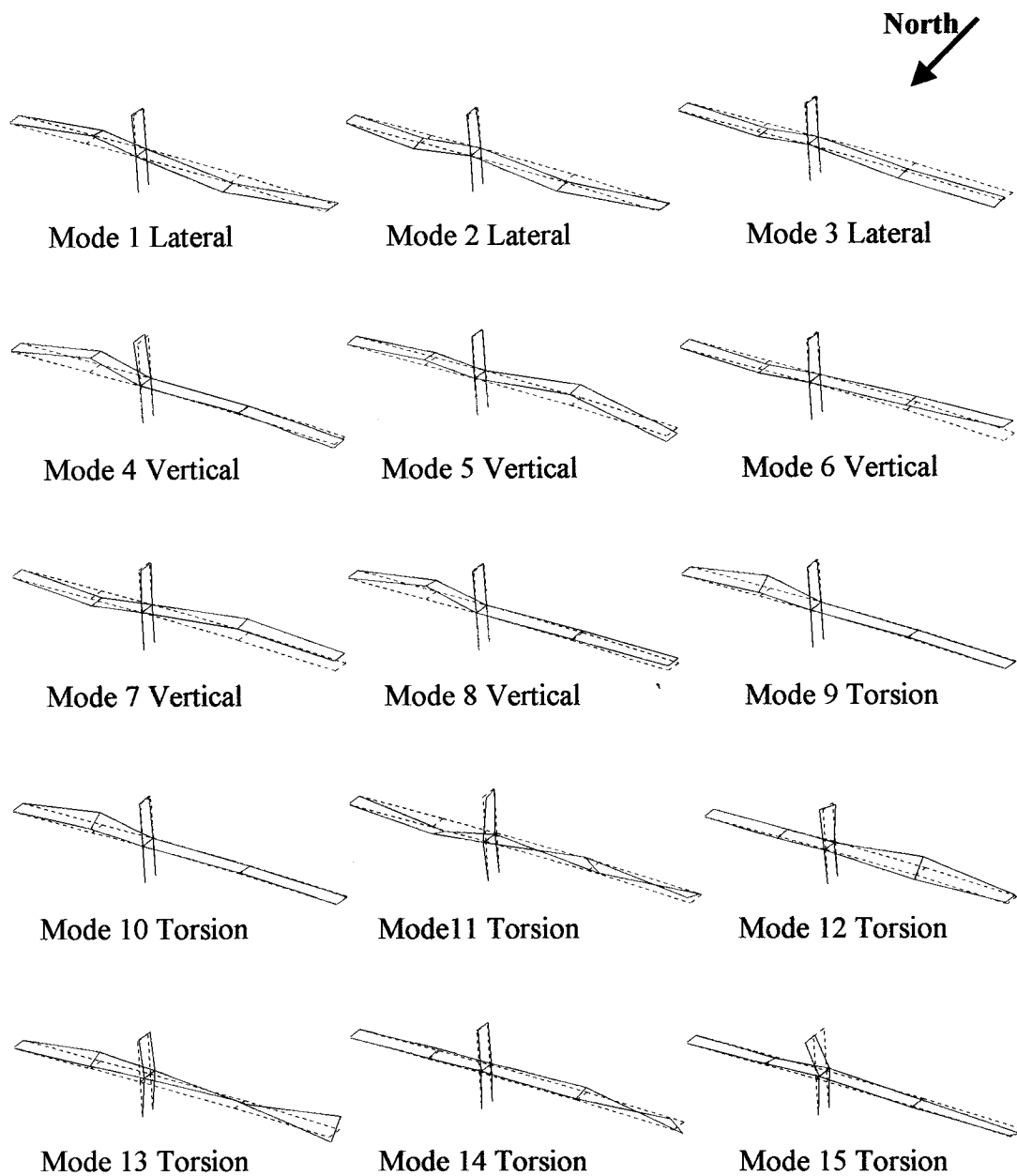
Figure 4.28: The identified mode shapes results for 11:45 a.m. until 12:45 p.m.

North

Mode 1 Lateral — Mode 2 Lateral — Mode 3 Lateral

Mode 4 Vertical — Mode 5 Vertical — Mode 6 Vertical

Mode 7 Vertical — Mode 8 Vertical — Mode 9 Torsion

Mode 10 Torsion — Mode 11 Torsion — Mode 12 Torsion

Mode 13 Torsion — Mode 14 Torsion — Mode 15 Torsion
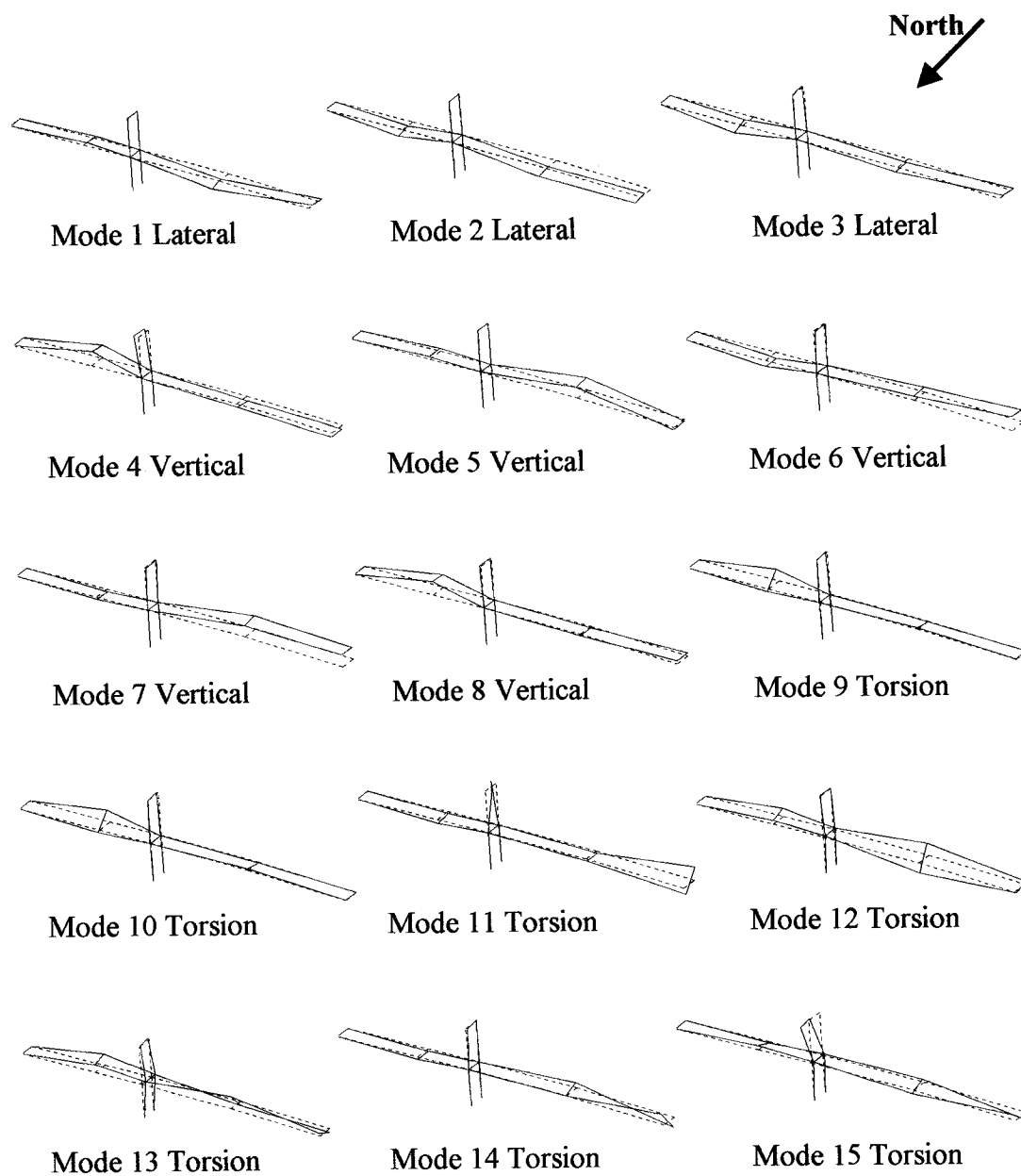
Figure 4.29: The identified mode shapes results for 04:45 p.m. until 05:45 p.m.

4.5.5 Discussion of results

In order to further compare the frequency results from the NASTRAN output and from the MIMO procedure, the following tables present these results. The results are very comparable as expected.

Frequency Number	April 14, 2003 8:45 a.m.	April 14, 2003 12:45 p.m.	April 14, 2003 5:45 p.m.
1	0.0600	0.0600	0.0596
2	0.0658	0.0660	0.0646
3	0.0732	0.0734	0.0737
4	0.0925	0.0851	0.0868
5	0.1426	0.1354	0.1394
6	0.1822	0.1701	0.1706
7	0.2045	0.1842	0.1895
8	0.2377	0.2242	0.2153
9	0.2719	0.2725	0.2750
10	0.3168	0.3136	0.3118
11	0.3740	0.3949	0.3789
12	0.4566	0.4391	0.4497
13	0.5381	0.5921	0.5252
14	0.6499	0.6696	0.5759
15	1.0424	1.0071	0.7659

Table 4.9: Corresponding NASTRAN frequency results for the above shown mode shapes.

116

Frequency Number	April 14, 2003 8:45 a.m.	April 14, 2003 12:45 p.m.	April 14, 2003 5:45 p.m.
1	0.0580	0.0593	0.0612
2	0.0692	0.0647	0.0652
3	0.0723	0.0726	0.0733
4	0.0979	0.0867	0.0877
5	0.1472	0.1366	0.1447
6	0.1900	0.1768	0.1727
7	0.2053	0.1819	0.1871
8	0.2205	0.2324	0.2103
9	0.2571	0.2586	0.2436
10	0.3196	0.3018	0.3080
11	0.4324	0.4127	0.4408
12	0.4840	0.4713	0.4859
13	0.5894	0.6552	0.5584
14	0.7290	0.7396	0.6153
15	1.0789	1.0376	0.8272

Table 4.10: Corresponding MIMO identification method frequency values for the above mentioned mode shapes.

The mode shapes analysis indicates the modes are essentially the same for all three different hours, without any significant change to the general shape of the identified mode shapes. In addition the identified modal frequencies are essentially very close to the first ten modes, while there is a more significant percentile change in the higher order frequencies.

In addition, it can clearly be observed from the real-time monitoring, that a statistically significant collection of long records is needed in order to be able to recognize any pattern of change. The real time monitoring method is an ideal method to utilize in collecting a long record of data.

117

4.6   Optimum number of sensors on the Vincent Thomas Bridge

The number of sensors on the Vincent Thomas Bridge is far from being adequate for obtaining sufficient spatial resolution of the identification results. Therefore, this part of the study focuses on determining the optimal number of sensors needed in order to perform a reliable structural damage detection investigation. The main focus of this section consists of generating synthetic data via a very detailed finite element model of the bridge, and then utilizing the identification approach under discussion to detect the pre-established structural changes.

4.6.1   Description of the Finite Element Model for VTB

In order to have a more reliable approach to the structural changes of the VTB bridge a detailed finite element model was used in generating the synthetic data. The detailed finite element model consisted of a model similar to the one developed during the VTB seismic retrofit program. This study utilized a NASTRAN platform for performing the finite element analysis. The finite element model consisted of 11980 nodes. In addition the analysis of the suspension bridge included the following general features:

- Geometrically nonlinear formulation.
- Multiple support ground motion.

118

The bridge model was idealized as assemblies of finite elements in order to capture the complicated geometry, stiffness and inertia effects. Several elements were used in modeling, the VTB model could be categorized in four main categories, these categories are the bridge deck, towers, cable system, and boundary conditions. The following discusses some of the main elements of the suspension bridge:

The deck category included the stiffening trusses, lateral bracing, cross beams, stringers, and reinforced concrete deck. For the *stiffening trusses*, the chords, verticals, and diagonals were modeled with 3-D elastic beam elements. The *lateral braces* were modeled with 3-D truss elements. Elastic elements were used initially; significant inelastic behavior of the braces was evaluated using either the methodology of elastic/plastic tension. The *cross frames* were modeled with 3-D elastic beam elements. Plastic hinging elements were used where necessary. The *stringers* were modeled with 3-D elastic beam elements and inelastic behavior was again not anticipated. The *reinforced concrete deck* was modeled with elastic membrane elements, composite with the chords of the stiffening trusses. When tension stresses were high enough to crack the deck, the inelastic behavior of the deck was simulated by modeling with either:

- Strut (compression only) and tie elements.
- Inelastic concrete material.

The joints in the deck (and the dowels across the joints) were included in the model. The sharing of the lateral load between the lateral braces and the reinforced concrete deck, and the transfer of load (through the cross frames) from the deck to the lateral

119

bracing at the ends of the span, was of particular interest (since only the lateral bracing is connected to the wind shoes).

The tower category consisted of tower shaft, tower bases, tower struts, wind shoes, and anchorages. The *tower shafts* were modeled with 3-D beam elements. Although elastic elements were used initially, demand/capacity ratios were for peak stress versus critical or yield stress. The *tower bases* shafts were modeled with a grid of gap/impact elements to capture any rocking or uplift of the towers. The anchor bolts restraining the tower shafts were modeled with elastic/plastic truss elements (with initial stress). When there was significant yielding of the tower bases, the bottom portion of the tower shafts were modeled with membrane finite elements so the rounding of the tower bases was properly reflected in the global behavior of the bridge, and so that consistent forces and displacements were supplied for the detailed analysis of the tower bases. The *tower struts* were modeled with 3-D beam elements. The gusset plates were modeled with rigid beam elements. Elastic elements were used initially; significant inelastic behavior of the struts was evaluated using one of the following methodologies:

- Elastic/plastic tension only braces.

- Inelastic braces.

The *wind shoes* were modeled with gap/impact elements. The refinement of the modeling was dependent on the importance of the impact. Rayleigh damping was also included in the model. The anchorages were modeled with lumped masses, located at their center of gravity.

120

The third category was the cable system which consisted of main cables, suspenders, cable bents. The *main cables* were modeled with 3-D elastic truss elements. The model was finely discretized near the towers to capture the transverse forces on the substructure elements. Each *suspender* was modeled with a 3-D elastic truss element, no compression allowed, and the *cable bents* were modeled with 3-D beam elements. Plastic hinging elements were used when necessary.

The final category consisted of boundary structures, impedance matrices, damping, and links. For the *boundary structures*, the approach structures were modeled with boundary springs and masses. The *impedance matrices* were coupled 6×6 degree of freedom impedance matrices were used to support the model; stiffness, mass, and damping matrices were used beneath the anchorages and towers. The model was driven with equivalent force input derived so as to reproduce the free field motion in the absence of the structure. The *damping* was included as viscous dampers in the model since they were added to the VTB as part of the retrofit schemes. Linear dampers were used, or more general force-velocity relationships were used where appropriate. Dampers were added between the spans and the towers and cable bents. They were modeled with nonlinear damping elements with a force-velocity relationship of

$$F = (2.5 \text{ kip} \cdot \text{sec} / \text{in}) \cdot V, \text{ at the towers, and}$$

$$F = (5.0 \text{ kip} \cdot \text{sec} / \text{in}) \cdot V, \text{ at the cable bents bottom chords of the trusses.}$$

121

One damper was placed on each chord of the bridge, at each of the six expansion joints between the spans and the towers and cable bents. The *links* between the cable bent trusses were attached to the end verticals of the stiffening trusses at the floor truss top chords. The "Hinges" were inserted into the side span stiffening trusses, effective for vertical bending only. This was accomplished with the following details:

- Portions of the bottom chords of the stiffening trusses were removed at specific location points.

- New diagonal and vertical members were inserted into the model, adjacent to the hinges.

- New floor trusses were inserted into the model, at the locations of the hinges.

- End releases, simulating physical hinges, were inserted into the ends of the diagonal chord, and vertical members meeting at the hinges.

- Dampers with a force-velocity relationship of

  $F = (100 \text{ kip} \cdot \sec^{1/2} / \text{in}^{1/2}) \cdot V^{1/2}$ were put in place of the removed portion of the chord members.

- Structural fuses with a capacity 1600 kip were put in parallel with the dampers (to carry live load); these can break during the seismic excitation.

4.6.2 Description of the FEM analysis on the Vincent Thomas Bridge

The finite element model was used extensively to generate synthetic data through different scenarios. The goal of this study was to determine the optimum number of sensors needed to get a reliable evaluation of the bridge behavior. First of all, a

static evaluation of the bridge was performed to determine the highest stressed member of the bridge. The dynamic analysis was then performed by first applying a uniform white noise through a unit load in all directions at the deck, and the dynamic analysis was repeated after reducing the stiffness of the highest stressed member by 99% or virtually eliminating such a member.

The analyses were repeated several times utilizing 21, 39 and 75 sensors spaced equally throughout the bridge. It was found that most practical and optimal number of sensors was 75 sensors. Acceleration data from both un-damaged and damaged analyses were obtained from the FEM for 75 sensor locations on the deck. Figure 4.30 shows the global locations of these 75 sensors. It should be noted that the upper locations of these sensors only record the vertical motion, while the lower locations record both vertical and lateral motions.
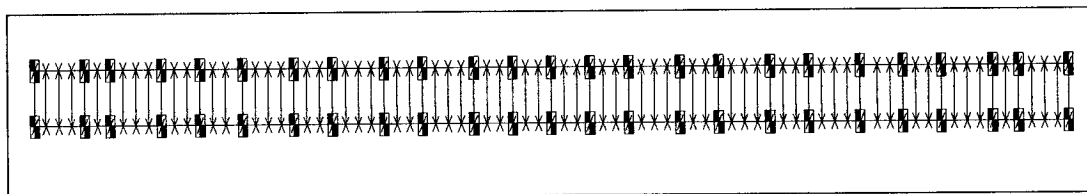
Figure 4.30: Deck sensors location of the FEM of the VTB model. The upper sensors record only vertical motions, while the lower ones records both vertical and lateral motions.

It was determined from this analysis that the 75 sensors were adequate to detect changes such as the idealized "damage" introduced in this study in the bridge. The next approach was to determine the minimum number of sensors one can use to detect changes in the bridge. Therefore the next part of the study was carried further

123

by utilizing the MIMO procedure with a "roving" set of different number of sensors. The roving method consisted of utilizing only selected numbers of the 75 sensors then shifting the fixed number of sensors and repeating the analysis again until the entire 75 sensors are utilized in the analysis. Three different sets of numbers were selected for this study, 9 channels at a time, 18 channels, and finally 36 channels. The following figures demonstrate the main idea behind the roving method.
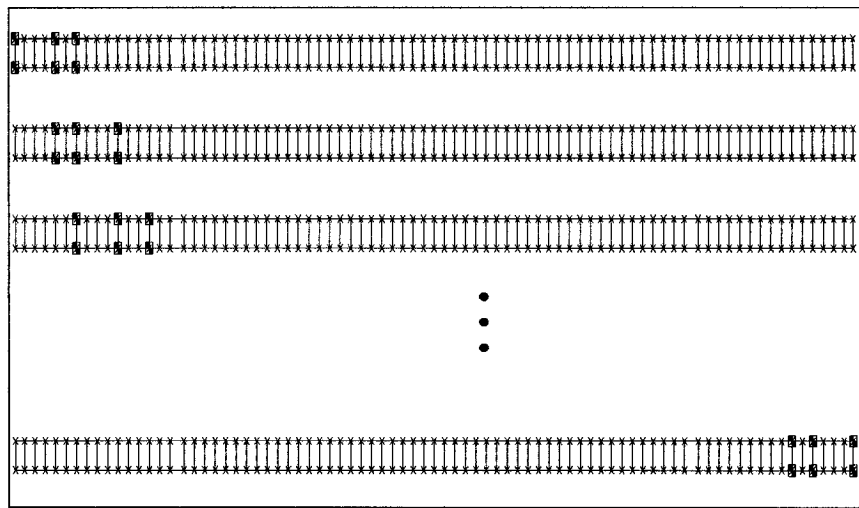
Figure 4.31: Roving method for 9 channels. The upper sensors record vertical motions only, while the lower sensors record both vertical and lateral motions.

124
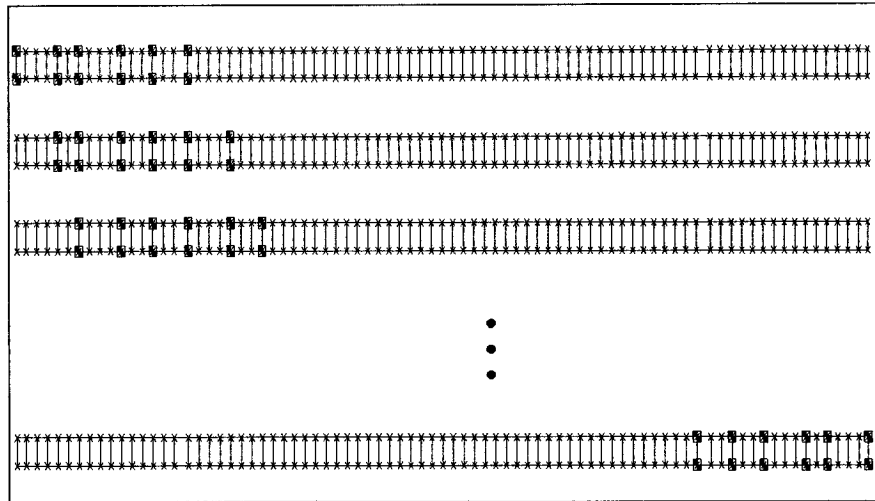
Figure 4.32: Roving method for 18 channels. The upper sensors record vertical motion only, while the lower sensors record both vertical and lateral motions.
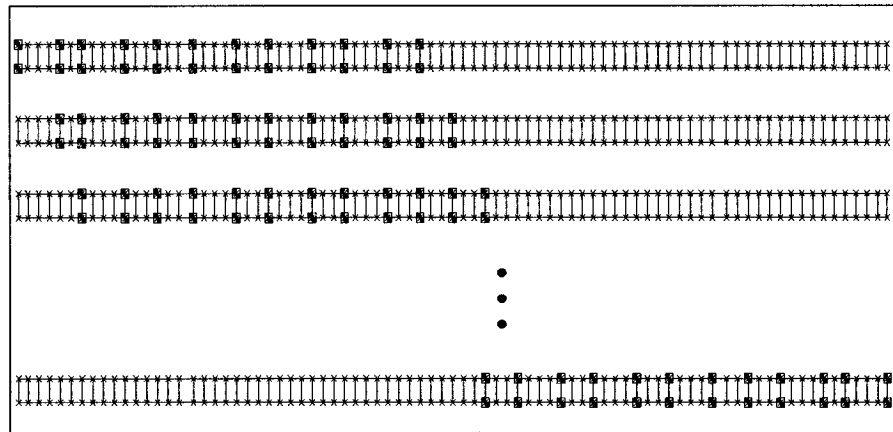
Figure 4.33: Roving method for 36 channels. The upper sensors record vertical motion only, while the lower sensors record both vertical and lateral motions.

125

4.6.3 Comparison of the identified results of the FEM schemes

The purpose of the study using simulated data from the finite element method was to determine the validity of the MIMO identification procedure, and to determine the optimum number of sensors needed for the method to provide reliable results. The various roving methods were implemented and the results were investigated. The following figure shows the comparison between the various sets. The results were normalized by each reference non-damage case. For instance the analysis included damage and non-damage for data sets with the same number of sensors, and the results were then normalized by the non-damaged case in accordance with the following equation:

$$\%Error = \frac{f_{NoDamage} - f_{Damage}}{f_{NoDamage}} \times 100 \qquad (4.21)$$

126
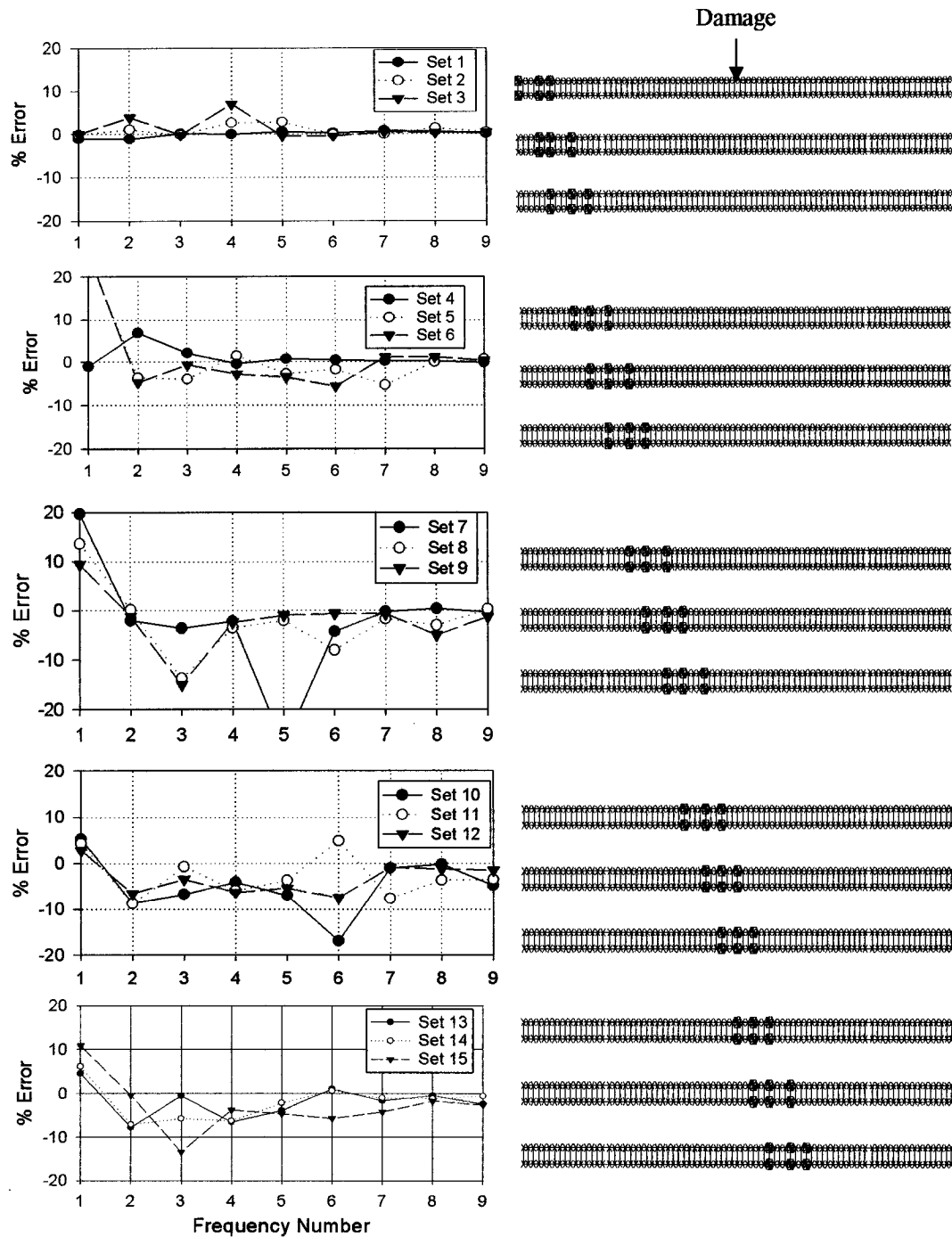
Figure 4.34a: Results of 9 roving channels throughout the deck.

127
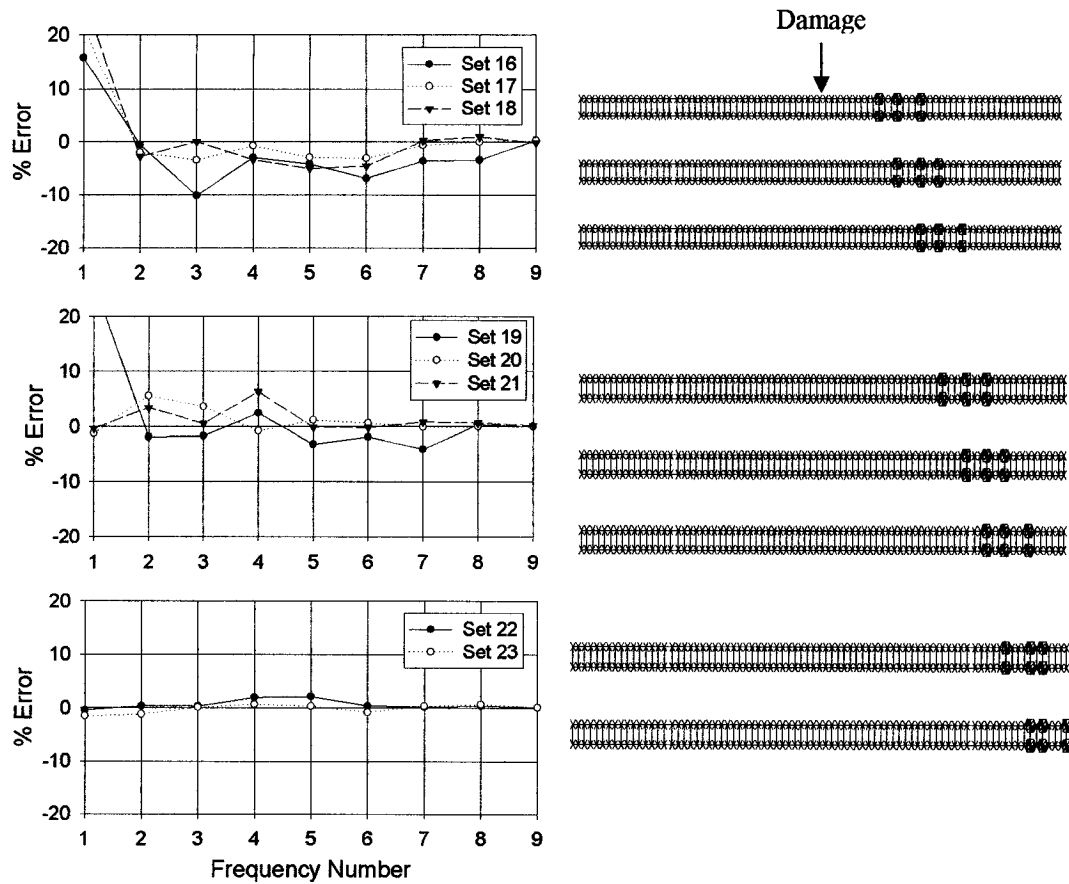
Figure 4.34b: Results of the 9 roving channels throughout the deck.
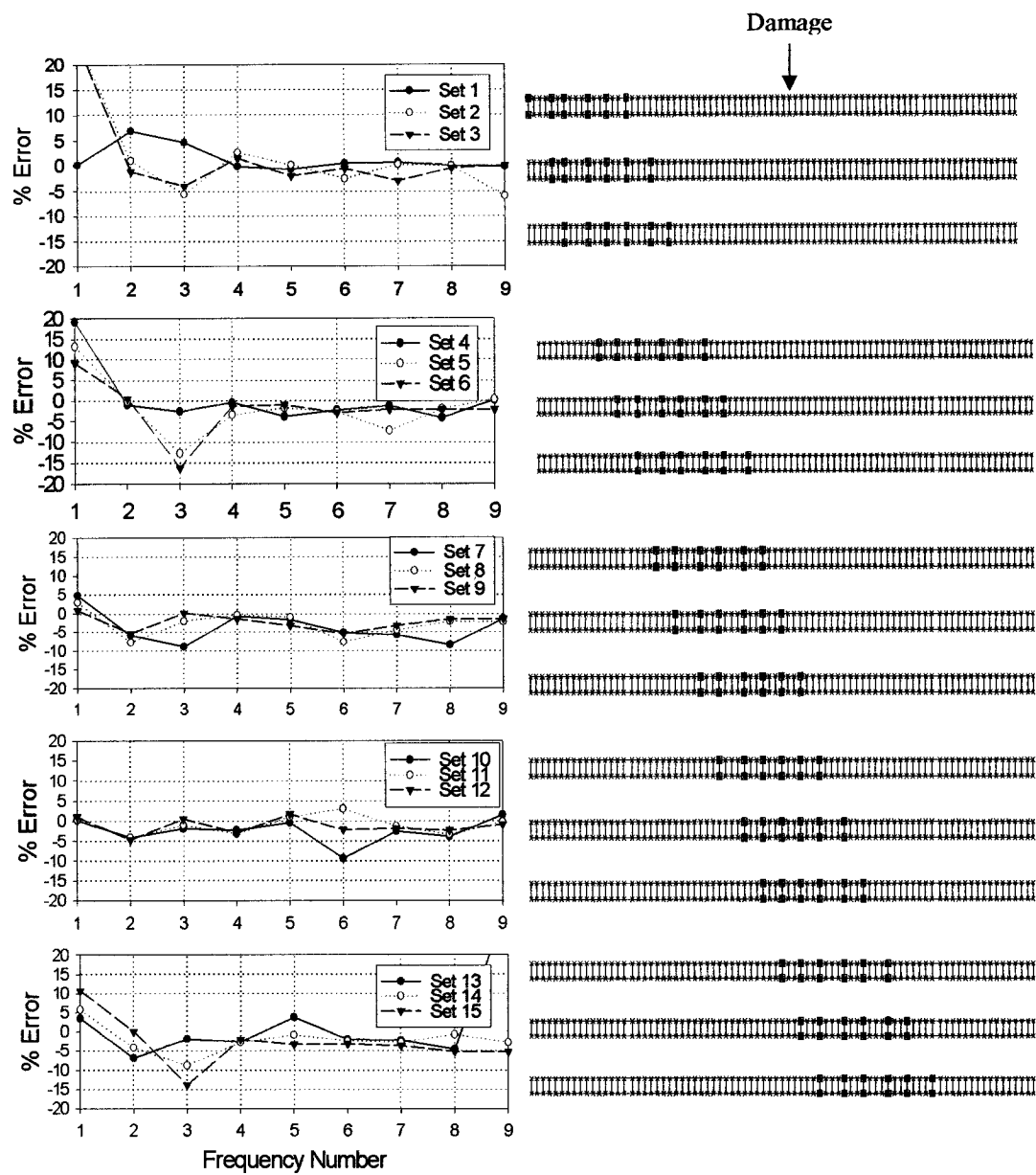
Figure 4.35a: Results of the 18 roving channels throughout the deck.

129
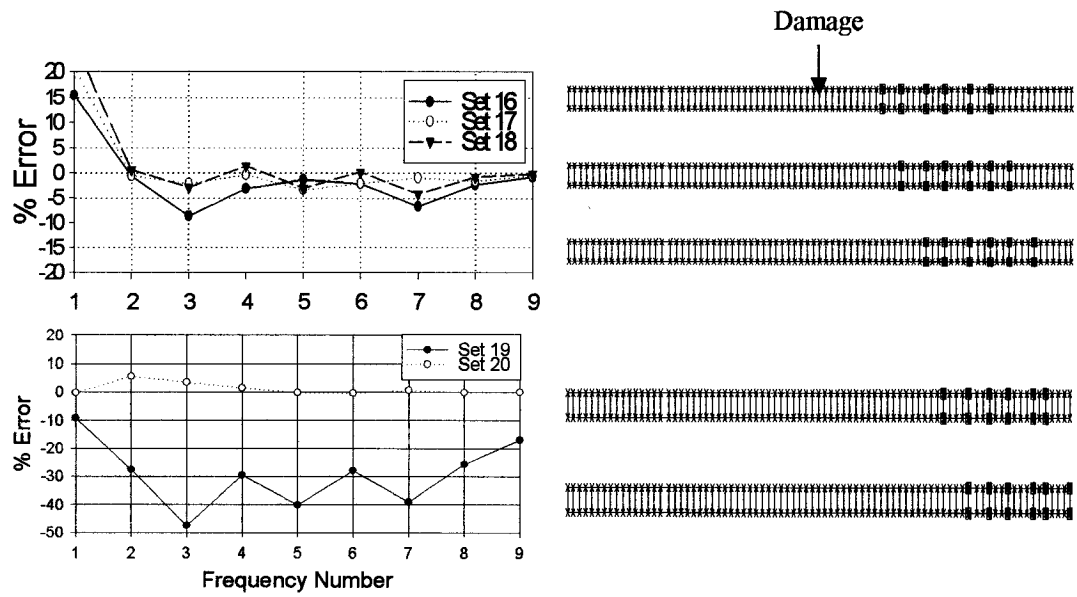
Figure 4.35b: Results of the remaining 18 roving channels throughout the deck.

130
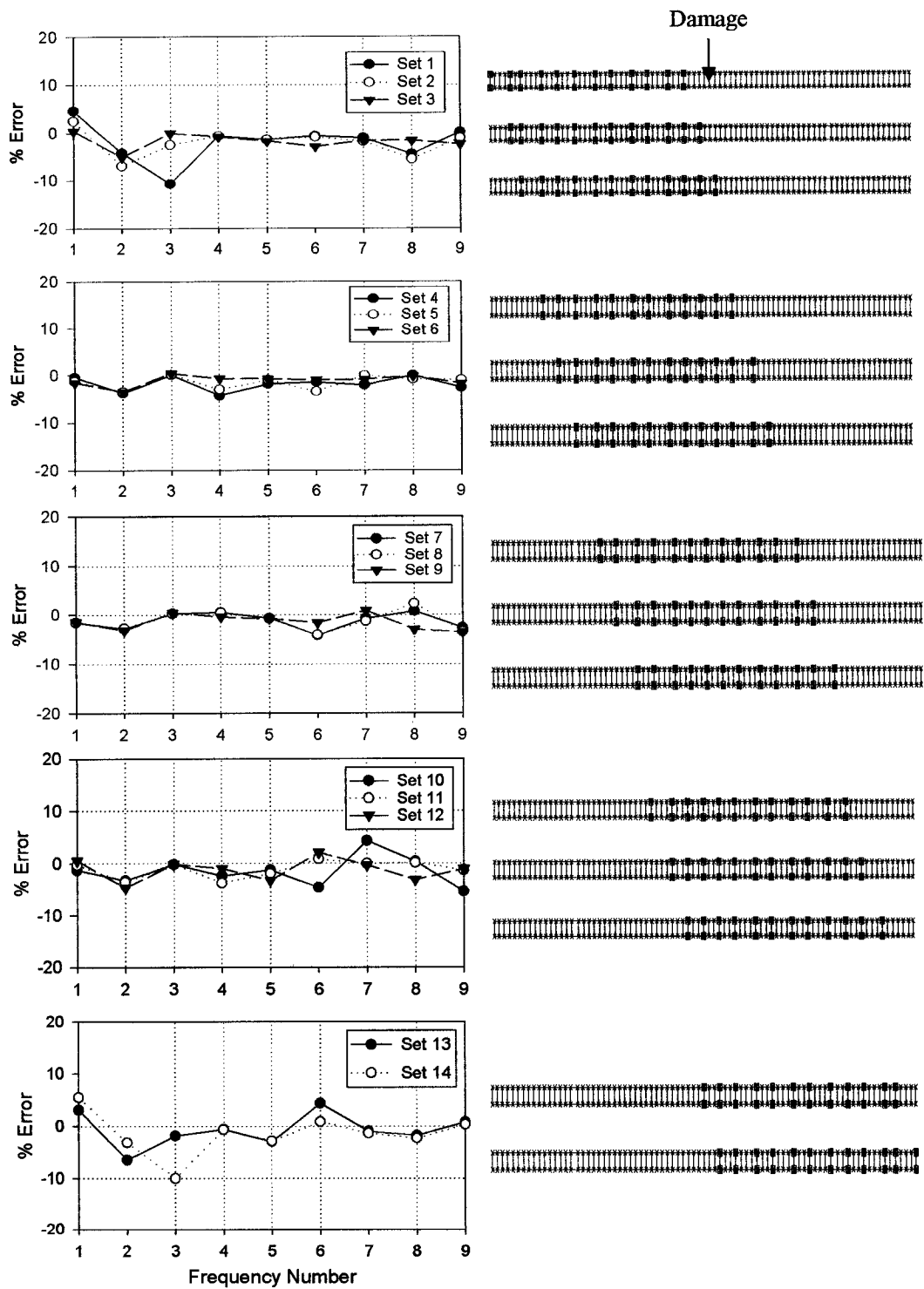
Figure 4.36: Results of the 36 roving channels throughout the deck.

4.6.4 Discussion

The advantage of having a detailed finite element model (FEM) is the ability to generate significant amounts of synthetic data and validate analytically any system identification method. This analysis indicated that the MIMO identification procedure is a viable method for system identification. The other part of the study was to determine the optimum number of sensors needed in order for the MIMO identification procedure to detect changes. The FEM was utilized to output 75 channels of acceleration data from both a non-damaged case and a damaged case. First, the 9 roving channels method of the 75 total was utilized, then the 18 channels and finally the 36 channels, as shown in earlier figures. It may be concluded from the 9 and 18 roving channels figures that significant percentage of error occurs in these methods. The percentage error ranges from 2% to 50%. However the 36-channels method seems to have a very small range of error. In addition, it can observed from the previously shown roving figures that the percentage of error seem to increase as the roving channels are closer to the damage location in the 9 and 18 roving channels, however in the 36 channels scheme the damage detection seem minimal.

One must be careful in analyzing these data. The high percentage of error could be attributed to the fact that as these channels move along the bridge deck, they are not detecting the dominate frequencies in that section of the bridge. This can be easily

132

shown through the increase of the number of sensors on the bridge. Therefore, from this discussion we can determine for this type of identification a uniform distribution of sensors on the bridge is more adequate in detecting changes than the roving method. The ideal number of sensors needed for this structure, in order to detect global changes, was established to be 75 sensors throughout the bridge.

4.7   Conclusion

This chapter tackled several aspects of system identification for a large scale system. The Vincent Thomas Bridge (VTB) provided a very challenging and realistic test bed. The utilizing of the Multi-input-multi-output identification procedure was validated via the use of both the real-time ambient monitoring data and via the complicated finite element model.

For the ambient vibration problem of the VTB, the reduced-order discrete system was developed based on 15 structural response locations, and 10 support inputs. However, since only the ambient response was measured, (i.e. no forced excitation measurements were available) the 15 response locations were utilized in the analysis. Since this represents a reduced-order, the modeling of this system will naturally incorporate some error due to the unavailable measurements. This inherent limitation due to low spatial resolution of the sensing, affects the range of conclusions which may be drawn from the identified reduced-order model.

It may be concluded in order for ambient vibration method to be effective, very long records need to be collected. Based on the analysis presented in this section, continuous records on the order of several days will be needed for "stable" statistical measurements of the system response.

This chapter demonstrated the difficulties encountered in utilizing the reduced-order method. These difficulties include the low spatial resolution of the sensor array and the significant dynamical changes of the structure due to ambient dynamic environment changes throughout the day. The capability of the method was demonstrated by the FEM synthetic data; however, in order to improve the validity of the reduced-order model the enhancement of the spatial resolution is needed through increasing the spatial resolution of sensor instrumentation.

134

Chapter 5

Frequency Response Method

5.1   Introduction

Frequency response analysis is a method used to compute structural response to

steady-state oscillatory excitation. In the frequency response analysis, the excitation

is explicitly defined in the frequency domain. All of the applied forces are known at

each forcing frequency. Forces can be in the form of applied forces and/or enforced

motions (displacements, velocities, or accelerations). Oscillatory loading is

sinusoidal in nature (Crandall and Mark, 1963).

The focus of this chapter is to analyze the validity of the frequency response method

in detecting changes in large-scale structures such as a long-span bridge. This

chapter will discuss the background of the transfer function method, the formulation

of the problem, the process by which the study was carried out, and the results.

5.2   Background Frequency Response Excitation Relation for Linear Time –
Invariant Systems

A linear and time-invariant vibratory system can be represented by a set of linear

differential equations of motions with constant coefficients. For example, a single

degree of freedom system can be described by a single second-order ordinary

differential equation. Therefore a two-degree-of-freedom system can be described by two second-order ordinary differential equations, and so on.

In general the excitation-response relation could be presented schematically by the excitation history $x(t)$ and the response history $y(t)$ as shown in Figure 5.1.

$$x(t) \longrightarrow \boxed{\text{Linear Time Invariant System}} \longrightarrow y(t)$$
Excitation   Response
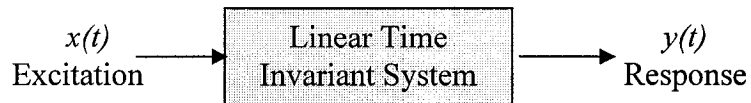
Figure 5.1: Schematic Presentation of Excitation-Response Relation.

As mentioned, this is the general form of the relation without any particular description of the parameter. However, when we consider a particular system, it is necessary to describe the precise nature of these parameters. If $x(t)$ is a specific deterministic time history, it is possible to get a specific answer for $y(t)$ by integrating the differential equation of motion with specific initial conditions. There are many techniques for obtaining solutions for linear differential equations with constant coefficients. There are two distinct methods for solving such equations. The first method is referred to as the frequency response method with Fourier integral and the second is the time domain method referred to as impulse response with superposition of the convolution integral. The two methods are essentially Fourier transforms of each other and hence directly related. This section will introduce the theoretical background of each method, and then perform a complete

136

comparison with a five-degree-of-freedom model analysis in order to verify the similarities of results from these methods.

5.2.1 Frequency Response Method

The response of linear time-invariant systems with a steady state simple harmonic motion is also steady state simple harmonic motion at the same frequency. The phase and amplitude of such a response is also dependent on the frequency. The frequency response is a complex quantity $H(w)$ described by its dependence on amplitude and phase. When the excitation is the real part of e^{iwt}, then the response is the real part of $H(w)\,e^{iwt}$. However the complex frequency response $H(w)$ is analytically obtained by expanding the excitation $x(t)$ as $x = e^{iwt}$ and hence will yield:

$$y = H(w)\ e^{iwt} \tag{5.1}$$

in the differential equation of motion, by canceling e^{iwt} terms and solving for $H(w)$.

The information presented in the frequency response $H(w)$ for all frequencies is sufficient to obtain the response $y(t)$ to an arbitrary known excitation $x(t)$. This is the well known principle of superposition. This principle applies to linear systems and is performed in the frequency domain utilizing the Fourier transform method. For instance if $x(t)$ is periodic, then it can be deconstructed into sinusoids forming a Fourier series. Hence the response to each separate sinusoid is provided by $H(w)$.

137

These responses form a new Fourier series that represent the response $y(t)$. The case when $x(t)$ is not periodic, will result in a Fourier transform of the form

$$x(w) = \int_{-\infty}^{\infty} x(t)e^{-iwt} \ dt \qquad (5.2)$$

The superposition concept is valid for each frequency component. This results in the following equation as the Fourier transform of the response $y(t)$.

$$Y(w) = H(a)X(w) \qquad (5.3)$$

The response is then represented by the Fourier integral.

$$y(w) = \frac{1}{2\pi} \int_{-\infty}^{\infty} Y(w)e^{iw\tau} \ d\tau \qquad (5.4)$$

The general input-output relation can be represented by reconstructing the above mentioned equation to the following general form:

$$y(t) = \frac{1}{2\pi} \int_{-\infty}^{\infty} \int_{-\infty}^{\infty} H(w)e^{iwt} \ x(\tau)e^{-iw\tau} d\tau \ dw \qquad (5.5)$$

Knowledge of $H(w)$ will allow evaluation of equation 5.5 to give the response $y(t)$ for an arbitrary excitation $x(t)$. The general input-output relation represented by equation 5.5 is very important in random vibration analysis. Such a relation holds for every corresponding pair of samples in the input and output random process.

5.3   Analysis

The above mentioned transfer response function is the theoretical background of the method. In order to evaluate the frequency response method, several study cases were evaluated based on the use of finite element method (FEM) frequency response

138

function models. The first step of the study was to validate the FEM frequency response method. Next, the study considered the complex long-span bridge structure of the Vincent Thomas Bridge. The following section summarizes the analysis performed.

5.3.1 Description of Modal Frequency Analysis

The modal frequency response analysis is the alternate approach used in the finite element model in order to compute the frequency response of a structure. Mode shapes of the structure are used in this method to reduce the size, uncouple the equations of motion (when modal or hence no damping is used), and therefore make the numerical solution more efficient. Since the mode shapes are typically computed as part of the characterization of the structure, modal frequency response is a natural extension of a normal modes analysis. The first step of the formulation is to transform the variables from physical coordinates $\{u(\omega)\}$ to modal coordinates $\xi(\omega)$ in accordance with the following equation (Berkely 1996):

$$\{x\} = [\phi]\{\xi(\omega)\}e^{i\omega t} \tag{5.8}$$

The mode shapes $[\phi]$ are used to transform the problem in terms of the behavior of the modes as opposed to the behavior of the grid points. Equation (5-8) represents an equality if all modes are used; however, because all modes are rarely used, the equation usually represents an approximation. To proceed, temporarily ignore all damping, which results in the undamped equation for harmonic motion

$$-\omega^2[M]\{x\} + [K]\{x\} = \{P(\omega)\} \tag{5.9}$$

139

at forcing frequency ω. Substituting the modal coordinates in Eq. (5.8) for the physical coordinates in Eq. (5.9) and dividing by $e^{i\omega t}$, the following is obtained:

$$-\omega^2[M][\phi]\{\xi(\omega)\}+[K][\phi]\{\xi(\omega)\} = \{P(\omega)\} \qquad (5.10)$$

Now, this is the equation of motion in terms of the modal coordinates. At this point, however, the equations remain coupled. To uncouple the equations, pre-multiply by $[\phi]^T$ to obtain

$$-\omega^2[\phi]^T[M][\phi]\{\xi(\omega)\}+[\phi]^T[K][\phi]\{\xi(\omega)\} = [\phi]^T\{P(\omega)\} \qquad (5.11)$$

where

$[\phi]^T[M][\phi] =$ modal (generalized) mass matrix

$[\phi]^T[K][\phi] =$ modal (generalized) stiffness matrix

$[\phi]^T\{P\} =$ modal force vector

The final step uses the orthogonality property of the mode shapes to formulate the equation of motion in terms of the generalized mass and stiffness matrices, which are diagonal matrices. These diagonal matrices do not have the off-diagonal terms that couple the equations of motion. Therefore, in this form the modal equations of motion are uncoupled. In this uncoupled form, the equations of motion are written as a set of uncoupled single degree-of-freedom systems as

$$-\omega^2 m_i\xi_i(\omega)+k_i\xi_i(\omega) = p_i(\omega) \qquad (5.12)$$

where

$m_i = $ i-th modal mass

140

k_i = i-th modal stiffness

p_i = i-th modal force

The modal form of the frequency response equation of motion is much faster to solve than the direct method because it is a series of uncoupled single degree-of-freedom systems.

Once the individual modal responses $\xi_i(\omega)$ are computed, physical responses are recovered as the summation of the modal responses using

$$\{x\} = [\phi]\{\xi(\omega)\}e^{i\omega t} \qquad (5.13)$$

These responses are in complex form (magnitude/phase or real/imaginary) and are used to recover additional output quantities.

It is possible not all of the computed modes are required in the frequency response solution. One needs to retain, at a minimum, all the modes whose resonant frequencies lie within the range of forcing frequencies. For example, if the frequency response analysis must be between 200 and 2000 Hz, all modes whose resonant frequencies are in this range should be retained. In the present analysis, over 1280 frequencies were included. This guideline is only a minimum requirement, however. For better accuracy, all modes up to at least two to three times the highest forcing frequency should be retained. In the example where a structure is excited to between 200 and 2000 Hz, all modes from 0 to at least 4000

141

Hz should be retained. The frequency range selected in the eigenvalue range to be included is one means to control the modes used in the modal frequency response solution.

5.3.2   Validation of the FEM

The FEM was validated by applying two different scenarios on a five degree of freedom system. The system consisted of five masses of 5 unites connected in series with springs with stiffness, k = 5000 unites, and critical damping of 5%. The first scenario consisted of the impulse response method. The system was subjected to a unit impulse for a duration of 0.01 second. The synthetic recording characteristics consisted of a sampling rate of 1000 Hz for 100 seconds, a total 100,000 time steps, for a frequency range from 1 to 10 Hz. The formulation of the impulse response consists of the following equations of motion for the uncoupled five degree of freedom system:

$$[M]\{\ddot{\xi}\} + [C]\{\dot{\xi}\} + [K]\{\xi\} = \{P\} \tag{5.14}$$

The next step is to utilize the Duhamel integral to obtain $\{\ddot{\xi}\}, \{\dot{\xi}\}, \{\xi\}$ for all degree of freedoms. The determining of the acceleration is accomplished by multiplying of the transpose of mode shape functions as follows:

$$\{\ddot{x}\} = [\phi]^T \{\ddot{\xi}(\omega)\} \tag{5.15}$$

Finally an FFT is performed on the acceleration records and compared to the frequency response function of the system as discussed earlier. Figure 5.2 shows the comparison between these two methods. It can be observed that the two methods

142

have a good match in the specified frequency ranges. This step was done to validate

the FEM frequency response method.

Comparison of FRF
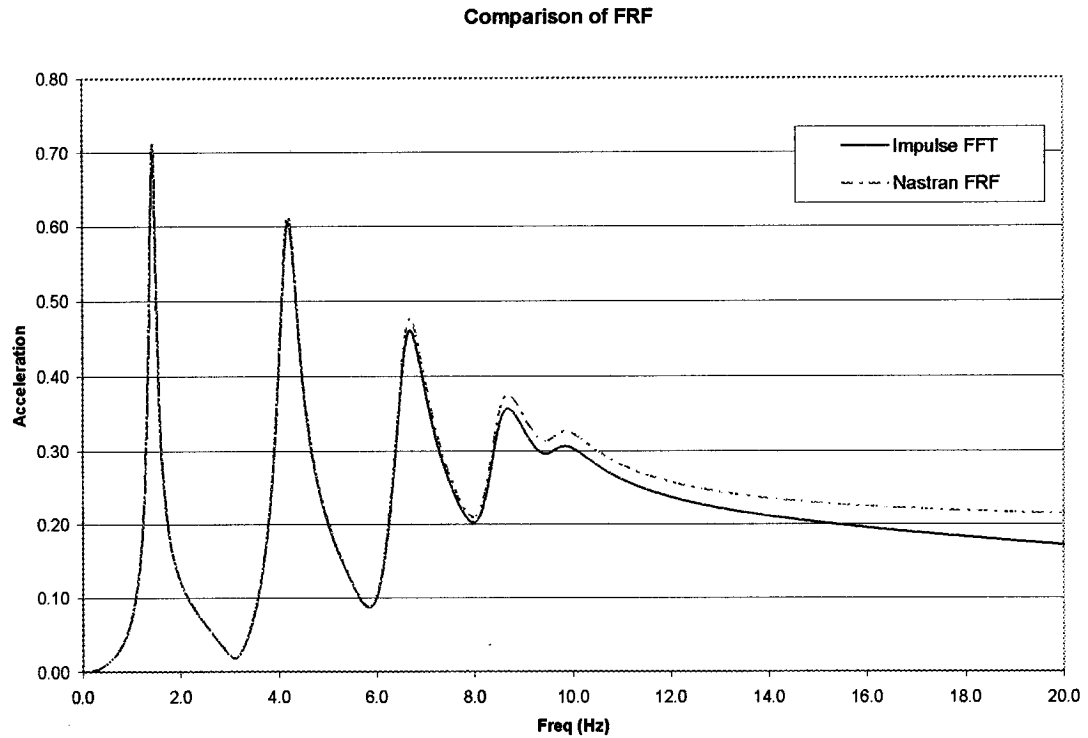
Figure 5.2: Comparison between the FFT of the impulse response and the frequency
response method.

It can observed that the above figure that the two methods have a good comparison

within the frequency range specified in the validation, which was 10 Hz for this

study. It was concluded from this comparison that the finite element frequency

response method is adequate to be utilized as an identification tool.

143

5.3.3 Description of the Case Studies

Since the comparison between the impulse response and the NASTRAN frequency response approaches revealed promising results, the study progressed to the more complicated bridge model. The study focused on analyzing the complex finite element model already developed for the Vincent Thomas Bridge. This model was already discussed in previous chapter. The model consists of 11980 nodes. Figure 5.3 depicts the FEM of the Vincent Thomas Bridge. The load applied to the deck consisted of a unit impulse load at selected nodes in all directions on the deck of the bridge. Figure 5.4 shows the loading scheme of the bridge deck.
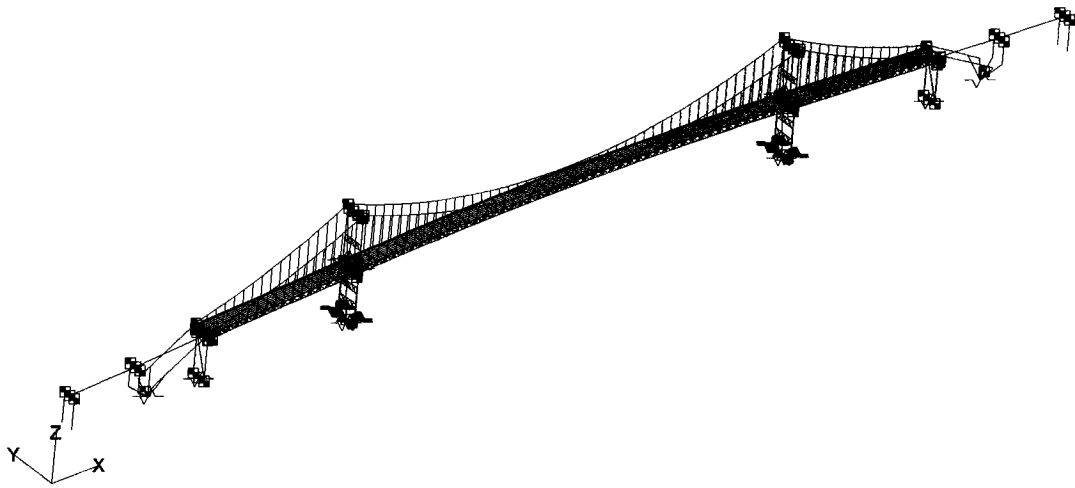
Figure 5.3: Finite Element Model of the Vincent Thomas Bridge.

144
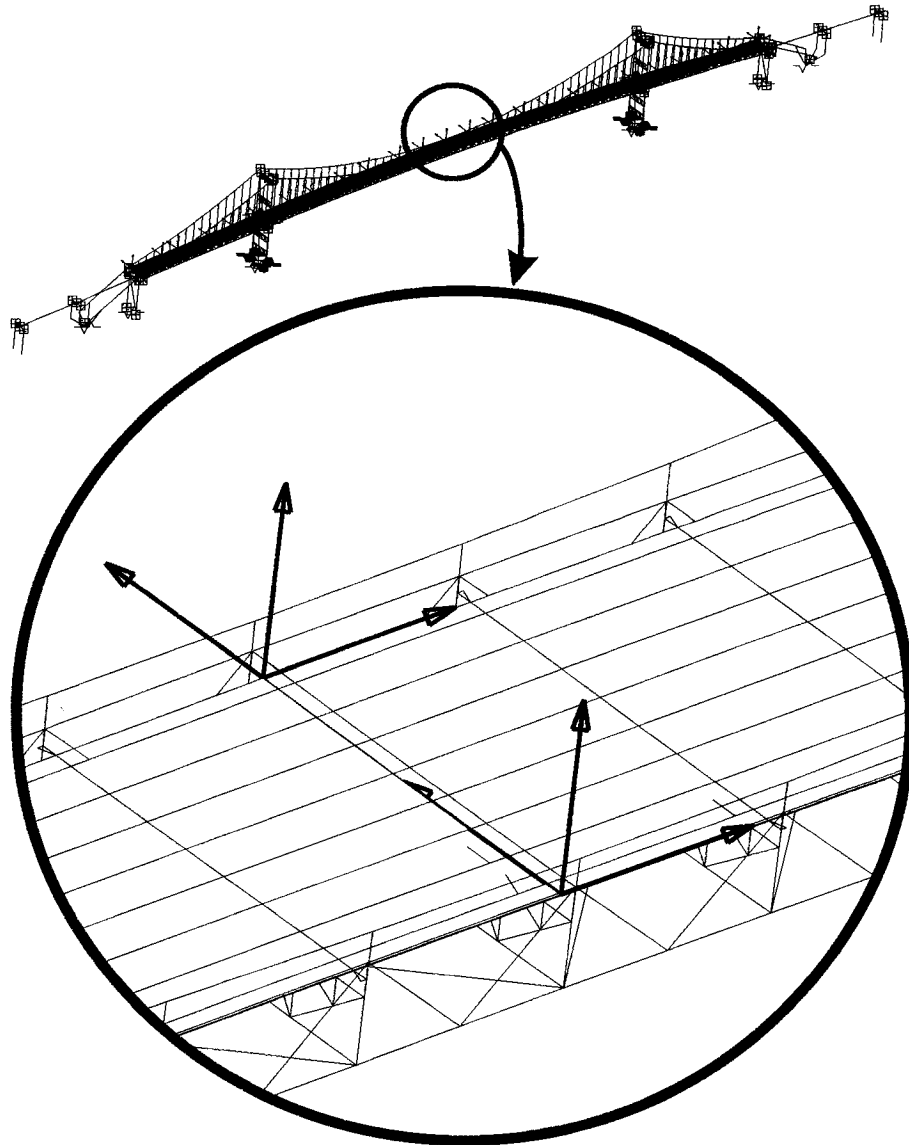
Figure 5.4: Loading scheme of the bridge deck.

5.4   Discussions

The analysis consisted of applying a unit impulse load at each load node shown in

Figure 5.4 and measuring the response for all other nodes on the bridge. In order to

have a meaningful analysis, several cases were evaluated. First of all, the base no-

damage case had to be developed as the reference case. Such a case represents the

145

response of the bridge without any structural modifications. This was established by applying the unit impulse loads and measuring the response to every node throughout the structure. The next case was to perform structural changes on the bridge by determining the high stress level member which is located at the center of the bridge at the lower deck cord, reducing its stiffness by 99%, then applying the unit impulse load at every node and measuring the response similar to the reference case, and finally performing the comparison to determine if this method could determine and locate the changes in the structure.

In order to demonstrate the results of this method, five nodes were selected on the deck. These locations are shown in Figure 5.5.
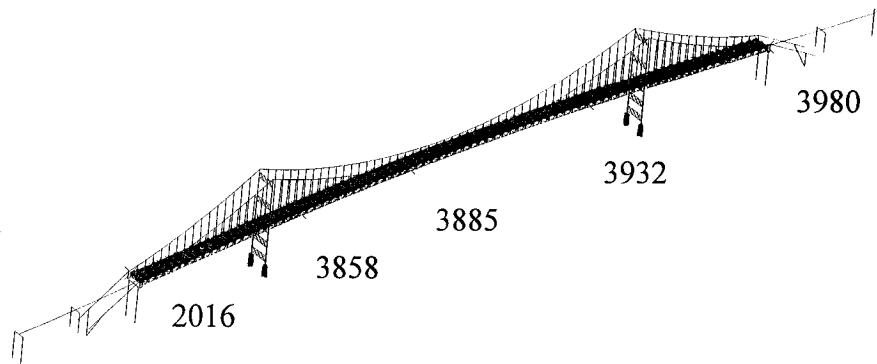
Figure 5.5: Selected nodes on the bridge deck

The frequency responses of these nodes were then compared to the reference case. The comparison results could be summarized as follows:

146

- Determining the transfer function of each node in all directions.

- Computing the area under the transfer function curve for the x, y, and z directions.

- Summing the area under the transfer function curves.

- Repeating the above steps for the damage case.

- Subtracting the difference between the damage and no-damage cases for each node.

- Normalizing the area with respect to the no-damage case.

The above steps are shown in Figure 5.6. This figure shows a comparison between the five nodes shown in Figure 5.5 of the vertical direction response for each node. The horizontal axis represents the distance along the bridge, It should be noted that the centerline of the bridge is located in the middle of the plot at number zero, and 15000 inches (1250 ft.) on each side of the centerline. The vertical axis is the normalized area percentage error, which represent the cumulative area difference under the transfer function curves normalized with respect to the referenced case. Therefore the response of nodes 2016 and 3980 show the least amount of area change, and therefore both of these curves are the closest to origin baseline. These nodes are located at each end of the bridge (Figure 5.3) where the influence would be very minimal as expected. As the nodes get closer to the damage location, the normalized error area under the curves increases. For example, node 3885 has the highest normalized area change, as it can observed from Figure 5.3 node 3885 is

147

located very close to the damaged area. This observation is very important considering the structural change is near that area.
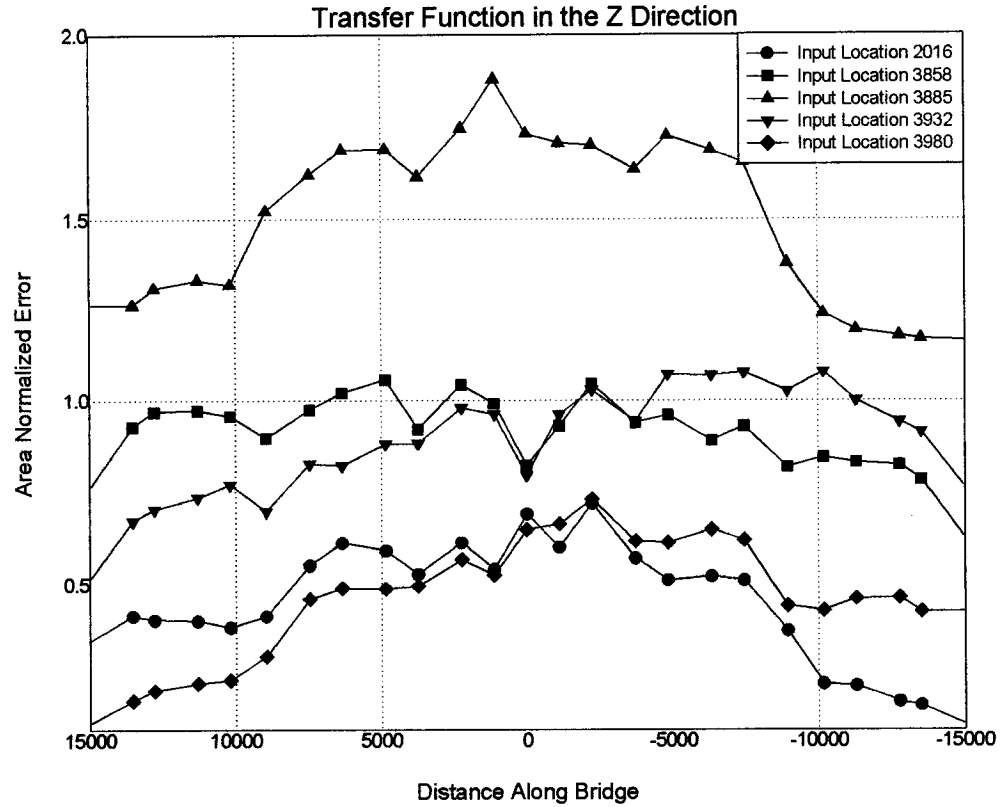
Figure 5.6: Comparison of the normalized error area of the transfer function of nodes along the bridge deck.

5.5   Conclusions

The above mentioned analytical study demonstrated the validity of the transfer function method for detecting changes in a complex structure. The study focused on synthetic generated data via the finite element method. The obvious follow up step of this study is to validate it on a complex experimental model. This method shows promising results for the structural health monitoring method for large complex structures such as bridges.

148

Chapter 6

Conclusions

This study has explored an array of system identifications and modeling approaches for large, complex dynamic systems. Significant effort was focused on the validation of a previously-developed multi-input/multi-output (MIMO) identification technique. However, prior to even validating this method, various factors, including the accuracy of using only acceleration measurements to obtain integrated velocities and displacements, were evaluated in order to assure the identification results would be as accurate as possible. Hence, the first step was to develop and validate the data processing algorithm, which included the integration technique of acceleration data through comparison with physical measurements, and through the use of a vision-based method, in order to obtain direct deformation measurements. The validation studies were performed in the laboratory and on the Vincent Thomas Bridge.

The data processing algorithm was validated both in the laboratory and on simulated data similar to what can be expected from a large-scale dispersed structural system. The study was performed on a range of frequencies with simulated noisy data in order to assure that the data processing will capture the dominant frequencies and accurately determine both velocities and displacements. This method proved to be extremely accurate on both laboratory and synthetic simulated data. The data processing algorithm is very much needed in order to obtain accurate system

149

identification results. The algorithm was further validated by the use of the vision-based measuring method to obtain direct displacement measurements from the VTB.

The vision-based method was first calibrated in the laboratory in order to assure its effectiveness in the field. Then it was deployed on the VTB for actual field implementation. This technique has also proven to be quite accurate in directly obtaining the displacement of large-scale structures. As demonstrated in an earlier chapter, this method has significant advantages as compared to the commonly used GPS method, mainly the accuracy of acquired data. In addition, this method is not restricted to measuring the motion of bridges and similar large-scale structures, but can be used on any size structural system.

The next step of the study was to obtain very long acceleration records in order to minimize the ambient affecting factors, including varying traffic loads, wind, varying temperatures, and rain. These long acceleration records were obtained through the use of the real-time monitoring system installed in early 2003 on the VTB. Data were then processed utilizing the MIMO identification technique. In addition, the identification technique was utilized on synthetic simulation studies of a large complex finite element model of the VTB, and subsequently used on both ambient vibration and strong motions acceleration data from the VTB.

The MIMO identification technique showed promise for detecting changes in large complex structures; however, several factors need to be recognized in order to have a

150

more reliable technique. The number of instruments utilized on the VTB was not near enough to accurately determine the location of the damage. The spatial resolution of these instruments was sufficient to determine the global changes of the system, but not a local change. In addition, for ambient vibration, the monitoring has to be performed for long periods of time, on the order of days, for the statistical averages to be more accurate. A minimum of two days of continuous recording needs to be completed in order for the system to stabilize with regard to environmental effects such as temperature, wind, and rain.

While continuously recording ambient measurements from the VTB through the use of the above mentioned real-time monitoring system, a small earthquake with a magnitude of 5.4M struck Big Bear City. Data was collected and analyzed via the MIMO identification technique. Additionally, a detailed ambient vibration analyses was performed on the large sets of acceleration data collected from the VTB. This analysis indicated the number of sensors on the bridge was far from adequate in order to perform system identification.

Simulation analyses were performed on synthetically generated data from a complex finite element model of the bridge. The simulation studies were focused on determining the optimum number of sensors needed to perform system identification. First a roving technique was implemented with a set number of sensors ranging from 9 to 36 being placed at one end of the bridge while synthetic motion was generated. Next, the sensors were moved over one step. This process was repeated over and

151

over again until the sensors reached the other end of the bridge. This method proved to be inconsistent as changes varied significantly along the bridge deck. The reason for this inconsistency could be attributed to several factors, including modeling errors and the low spatial resolution of these sensors. Furthermore these sensors detected different dominant frequencies in the roving range as they moved along the bridge deck. All these factors could have affected the results significantly; hence it was determined the roving method is not adequate for detecting global structural changes. Clearly, a dense uniform distribution of sensors is a more accurate approach.

Lastly, a forced-excitation approach to obtain the VTB transfer functions was studied. This technique was found to be a fairly accurate method in detecting and locating structural modifications in large-scale structures.

6.1   Recommendation for Future Research

There are numerous technical hurdles which must be investigated and resolved before the full promise of the important emerging field of SHM of dispersed civil structures, including long-span bridges, is realized, thus leading to a reliable and useful SHM methodology ready for field implementation.

The development of some powerful analysis tools for extracting useful information about the detection, location, and quantification of changes in the structural

152

parameters of monitored bridges such as the VTB can be quite useful to the owners of such structures. To minimize the environmental changes in a large complicated structure, it is recommended that traffic count, rain, wind and temperature gauges be installed and monitored. Furthermore, the monitoring should be of a continuous nature in order to obtain adequate statistics. Based on obtained results from the MIMO identification technique, the number of instruments on the VTB should be at least of two orders of magnitude more in order to accurately capture the modal characteristics and increase the reliability of the damage detection.

Based on the experimental results obtained from this research, it is also recommended that additional verification be performed on the vision-based method. In order to enhance surveillance capabilities, and high-fidelity monitoring of field deformation measurements at selectable locations and orientations, and increase the reliability of the vision-based measuring method, several cameras should be installed on the ground level and multiple targets on the bridge should be monitored. Figure 6.1 depicts the schematics of this recommendation.

153

Optical Displacement Tracking
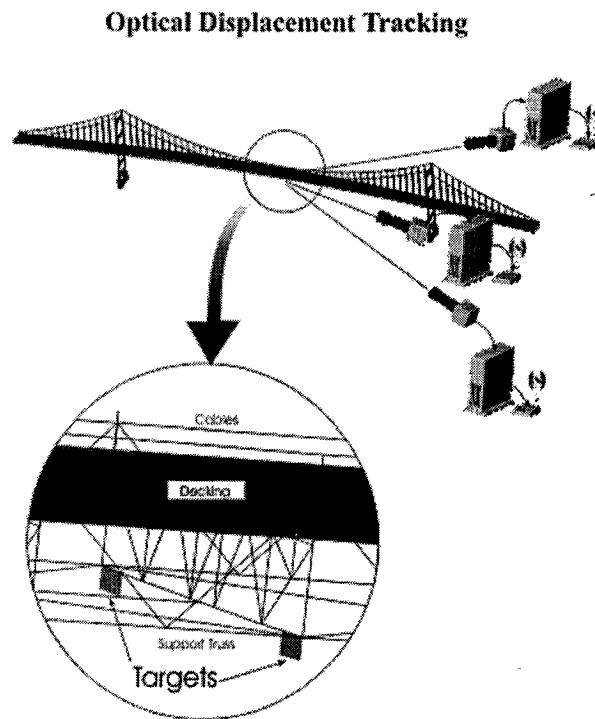
Figure 6.1: Schematic locations of the recommended additional vision-based monitoring.

Another important recommendation is that the finite element model of any complicated structure should be validated through the use of forced-excitation. As it was successfully demonstrated, this method is a powerful tool in identifying damage; it is also a powerful tool in determining the base line system matrices, and the dominant frequencies of such structures. The forced-excitation method is a general identification technique for other types of structural systems. Since most structural vibration designs are based on a developed finite element model and several factors can not be modeled accurately during the analysis phase, the finite element model should be validated via forced vibration tests. Several methods could be utilized

154

including the snap-back tests and the impact load tests. The input force is known in these tests, thus leading to a more accurate determination of the system motions. After the validation of the finite element model is accomplished, one can perform any sort of simulation and analysis on the calibrated model. In addition any further analysis performed on such structures will now be highly reliable.

Furthermore, for new large-scale structures the validation of the mathematical model, and the vibration analysis should be conducted prior to putting the structure in service. Then the base reference line condition can be easily developed, and the monitoring can begin. Monitoring of the structure will decrease the maintenance costs and assure a more reliable functioning structural system in the long run.

155

References

Abdel-Ghaffar, A.M., and Housner, G.W., 1977, "An Analysis of the Dynamic Characteristics of a Suspension Bridge by Ambient Vibration Measurement," California Institute of Technology, Earthquake Engineering Research Laboratory, EERL 77-01.

Achenbach, J.D., Moran, B., and Zulfiqar, A., 1997, "Techniques and Instrumentation for Structural Diagnostics," *Proceedings of the 2nd International Workshop on Structural Health Monitoring, Current Status and Perspectives*, 179-190.

Agbabian, M.S., and Masri, S.F. (eds) 1988, *Proceedings of the International Workshop on Nondestructive Evaluation for Performance of Civil Structures*, Civil Engineering Dept., Publication No.M8805, University of Southern California, Los Angeles, CA.

Agbabian, M.S., Masri, S.F., Miller, R.K., and Caughey, T.K., 1987 "A System Identification Approach to the Detection of Changes in Structural Parameters," in *Structural Safety Evaluation Based on System Identification Approaches*, Proceedings of the Workshop at Lambrecht/Pfatz, edited by H.G. Natke and J.T.P. Yao, Frieder Vieweg & Sohn, Braunschweig, 1988, 341 - 356.

Agbabian, M.S., Masri, S.F., Miller, R.K., and Caughey, T.K., 1991, "System Identification Approach to Detection of Structural Changes," *Journal of Engineering Mechanics*, **117**(2), 370-390.

Aktan, A.E., Catbas, F.N., Grimmelsman, K.A., and Tsikos, C.J., 2000, "Issues in Infrastructure Health Monitoring for Management," *Journal of Engineering Mechanics*, **126**(7), 711-724.

Alampalli, S., and Cioara, T., 2000, "Selective Random Decrement Technique for Processing Bridge Vibration Data," *Structural Materials Technology IV, Nondestructive Testing Conference Proceedings*, 75-80.

Audenino, A.L., and Belingardi, G., 1996, "Processing of Simultaneous Mechanical Random Response Signals: Integration, Differentiation and Phase Shift Correction," *Mechanical System and Signal Processing*, **10**, 277-291.

Behr, J. A., Hudnut, K., and King, N., 1998, "Monitoring Structural Deformation at Pacoima Dam, California Using Continuous GPS," *Proceedings 11th International Technical Meeting of Satellite Division of the Institute of Navigation* [ION GPS-98; Nashville, TN], 59-68.

156

Blakely K., Editor, 1996, "MSC/NASTRAN V68 Basic Dynamic Analysis User's Guide."

Casciati, F., 2002, *Proceedings of the Third World Conference on Structural Control* (Como, Italy, 7 - 11 April).

Casciati, F., Maganotte, G. (eds), 2000, *Structural Control for Civil and Infrastructure*, Proceedings of the Third International Workshop on Structural Control (Paris, France, 6-8 July).

Celebi, M., Prescott, W., Stein, R., Hudnut, K., Behr, J., and Wilson, S., 1999, "GSP Monitoring of Dynamic Behavior of Long-period Structures," *Earthquake Spectra,* **15**, 55-66.

Celebi, M., Sanli, A., 2002, "GPS in Pioneering Dynamic Monitoring of Long-period Structures," *Earthquake Spectra,* **18**, 47-61.

Chang, F.K. (editor), 1997, *Structural Health Monitoring: Current Status and Perspectives,* Proceeding International Workshop on Structural Health Monitoring, Stanford University.

Chang, F.K. (editor), 2001, *Structural Health Monitoring: Current Status and Perspectives,* Proceeding Third International Workshop on Structural Health Monitoring, Stanford University.

Chang, F.K. (editor), 2003, *Structural Health Monitoring: Current Status and Perspectives,* Proceeding Fourth International Workshop on Structural Health Monitoring, Stanford University.

Chang et al, 2002, Proceedings of the First European Workshop on Structural Health Monitoring, Ecole Normale Superior de Cachan (Paris, France, 10-12 July).

Chen, J., *Proceedings of the Second International Workshop on Structural Control,* 18-21 December , Hong Kong University of Science and Technology, (Hong Kong, China, 18-21 December)..

Chong, K.P., 1997, "Health Monitoring of Civil Infrastructures," *Proceedings of the 2nd International Workshop on Structural Health Monitoring, Current Status and Perspectives,* (Sept. 18-20), 339-350.

Crandall, S.H., Mark, W.D., 1963, "Random Vibration in Mechanical Systems," Academic Press Inc.

157

Doebling, S.W., Farrar, C.R., Prime, M.B., and Shevitz, D.W., 1996, "Damage Identification and Health Monitoring of Structural and Mechanical Systems from Changes in their Vibrations Characteristics: A Literature Review." Technical Report LA-13070-MS, Los Alamos National Laboratory.

FWSHM, 2002, *Proceedings of the First European Workshop on Structural Health Monitoring*, Ecole Normale Superieure de Cachan, (Paris, France, 10-12 July).

Farrar, C.R., and Doebling, S.W., 1999, "Damage Detection II: Field Applications to Large Structures," *Analysis and Testing*, J.M.M. Silva and N.M.M. Maia, (eds.), Nato Science Series, Kluwer Adademy, (Dordrecht, The Netherlands).

Farrar, C.R., Doebling, S.W., and Nix, D.A., 2001, "Vibration-Based Structural Damage Identification," *The Royal Society, Philosophical Transactions: Mathematical, Physical and Engineering Sciences*, **359**, 130-149.

Farrar, C.R., and Doebling, S.W., 1997, "Lessons Learned from Applications of Vibration-Based Damage Identification Methods to a Large Bridge Structure," *Proceedings of the 2nd International Workshop on Structural Health Monitoring, Current Status and Perspectives*, (September 18-20), 351-370.

Farrar, C.R., and Jauregui, D.A., 1998, "Comparative Study of Damage Identification Algorithms Applied to a Bridge: 1. Experiment," *Smart Materials and Structures*, **7**, 704-719.

Fraser, C.S., Shortis, M.R., 1995, "Metric Exploitation of Still Video Imagery," *Photogrammetric Record*, **15 (85)**, 107-121.

Fraser, C.S., Riedel, B., 2000, "Monitoring the Thermal Deformation of Steel Beams via Vision Metrology," *ISPRS Journal of Photogrammetry & Remote Sensing*, **55 (4)**, 268-276.

Gattuli, V., and Romeo, F., 2000, "Integrated Procedure for Identification and Control of MDOF Structures," *Journal of Engineering Mechanics*, 126(7), 730-737.

IABMAS, 2002, Proceedings of *the First International Conference on Bridge Maintenance, Safety and Management*, (Barcelona, Spain, 14-17 July).

ICANCEER, 2002, *Proceedings of the International Conference on Advances and New Challenges in Earthquake Engineering Research*, (Harbin and Hong Kong, China, 15-20 August).

Hanagud, S., and Luo, H., 1997, "Damage Detection and Health Monitoring Based on Structural Dynamics," *Proceedings of the 2nd International Workshop on Structural Health Monitoring, Current Status and Perspectives,* (September 18-20), 715-726.

Housner, G.W., and Masri, S.F. (eds), 1990, *Proceedings of the U.S. National Workshop on Structural Control Research,* (University of Southern California, 25-26 October), USC Publication No. M9013, ISBN 0-9628908-0-4.

Housner, G.W., Masri, S.F., Casciati, F., and Kameda, H. (eds), 1992, *Proceedings of the U.S.-Italy-Japan Workshop/Symposium on Structural Control and Intelligent Systems,* (Sorrento, Italy, 13-15 July),

Housner, G.W., Masri, S.F., editors), (1993), *Proceedings of the International Workshop on Structural Control,* (Honolulu, Hawaii, 3-5 August), USC Publication No. CE-9311, ISBN 0-9628908-2-0.

Housner, G.W., Masri, S.F., and Chassiakos, A.G., (eds), 1995, *Proceedings of the First World Conference on Structural Control,* Civil Engineering Dept, University of Southern Calif., (Los Angeles, CA, 3-5 August) ISBN 0-9628908-3-9.

Housner, G.W. and Masri, S.F., 1996, "Structural Control Research Issues Arising out of the Northridge and Kobe Earthquakes," *Proc Eleventh World Conference on Earthquake Engineering,* (Acapulco, Mexico 23-28 June).

Housner, G.W. and Kobori, T., 1996, *Proceedings of the Joint U.S.-Japan Workshop on Mitigation of Urban Disasters: Cooperative Research on Structural Control,* (Kyoto, Japan, 14-15 March).

Housner, G.W., Bergman, L.A., Caughey, T.K., Chassiakos, A.G., Claus, R.O., Masri, S.F., Skelton, R.E., Soong, T.T., Spencer, B.F., and Yao, J.T.P., 1997, "Structural Control: Past, Present and Future," ASCE *Journal of Engineering Mechanics,* (Special Issue), **123**(9), 897-971.

Hyzak, M., Leach, M., and Duff, K., 1997, "Practical application of GPS to bridge deformation monitoring," *Proceedings, Permanent Committee Meeting and Symp., International Federation of Surveyors (FIG), May.*

IBMAS, 2002, Proceedings of *the First International Conference on Bridge Maintenance, Safety and Management,* (Barcelona, Spain, 14-17 July).

Inman, R. J. 1994, Engineering Vibration, Prentice Hall, 560.

159

Knecht, A., Manetti, L., 2001, "Using GPS in Structural Health Monitoring," *Proceedings of SPIE's Eighth Annual Symposium on Smart Structures and Materials,* (Newport Beach, California, 4-8 March).

Kondo, H., and Cannon, M.E., 1995, "Real-time Landslide Detection System Using Precise Carrier Phase GPS," *ION GPS95 Conference Proceedings,* The Institute of Navigation, (Palm Springs, CA).

Lee, G.C., and Liang, Z., 1999, "Development of a Bridge Monitoring System," *Proceedings of the 2nd International Workshop on Structural Health Monitoring,* (September 18-20), 349-358.

Marwala, T., 2000, "Damage Identification Using Committee of Neural Networks," *Journal of Engineering Mechanics,* **126**(1), 43-50.

Masri, S.F., Nakamura, M., Chassiakos, A.G., and Caughey, T.K., 1996, "A Neural Network Approach to the Detection of Changes in Structural Parameters," ASCE *Journal of Engineering Mechanics,* **122**(4), 350 - 360.

Masri, S.F., 2003, Personal communication with Dr. Sami F. Masri.

Masri, S.F., 1994, "A Hybrid Parametric/Nonparametric Approach for the Identification of Nonlinear Systems," *Probabilistic Engineering Mechanics,* **9**, 47-57.

Masri, S.F., and Caughey, T.K., 1979, "A Nonparametric Identification Technique for Nonlinear Dynamic Problems," *ASME Journal of Applied Mechanics,* **46**(2), 433-447.

Masri, S.F., Chassiakos, A.G., and Caughey, T.K., 1993, "Identification of Nonlinear Dynamic Systems Using Neural Networks," *ASME Journal of Applied Mechanics,* **60**(3), 123-133.

Masri, S.F., Nakamura, M., Chassiakos, A.G., and Caughey, T.K., 1996, "Neural Network Approach to Detection of Changes in Structural Parameters," *Journal of Engineering Mechanics,* **122**(4), 350-360.

Masri, S.F., Miller, R.K., Sassi, H., and Caughey, T.K., 1984, "A Method for Reducing the Order of Nonlinear Dynamic Systems," *Journal of Applied Mechanics,* **51**(6), 391-398.

Masri, S.F., Miller, R.K., Saud, A.F., and Caughey, T.K., 1987, "Identification of Nonlinear Vibrating Structures: Part I – Formulation," *ASME Journal of Applied Mechanics,* **54**(12), 918-922.

160

Masri, S.F., Smyth, A.W., Chassiakos, A.G., Caughey, T.K., and hunter, N.F., 2000, "Application of Neural Networks for Detection of Changes in Nonlinear Systems," *Journal of Engineering Mechanics,* **126**(7), 666-683.

Masri, S.F., Smyth, A.W., and Chassiakos, A.G., 1998, "Detection of Structural Changes through Nonlinear System Identification Approaches," *Asia-Pacific Workshop on Seismic Design & Retrofit of Structures,* (August 10-12), 425-439.

Masri, S.F., Smyth, A.W., Chassiakos, A.G., Nakamura, M., and Caughey, T.K., 1999, "Training Neural Networks by Adaptive Random Search Techniques," *Journal of Engineering Mechanics,* **125**(2), 123-132.

Natke, H.G. and Yao, J.T.P. (eds), 1988, *Structural Safety Evaluation Based on System Identification Approaches,* Frieder Vieweg & Sohn, Braunschweig.

Natke, H.G.; Tomlinson, G.R; and Yao, J.T.P. (eds), 1993, *Proceedings of the International Workshop on Safety Evaluation Based on Identification Approaches Related to Time Variant and Nonlinear Structures,* (Lambrecht, Germany, 6-9 September), Vieweg, Weisbaden, ISBN 3-528-06535-4,

Nakamura, S., 2000, "GPS Measurement of Wind-induced Suspension Bridge Girder Displacements," *Journal Structural Engineering.,* **126**, 1413-1419.

Olaszek, P., 1999, "Investigation of the Dynamic Characteristics of Bridge Structures Using a Computer Vision Method," *Measurement,* **25**(3), 227-236.

Park, K.C., Reich, G.W., and Alvin, K.F., 1997, "Structural Damage Detection Using Localized Flexibilities," *Proceedings of the 2nd International Workshop on Structural Health Monitoring, Current Status and Perspectives,* (September 18-20), 125-139.

Pridham, B.A., Wilson, J.C., 2001, "Subspace Identification of Vincent Thomas Suspension Bridge Ambient Vibration Data," *Proceedings of the 20th International Modal Analysis Conference, Los Angeles, California,* 596-604.

Radulescu, D. and Radulescu C., 2003, personal communication with Misters Dan and Costin Radulescu.

Rainer, J. H.,and Selst, V.A., 1976, "Dynamic Properties of Lions' Gate Suspension Bridge," ASCE / EMD Specialty Conference on Dynamic Response of Structures: Instrumentation, Testing Methods and System Identification, University of California, (Los Angeles, CA, 30-31 March).

Roberts, G. W., Dodson, A. H., 1998, "A Remote Bridge Health Monitoring System Using Computational Simulation and GPS Sensor Data," *Seismological Society of America*, **25**(4), 299-308.

Roberts, G. W., Dodson, A. H., Brown, C. J., Karuna, R., Evans, R. A., 2000, "Monitoring the Height Deformation of Humber Bridge by GBS, GLONASS and Finite Element Modeling," IAG Symposia, Springer-Verlag, (Berlin, Germany) **121**, ISBN 3-540-67002-3, 355-360, Berlin, 2000.

SHMISIS, 2002, *Proceedings of First International Workshop on Structural Health Monitoring of Innovative Civil Engineering Structures*, Structural Health Monitoring Intelligent Sensing for Innovation Structures, (Winning, Manitoba, Canada, 19-20 September).

Shinozuka, M., Ghanem, R., Houshmand, B., and Mansouri, B., 2000, "Damage Detection in Urban Areas by SAR Imagery," *Journal of Engineering Mechanics*, **126**(7), 769-777.

Symth A. W., 1998, "Analytical and experimental studies in system identification and monitoring in context of structural control," *Ph.D. Dissertation*, University of Southern California.

Smyth, A.W., Masri, S.F., Caughey, T.K., and Hunter, N.F., 1999, "Surveillance of Mechanical Systems on the Basis of Vibration Signature Analysis," *ASME Journal of Applied Mechanics*.

Smyth, A.W., Masri, S.F., Chassiakos, A.G., and Caughey, T.K., 1999, "On-Line Parametric Identification of MDOF Nonlinear Hysteretic Systems," *Journal of Engineering Mechanics*, **125**(2), 133-142.

Smyth, A. W., Masri, S.F., Caughey, T.K., and Hunter, N.F., 2000, "Surveillance of Mechanical Systems on the Basis of Vibration Signature Analysis," ASME *Journal of Applied Mechanics*, **67**(3), 540-551.

Smyth, A. W., Masri, S.F., 2001, "Nonlinear System Identification and Structural Health Monitoring of Bridges Through the Use of Reduced-Order Models, " *Proceeding IABSE Conference on Cable-Supported Bridges*, (Seoul, Korea, 12-14 June).

Smyth, A.W; Pei, J-S; and Masri, S.F., 2002, "System Identification of the Vincent Thomas Suspension Bridge using Earthquake Records," *Intl Jnl Earthquake Engineering and Structural Dynamics*, June.

Smyth, A., Pei, J, 2000, "Integration of Measured Response Signals for Nonlinear Structural Health Monitoring," *Proceedings of the Workshop on Nonlinear Structural Control*, University of Southern California.

Sohn, H., Dzwonczyk, M., Straser, E.G., Kiremidjian, A.S., Law, K.H., and Meng, T., 1999, "An Experimental Study of Temperature Effect on modal Parameters of the Alamosa Canyon Bridge," *Engineering and Structural Dynamics* **28**, 879-897.

Sohn, S., Farrar, C.R., Hunter, N.F., and Worden, K., 2001, "Structural Health Monitoring Using Statistical Pattern Recognition Techniques," *ASME Journal of Dynamics Systems, Measurement and Control: Special Issue on Identification of Mechanical Systems*.

Sohn, H., and Farrar, C.R., 2001, "Damage Diagnosis Using Time Series Analysis of Vibration Signals," *Smart Materials and Structures*, **10**, 1-6.

Sohn, H., and Law, K.H., 2001, "Extraction of Ritz Vectors from Vibration Test Data," *Mechanical Systems and Signal Processing*, **15**(1), 213-226.

Szewezyk, P. and Hajela, P., 1994, "Damage Detection in Structures Based on Feature-Sensitive Neural Networks," *Jnl of Computing in Civil Engineering*, ASCE, **8**(2), 163-178.

Teague, E. H., How, J. P., Lawson, L. G., and Parkinson, B. W., 1995, "GPS as a Structural Deformation Sensor," *Proceedings of AIAA Guidance, Navigation and Control Conference*, Baltimore, MD, August.

Vanik, M.W., Beck, J.L., and Au, S.K., 2000, "Bayesian Probabilistic Approach to Structural Health Monitoring," *Journal of Engineering Mechancis*, Vol. **126**(7), 738-745.

Vestroni, F., and Capecchi, D., 2000, "Damage Detection in Beam Structures Based on Frequency Measurements," *Journal of Engineering Mechanics*, **126**(7), 761-768.

Wahbeh, A. M., Caffrey, J. P., Masri S.F., 2003, "A Vision-based Approach for the Direct Measurement of Displacement in Vibrating Systems," *Smart Materials and Structures Journal*, **12**, 785-794.

Wieser, A., Brunner, F. K., 2002, "Analysis of Bridge Deformation using Continuous GPS Measurements," *Proceedings of INGEO Bratislava*, November.

Wolfe, R.W; Masri, S.F; and Caffrey, J.C., (2002), "Some Structural Health Monitoring Approaches for Nonlinear Hydraulic Dampers," *Journal of Structural Control*, **9**(1), 5-18

163

Woodhouse, N.G., Robson, S., Eyre, R., 1999, "Vision Metrology and Three Dimensional Visualization in Structural Testing and Monitoring," *Photogrammetric Record*, **16**(94), 625-641.

Worden, K., 1990, "Data Processing and Experimental Design for the Restoring Force Method, Part I: Integration and Differentiation of Measured Time Data," *Mechanical Systems and Signal Processing*, **4**, 295-319.